

SANDIA REPORT

SAND99-2691

Unlimited Release

Printed October 1999

Development of Zinc/Bromine Batteries for Load-Leveling Applications: Phase 2 Final Report

Nanch Clark, Phillip Eidler and Peter Lex

Prepared by
Sandia National Laboratories
Albuquerque, New Mexico 87185 and Livermore, California 94550

Sandia is a multiprogram laboratory operated by Sandia Corporation,
a Lockheed Martin Company, for the United States Department of
Energy under Contract DE-AC04-94AL85000.

Approved for public release; further dissemination unlimited.



Sandia National Laboratories

Issued by Sandia National Laboratories, operated for the United States Department of Energy by Sandia Corporation.

NOTICE: This report was prepared as an account of work sponsored by an agency of the United States Government. Neither the United States Government, nor any agency thereof, nor any of their employees, nor any of their contractors, subcontractors, or their employees, make any warranty, express or implied, or assume any legal liability or responsibility for the accuracy, completeness, or usefulness of any information, apparatus, product, or process disclosed, or represent that its use would not infringe privately owned rights. Reference herein to any specific commercial product, process, or service by trade name, trademark, manufacturer, or otherwise, does not necessarily constitute or imply its endorsement, recommendation, or favoring by the United States Government, any agency thereof, or any of their contractors or subcontractors. The views and opinions expressed herein do not necessarily state or reflect those of the United States Government, any agency thereof, or any of their contractors.

Printed in the United States of America. This report has been reproduced directly from the best available copy.

Available to DOE and DOE contractors from
Office of Scientific and Technical Information
P.O. Box 62
Oak Ridge, TN 37831

Prices available from (703) 605-6000
Web site: <http://www.ntis.gov/ordering.htm>

Available to the public from
National Technical Information Service
U.S. Department of Commerce
5285 Port Royal Rd
Springfield, VA 22161

NTIS price codes
Printed copy: A19
Microfiche copy: A01



SAND99-2691
Unlimited Release
Printed October 1999

Development of Zinc/Bromine Batteries for Load-Leveling Applications: Phase 2 Final Report

Nancy Clark
Energy Storage Systems Department
Sandia National Laboratories
P.O. Box 5800
Albuquerque, New Mexico 87185-0613

Phillip Eidler
Peter Lex
ZBB Technologies, Inc.
11607 W. Dearbourn Ave.
Wauwatosa, WI 53226

Sandia Contract No. 40-8965

Abstract

This report documents Phase 2 of a project to design, develop, and test a zinc/bromine battery technology for use in utility energy storage applications. The project was co-funded by the U.S. Department of Energy Office of Power Technologies through Sandia National Laboratories. The viability of the zinc/bromine technology was demonstrated in Phase 1. In Phase 2, the technology developed during Phase 1 was scaled up to a size appropriate for the application. Batteries were increased in size from 8-cell, 1170-cm² cell stacks (Phase 1) to 8- and then 60-cell, 2500-cm² cell stacks in this phase. The 2500-cm² series battery stacks were developed as the building block for large utility battery systems. Core technology research on electrolyte and separator materials and on manufacturing techniques, which began in Phase 1, continued to be investigated during Phase 2. Finally, the end product of this project was a 100-kWh prototype battery system to be installed and tested at an electric utility.

Contents

Executive Summary	ES-1
1. Introduction.....	1-1
2. Advances in Core Technology	2-1
Electrode Substrate Resistivity	2-1
Cathode Activation Layer.....	2-1
Carbon Paper Cathode Layer	2-2
Cathode Layer Adhesive	2-2
Cycled Battery Electrodes.....	2-2
Terminal Electrode Development.....	2-4
Separator Development	2-5
Quaternary Complexing Agents	2-6
Bromine Distribution and Evaporation Study.....	2-8
Experimental Complexing Agent.....	2-10
Zinc Plating.....	2-11
3. Battery Design, Fabrication, and Qualification	3-1
Battery Design	3-1
Stack and Battery Assembly	3-1
4. Battery Testing.....	4-1
8-cell, 1170-cm ² , 1-kWh Battery Testing.....	4-1
Battery V1-67 (1 kWh)	4-1
Battery V1-68.....	4-1
Battery V1-69.....	4-4
Battery V1-70.....	4-5
Battery V1-71.....	4-5
Battery V1-72.....	4-5
Battery V1-73.....	4-8
Battery V1-74.....	4-8
Battery V1-75.....	4-9
Battery V1-76.....	4-9
Battery V1-77.....	4-11
Battery V1-78.....	4-12
Battery V1-79.....	4-12
Battery V1-80.....	4-12
Battery V1-81.....	4-13
Battery V1-83.....	4-15
Battery V1-84.....	4-15
Battery V1-85.....	4-15
Battery V1-86.....	4-16
8-cell, 2500-cm ² , 2-kWh Battery Stacks	4-16
Battery V25-01-08.....	4-19
Battery V25-02-08.....	4-19
Battery V25-03-08.....	4-21
Battery V25-04-08.....	4-21
Battery V25-05-08.....	4-21
Battery V25-06-08.....	4-21
Battery V25-07-08.....	4-23

Contents (continued)

Battery V25-10-08.....	4-23
Battery V25-12-08.....	4-23
Battery V25-13-08.....	4-25
Battery V25-27-08.....	4-25
Battery V25-30-08.....	4-25
Battery V25-32-08.....	4-27
Battery V25-33-08.....	4-27
Battery V25-37-08.....	4-27
60-cell, 2500-cm ² Battery Stack Qualification.....	4-29
Batteries Delivered for Testing at SNL	4-29
SNL518 (8-cell, 1-kWh)	4-29
SNL526 (50-cell, 15-kWh)	4-29
5. Additional Battery Testing.....	5-1
No-strip Cycling	5-1
Overtoltage and Internal Resistance (IR) Testing.....	5-3
High-rate Discharge.....	5-6
Electrode Reconditioning	5-6
Effect of Orientation on Battery Performance.....	5-8
Simplified Frequency Regulation/Spinning Reserve (SFRSR) Testing.....	5-9
Low-temperature Study	5-10
Electrolyte Utilization Study	5-11
Stand Heating Study	5-11
Gas Generation at the Anode.....	5-12
Nonflow Zinc/Bromine Battery	5-12
6. 2500-cm² Battery Design.....	6-1
Cell Stack Design	6-1
Heating/Cooling Requirements	6-1
Thermodynamic Efficiency	6-1
Practical Cooling Requirements.....	6-2
Environmental Impact	6-3
Zinc Bromide and Zinc Chloride	6-3
Bromine	6-3
Quaternary Ammonium Ion Salts	6-4
7. Battery System Design and Manufacture.....	7-1
Battery Stack Manufacturing	7-1
2-kWh Control Station.....	7-2
100-kWh Deliverable Battery Design	7-2
Battery Controller and Software.....	7-4
100-kWh Battery System Manufacturing	7-6
8. Summary and Conclusions	8-1
9. References.....	9-1
10. Publications	10-1

Figures

2-1.	Overvoltage vs. Number of Cycles for Cycled Battery Electrodes.....	2-3
2-2.	Overvoltage vs. Electrochemical Surface Area for Cycled Battery Electrodes.....	2-3
2-3.	Volume of Second-phase in Load-leveling Electrolyte.....	2-9
2-4.	Bromine Concentration in Second-phase for Load-leveling Electrolyte.....	2-9
2-5.	Bromine Concentration in Catholyte Aqueous Layer for Load-leveling Electrolyte.....	2-10
2-6.	Beaker-scale Overvoltage Curves for Bromine Electrodes at 30°C.....	2-12
2-7.	Effect of Temperature on Overvoltage of Bromine Electrodes for Various Complexing Agents.....	2-12
4-1.	Cycle Efficiencies for Battery V1-67 (Includes Baseline and No-strip Cycles).....	4-4
4-2.	Baseline Cycle Efficiencies for Battery V1-68.....	4-5
4-3.	Baseline Cycle Efficiencies for Battery V1-69.....	4-6
4-4.	Baseline Cycle Efficiencies for Battery V1-71.....	4-6
4-5.	Baseline Cycle Efficiencies for Battery V1-72.....	4-7
4-6.	Baseline Cycle Efficiencies for Battery V1-73.....	4-8
4-7.	Baseline Cycle Efficiencies for Battery V1-74.....	4-9
4-8.	Baseline Cycle Efficiencies for Battery V1-75.....	4-10
4-9.	Baseline Cycle Efficiencies for Battery V1-76.....	4-10
4-10.	Baseline Cycle Efficiencies for Battery V1-77.....	4-11
4-11.	Baseline Cycle Efficiencies for Battery V1-78.....	4-12
4-12.	Baseline Cycle Efficiencies for Battery V1-79.....	4-13
4-13.	Baseline Cycle Efficiencies for Battery V1-80.....	4-14
4-14.	Baseline Cycle Efficiencies for Battery V1-81.....	4-14
4-15.	Baseline Cycle Efficiencies for Battery V1-83.....	4-15
4-16.	Baseline Cycle Efficiencies for Battery V1-84.....	4-16
4-17.	Baseline Cycle Efficiencies for Battery V1-85.....	4-17
4-18.	Baseline Cycle Efficiencies for Battery V1-86.....	4-17
4-19.	Baseline Cycle Efficiencies for Battery V25-01-08.....	4-20
4-20.	Baseline Cycle Efficiencies for Battery V25-02-08.....	4-20
4-21.	Baseline Cycle Efficiencies for Battery V25-04-08.....	4-21
4-22.	Baseline Cycle Efficiencies for Battery V25-05-08.....	4-22
4-23.	Baseline Cycle Efficiencies for Battery V25-06-08.....	4-22
4-24.	Baseline Cycle Efficiencies for Battery V25-07-08.....	4-23
4-25.	Baseline Cycle Efficiencies for Battery V25-10-08.....	4-24
4-26.	Baseline Cycle Efficiencies for Battery V25-12-08.....	4-24
4-27.	Baseline Cycle Efficiencies for Battery V25-13-08.....	4-25
4-28.	Baseline Cycle Efficiencies for Battery V25-27-08.....	4-26
4-29.	Baseline Cycle Efficiencies for Battery V25-30-08.....	4-26
4-30.	Baseline Cycle Efficiencies for Battery V25-32-08.....	4-27
4-31.	Baseline Cycle Efficiencies for Battery V25-33-08.....	4-28
4-32.	Baseline Cycle Efficiencies for Battery V25-37-08.....	4-28
4-33.	Baseline Cycle Efficiencies for Battery SNL518.....	4-30
4-34.	Baseline and No-strip Cycle Efficiencies for Battery SNL526.....	4-31
5-1.	Energy Efficiency over a Set of Six Consecutive Cycles without Stripping.....	5-2
5-2.	Overvoltage Losses for Battery V1-74 Measured by the Current-interrupt Method.....	5-4
5-3.	IR Losses for Battery V1-74 Measured by the Current-interrupt Method.....	5-4
5-4.	Battery Overvoltage Losses versus Cycle Life.....	5-5
5-5.	Battery IR Losses versus Cycle Life.....	5-5
5-6.	Overvoltage and IR Losses During Discharge Cycle (V1-80, 1-kWh).....	5-6
5-7.	Discharge Voltage Profiles for a 60-Cell, 2500-cm ² Battery Stack.....	5-7
5-8.	SFRSR Cycle for Zinc/Bromine Battery.....	5-10
7-1.	Depiction of a 33-kWh Battery Module.....	7-3
7-2.	Front and Back Views of the 100-kWh HazMat Building.....	7-4
7-3.	Detailed View of 33-kWh Battery Module.....	7-5

Tables

2-1.	Cathode Layer Properties for Various Types of Adhesives.....	2-2
2-2.	Overvoltage and Surface Area for Cycled and Uncycled Bromine Electrodes	2-4
2-3.	Resistance of Carbon Plastic Test Samples	2-5
2-4.	Resistance of Terminal Electrode Samples.....	2-5
2-5.	Properties of Experimental Separator Materials.....	2-6
2-6.	Properties of Vendor-prepared Separator Compositions	2-7
2-7.	Experimental Separator Results.....	2-7
2-8.	Bromine Diffusion for Experimental Separators—Contribution from Complex and Aqueous Phases	2-8
2-9.	Quaternary Complexing Agent Comparison	2-8
2-10.	Single-Cell Battery Efficiencies for Experimental Quaternary Complexing Agents	2-11
2-11.	Aqueous Bromine Concentration and Evaporation Rates for Experimental Quaternary Complexing Agents	2-11
4-1.	V-Design Battery Stack Performance.....	4-2
4-2.	Overview of 8-cell, V-Design Battery Testing	4-3
4-3.	Cycle Efficiencies for Battery V1-67	4-4
4-4.	Overview of 8-cell, 2500-cm ² Battery Testing.....	4-18
4-5.	Performance of 60-cell, 2500-cm ² Stacks	4-19
4-6.	Final Average Efficiencies of Battery SNL518	4-29
5-1.	No-strip Cycle Efficiencies for Battery V1-60.....	5-1
5-2.	Average of Six No-strip Cycles Compared to Baseline Cycle Results	5-2
5-3.	Performance of Battery V25-07-08 During Consecutive Cycles Without Stripping	5-3
5-4.	Effect of Discharge Rate on Performance for a 60-cell, 2500-cm ² Battery Stack	5-7
5-5.	Baseline Cycle Efficiencies Before and After Electrode Reconditioning	5-8
5-6.	Cycle Efficiencies for Vertical and Horizontal Orientation for Battery VL-15	5-8
5-7.	Constant-power Discharge Tests	5-9
5-8.	Frequency Regulation Discharge for Battery V1-64	5-10
5-9.	V1-50 Frequency Regulation Efficiencies.....	5-11
5-10.	Zinc Utilization Study for Battery V1-62	5-11
5-11.	Energy Efficiencies for Single-cell Nonflow Battery During Stand-Loss Cycling.....	5-13
6-1.	Calculated Heat* and Electrical Power in a Single Cell for a Constant-current Cycle at 25 A	6-2
6-2.	Battery Cooling Requirements.....	6-3
7-1.	100-kWh Battery Specifications	7-6
7-2.	Fault and Shutdown Conditions for 100-kWh Battery	7-7

Acronyms

Cp	heat capacity
DOE	U.S. Department of Energy
ESSP	Energy Storage Systems Program
IR	internal resistance
JCBGI	Johnson Controls Battery Group, Inc.
MEP	N-ethylpyrrolidinium bromide
MEM	N-ethylmorpholinium bromide
PCS	power conversion system
PLC	programmable logic controller
rpm	revolutions per minute
SFRSR	Simplified Frequency Regulation and Spinning Reserve
SNL	Sandia National Laboratories
T&D	transmission and distribution
ZBB	ZBB Technologies, Inc.

Intentionally Left Blank

Executive Summary

The U.S. Department of Energy (DOE) has long recognized the potential for utility energy storage and is currently supporting programs to develop advanced battery systems, such as the zinc/bromine battery, for these applications. The zinc/bromine battery development program is being cost-shared with the DOE through the Energy Storage Systems Program (ESSP) at Sandia National Laboratories (SNL). The objectives of the zinc/bromine battery development program are to design, fabricate, evaluate, and optimize a zinc/bromine battery system suitable for electric utilities.

The zinc/bromine load-leveling battery development contract was partitioned at the outset into two phases of equal length. Phase 1 (Contract No. 40-8965) was completed at Johnson Controls Battery Group, Inc. (JCBGI). Phase 2 was started at JCBGI but was transitioned to another company when JCBGI sold the business. The technology was acquired by ZBB Technologies, Inc. (ZBB), and the fabrication and troubleshooting of the final deliverable system was completed under Contract No. AF-5435.

Phase 1 started in September 1990 and continued through December 1991. In Phase 1, zinc/bromine battery technology was advanced to the point that it was clear that the technology was viable and that it would be an appropriate choice for electric utilities wishing to use stationary energy storage facilities. Criteria were established that addressed most of the problems that had been observed in previous development efforts. The performances of 8-cell and 100-cell laboratory batteries demonstrated that the criteria were met or exceeded.

In Phase 2, a 100-kWh battery was built, and demonstration of the complete 100-kWh battery system was initiated. At the same time, work continued on identifying improved assembly techniques and operating conditions. This report details the results of the efforts carried out in Phase 2. The highlights are listed below.

- The performance of 1170-cm² vibration-welded battery stacks gradually improved during the course of the contract. Battery V1-79 completed 1036 deep-discharge cycles before the energy efficiency declined by 10% from the peak value of 76.0%.
- A new cycling regime that is more appropriate for the electric utility industry, the Simplified Frequency Regulation and Spinning Reserve

(SFRSR) test, was explored using a cyclor on loan from SNL.

- A stand-test procedure was developed using a 50-cell stack. The test was used to measure the heat generated during the stand and to calculate bromine transport. As anticipated, the battery warmed, and the average bromine transport decreased during a stand. Battery orientation studies indicated that the transport current was higher when the cell stack was mounted horizontally. Beaker-scale tests to measure hydrogen gassing were developed and conducted.
- Mini-cell tests showed favorable results with one experimental quaternary complexing agent. Another experimental quat appeared to complex the bromine too tightly and gave poor battery performance.
- Special tests with battery V1-71 were conducted to simulate utility-type cycle regimes. In four trials, this battery completed 52, 56, 69, and 78 continuous one-hour charge/one-hour discharge cycles before the 1.0-V/cell low-voltage cutoff was reached.
- An electrode reconditioning process demonstrated significant improvements in efficiencies for three poorly performing batteries. The process appears to be much more successful if it is performed before the battery energy efficiency is allowed to get too low. Improved life expectancies were demonstrated when the procedure was performed regularly.
- A 60-cell, 2500-cm² battery stack delivered greater than 19 kWh when it was discharged over a three- to six-hour period.
- Modifications in the design of the 2500-cm²-series flow frames demonstrated improved battery performance. Energy efficiencies as high as 78% were observed on baseline cycles for 8-cell stacks. Stacks with 60 cells have achieved 77% energy efficiency.
- Several battery stacks were manufactured with experimental battery separators that demonstrated better properties than the standard zinc/bromine battery separator in beaker-scale tests. Battery V1-86 achieved 80.2% energy efficiency

EXECUTIVE SUMMARY

- on baseline cycles and 81.2% energy efficiency on cycles without stripping. This is the best-performing battery stack to date.
- Eight 60-cell, 2500-cm² battery stacks were qualified for use in the 100-kWh deliverable battery system. Each stack achieved greater than 75% energy efficiency on baseline cycles.
 - A coating applied to the carbon plastic electrode substrate demonstrated a 50% reduction in the resistance of terminal electrodes. This corresponds to at least a 1% increase in voltaic efficiency.
 - A more conductive carbon plastic substrate was manufactured and demonstrated an increase in energy efficiency of about 2%.
 - Experimental separator materials were developed with 25% lower resistivity and a bromine transport rate 25% lower than that of the standard zinc/bromine battery separator.
 - Postmortem evaluation of battery electrodes confirmed the occurrence of increased overvoltage and decreased surface area of the cathode activation layer in cycled batteries.
 - A high-surface area bromine electrode was developed with two to three times the surface area of previously prepared electrodes. The surface area of electrodes at the end of the contract was about 10,000 cm²/cm², compared to 2000-3500 cm²/cm² for earlier electrodes. An electrode with an even higher surface area of 50,000 cm²/cm² was also developed, but was not tested in a battery. The higher surface areas are expected to extend the cycle life expectancy of the batteries.
 - Manufacture of the 100-kWh battery was completed. The design consists of three compartments containing battery modules and a compartment for electrical panels, a scrubber, and a heat exchanger. These are all contained in a sealed HazMat building.
 - Battery stacks with 2500-cm² electrode area are capable of withstanding 23 to 24 psi before bursting. Under normal operating conditions, the battery stack observes a pressure of 6 to 8 psi, so a safety factor of about 3 has been built into the battery stacks.
 - The wiring for the 100-kWh deliverable battery system was completed. Communication between a personal computer and four programmable logic controllers (PLCs) has been accomplished. The major components of the system were installed and were tested.
 - Three 33-kWh battery modules were installed in the 100-kWh building. Short cycling of these modules through the power conversion system (PCS) was initiated for calibration purposes and to test fault conditions. Electrical noise between the PCS and the battery delayed initial testing of the 100-kWh battery system, but methods were developed to eliminate the noise.

The most critical development during Phase 2 was the ability to assemble a battery stack that remains leak-free. The task of sealing the battery stack using vibration welding has undergone significant improvement resulting in a viable production process. Developments made in battery component materials and testing procedures have demonstrated improvements in battery performance and life expectancy.

A method of determining the thermal management properties of the battery and an introduction to the environmental aspects of the battery system are also presented in this report.

1. Introduction

Because of the increasing demand for high quality, low cost electricity in the United States, utilities will need to modify their generation as well as their transmission and distribution (T&D) resources in the future. Concerns relating to matters such as air quality and the potential health effects of electromagnetic fields may delay the installation of these energy resources. Therefore, utilities are currently examining alternatives to these upgrades that will allow them to remain competitive in the marketplace.

One economically attractive alternative to utility upgrades is the use of battery energy storage. Batteries can be charged during off-peak periods and provide the necessary energy to customers when it is needed. Batteries have traditionally been considered only as a load-leveling resource, but recently they have been investigated as a multipurpose energy-storage option. Some of the potential benefits include T&D deferral and improved power quality. Economic and environmental benefits to the utilities have been identified, but the acceptance of batteries as an energy-storage option depends on the development of a low cost, reliable battery system.

The U.S. Department of Energy (DOE) has long recognized the potential for utility energy storage and is currently supporting programs to develop advanced battery systems, such as the zinc/bromine battery, for these applications. The zinc/bromine battery development program is being cost-shared with the DOE through the Energy Storage Systems Program (ESSP) at Sandia National Laboratories (SNL). The objectives of the zinc/bromine battery development program are to design, fabricate, evaluate, and optimize a zinc/bromine battery system suitable for electric utilities.

Toward this end, SNL awarded a cost-shared contract for a multiphase research project to Johnson Controls Battery Group, Inc. (JCBGI). JCBGI completed Phase 1 of the contract, the results of which are documented in SAND99-1853, *Development of Zinc/Bromine Batteries for Load-Leveling Applications: Phase 1 Final Report*. JCBGI began work on Phase 2, but the technology was acquired by ZBB Technologies, Inc., (ZBB) where the work was completed as documented in this report.

The goal of Phase 1 was to demonstrate the viability of the zinc/bromine technology for use in load-leveling applications. During this phase, the size of the bat-

tery stacks was limited to 1170 cm². Scale-up to 2500-cm² stacks would begin in Phase 2 if Phase 1 results succeeded in demonstrating the technology's viability.

This viability of the technology was demonstrated in Phase I when a number of criteria were met, including the following:

1. Demonstrating leak-free battery stacks.
2. Demonstrating steady long-term operation by achieving more than 100 cycles with less than a 10% drop in energy efficiency.
3. Achieving energy efficiencies of approximately 75%.
4. Demonstrating six consecutive no-strip cycles.
5. Verifying battery cost of \$150/kWh or less.
6. Addressing safety issues associated with the battery.

Major progress during Phase 1 included refining battery components and manufacturing techniques, which minimized leaks and improved battery performance.

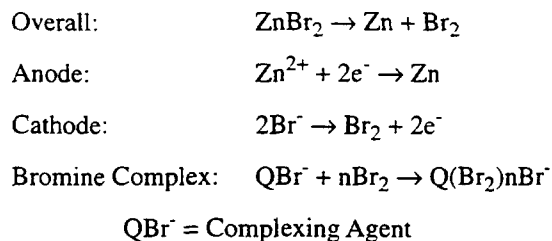
In Phase 2, the new 2500-cm² cell stacks, designed for an electric utility battery, were developed while core technology research continued. The end objective of Phase 2 was the demonstration of a 100-kWh system at a utility installation. Based on the results of this testing and utility interest, larger systems could be tested in the future.

The zinc/bromine battery differs from conventional lead/acid batteries because the electrolyte is circulated and stored external to the battery stack. The system consists of battery stacks, electrolyte storage reservoirs, and an electrolyte circulation system. The flowing electrolyte is necessary to ensure uniform zinc plating on the anode, to separate the reactive bromine from the electroplated zinc in the battery stack, and to improve thermal management. For more information on zinc/bromine batteries, see Chapter 37 of the *Handbook of Batteries*, by David Linden.

A bipolar electrode design is used to increase the specific energy of the battery. During charge, zinc is electroplated on the anode, and bromine is evolved at the cathode. A complexing agent in the electrolyte is

I. INTRODUCTION

used to reduce the reactivity and vapor pressure of the elemental bromine by forming a polybromide complex with the bromine. This minimizes the self-discharge of the battery and significantly improves the safety of the system. The complexed bromine is removed from the stacks with the flowing electrolyte and is stored in an external reservoir. On discharge, the complexed bromine is returned to the battery stacks, where zinc is oxidized to zinc ions and bromine is reduced to bromide ions. The electrochemical reactions during charge are given as follows:



The zinc/bromine battery stack contains nearly 100% plastic materials. Only a thin metal screen imbedded in the terminal electrodes is necessary to collect the electrical current in the x-y plane of the electrode. Plastic electrodes contain carbon for electrical conductivity

and glass to minimize warpage. Separators are microporous silica-filled polyethylene. Each electrode and separator is welded into a polyethylene frame that contains channels and diverters to distribute the flowing electrolyte uniformly across the face of the electrodes and separators. Alternating electrode and separator flow frames are then welded together between glass-filled polyethylene endblocks to form a hermetically sealed battery stack. A patented endblock design was developed to maintain the dimensional stability of the battery stack under pressure. The electrolyte normally flows through the battery stack under a pressure of 6-8 psi, and tests have demonstrated that the burst strength of the stack is about three times the operating pressure.

The potential advantages of the zinc/bromine technology include high specific energy (70 to 80 Wh/kg), rapid recharge (two to four hours), deep-discharge capability (100%), a finite self-discharge, and a built-in thermal management system. Inexpensive raw materials and mass-production manufacturing techniques give this battery system a potentially low initial cost (about \$150/kWh) and a stack replacement cost of about \$50/kWh.

2. Advances in Core Technology

This section describes improvements made in battery components. Improvements included lower-resistance electrode materials, cathode activation layers with increased electrochemical surface area, and separators with reduced bromine diffusion rates and lower resistance.

Electrode Substrate Resistivity

The carbon-filled plastic used for electrodes was produced by several compounding and extruding vendors. Several carbons were used at different concentrations. In general, the resistivity decreased as the amount of carbon black in the plastic increased. While the decrease in resistivity was expected, another, unexpected effect was that the plastic became more difficult to process as the carbon content increased. The resistivity of the carbon-plastic extruded sheets was reduced to 2 to 4 Ω -cm from that of the original material, which was about 8.6/ Ω -cm. New techniques to extrude and weld the carbon plastic have been developed.

Cathode Activation Layer

Early 8-cell and larger battery stacks reached the end of life at around 250–300 cycles. The cause of failure was most often a loss of activity of the porous, active carbon surface on the bromine electrode. Other cell stacks were found to develop a similar problem immediately following special tests. Therefore, work was undertaken to identify (a) the nature of the problem, (b) the cause, and (c) which active surface is more susceptible. This work was performed with small, 4-cm² electrode samples that were either cut from battery electrodes or specially prepared for the testing.

The cathode activation layer is a carbon coating that is applied to the bromine side of the carbon plastic electrode and is then heat-pressed into the plastic. This high-surface-area coating is necessary to compensate for the relatively low exchange current density for the bromine/bromide reaction on carbon. The life-limiting mechanism for earlier battery stacks was associated with the deterioration of the cathode activation layer, which caused a rapid increase in overvoltage near the end of battery life. Higher-surface-area cathode layers have demonstrated low electrode overvoltage and the ability

to increase the life expectancy of the battery. A great deal of work has been performed on increasing the electrochemical surface area of the bromine electrode.

The electroactive surface areas of bromine test electrodes are measured using a cyclic voltammetric method. The technique measures double-layer capacitance, which is directly proportional to the electroactive surface area of the electrodes.

Heat-press conditions were optimized for the fabrication of full-size bipolar electrodes made with Lot 11 carbon-plastic backbone. Full-size electrode heat-press conditions were evaluated and optimized via a combination of scratch-test physical testing and electrochemical surface area and overvoltage tests. Because of unstable electrode contacts, beaker-scale accelerated cycle-life tests cannot be run on samples of the full-size bipolar electrodes. However, the favorable test results for the new electrodes should translate into a favorably long cycle life. Similar test procedures were also used to optimize the heat-press conditions for terminal electrodes. The different mold requirements and increased viscosity of the thermally preworked terminal electrode carbon-plastic backbones necessitate developing optimum heat-press parameters that differ from those for the bipolar electrodes.

Optimizing the heat-press parameters produced low overvoltage as well as significantly higher surface areas than those seen previously. Bipolar electrodes were produced with 52-mV overvoltage at 250 mA/cm² and surface areas of 3600 cm²/cm². Terminal electrodes have been prepared with 43-mV overvoltage at 250 mA/cm² and surface areas of 5500 cm²/cm². Overvoltage of less than 100 mV at 250 mA/cm² is considered good. The highest surface areas before this optimization were 3000 cm²/cm² for bipolar electrodes and 2000 cm²/cm² for terminal electrodes. The higher surface areas appeared to correspond to longer lifetimes for zinc/bromine batteries.

A very-high-surface-area cathode layer has been developed and was tested in Battery V1-80. These bromine electrodes had high surface areas of 10,000 to 15,000 cm²/cm², as compared to 2000 to 3500 cm²/cm² for previous batteries. These new cathode layers have shown low overvoltage of 30 to 40 mV at 250-mA/cm² discharge rates and are expected to improve the life expectancy of the battery. The high-surface-area cathode layer demonstrated very good performance over the

first 900 cycles for Battery V1-80. Another type of cathode layer with an electrochemical surface area of about $50,000 \text{ cm}^2/\text{cm}^2$ has also been developed, but it was not tested in a battery.

Beaker-scale bromine electrodes prepared from a new carbon powder with a high specific surface area (about $3000 \text{ m}^2/\text{gm}$) were compared to electrodes prepared from the standard carbon, which has a surface area of $1200 \text{ m}^2/\text{gm}$. The results were not as promising as expected. Despite the higher-carbon-powder surface area, the electrodes made with the new carbon gave slightly lower electrochemical surface area and higher overvoltage (particularly at high current densities) than the standard carbon. The new carbon had a much smaller particle size than the standard carbon, and the carbon layer did not appear to be as thick as for the standard coating. The new carbon is small and flake-like. Consequently, the particles may have lain flat on the surface of the electrode substrate, resulting in a very thin carbon surface layer. These factors may have contributed to the lower active surface area observed for the new carbon powder.

Carbon Paper Cathode Layer

The carbon paper electrodes were assembled into Battery V1-75. The battery achieved good initial performance, but the performance declined significantly after only 16 baseline cycles. An internal leak was suspected, because of the appearance of complexed phase bromine in the anolyte reservoir during cycling. After testing, the electrodes showed a very good electrochemical surface area on the bipolar cathode, but the terminal cathode had very low surface areas. This is because the manufacture of the terminal electrode cathode layer was optimized for the carbon powder, but not for the carbon paper.

Cathode Layer Adhesive

A conductive adhesive is used to bond the cathode activation layer to the carbon plastic electrode substrate in the zinc/bromine battery. Overvoltage and surface area results for several adhesives are compared to the standard product in Table 2-1. The results indicate that each of the alternative materials could be a potential replacement for the standard adhesive. Each of these materials was also found to have good resistance to bromine.

Sample A is a commercial adhesive and was used to fabricate the electrodes used in Battery V25-33-08. The battery performed consistently over the first 127 baseline cycles with a very low overvoltage of $0.5 \text{ mV}/\text{cell}$ at a discharge rate of $14 \text{ mA}/\text{cm}^2$. Sample B was not used in a battery because it was not a commercial product.

The first attempts at using the new aqueous-based adhesive to make porous carbon layers resulted in good initial electrode performance, but very poor accelerated cycle-life performance. Research is needed to find a way of stabilizing the ohmic contact of the cathode layer, which may improve its cycle life.

Cycled Battery Electrodes

Samples of the electrode materials taken from cycled batteries showed a range of overvoltage and surface area values. Figure 2-1 indicates that there was little correlation between overvoltage and number of cycles, but Figure 2-2 shows a strong correlation between the electrochemical surface area and the overvoltage. The samples with low surface area exhibited high overvoltage.

Electrochemical overvoltage and surface area for bipolar and terminal battery bromine electrodes from recent teardowns are given in Table 2-2. It is clear from

Table 2-1. Cathode Layer Properties for Various Types of Adhesives

Adhesive Type	Overvoltage at $250 \text{ mA}/\text{cm}^2$ (mV)	Electrochemical Surface Area (cm^2/cm^2)
Standard	35	12,453
Sample A	42	12,876
Sample B	44	14,375

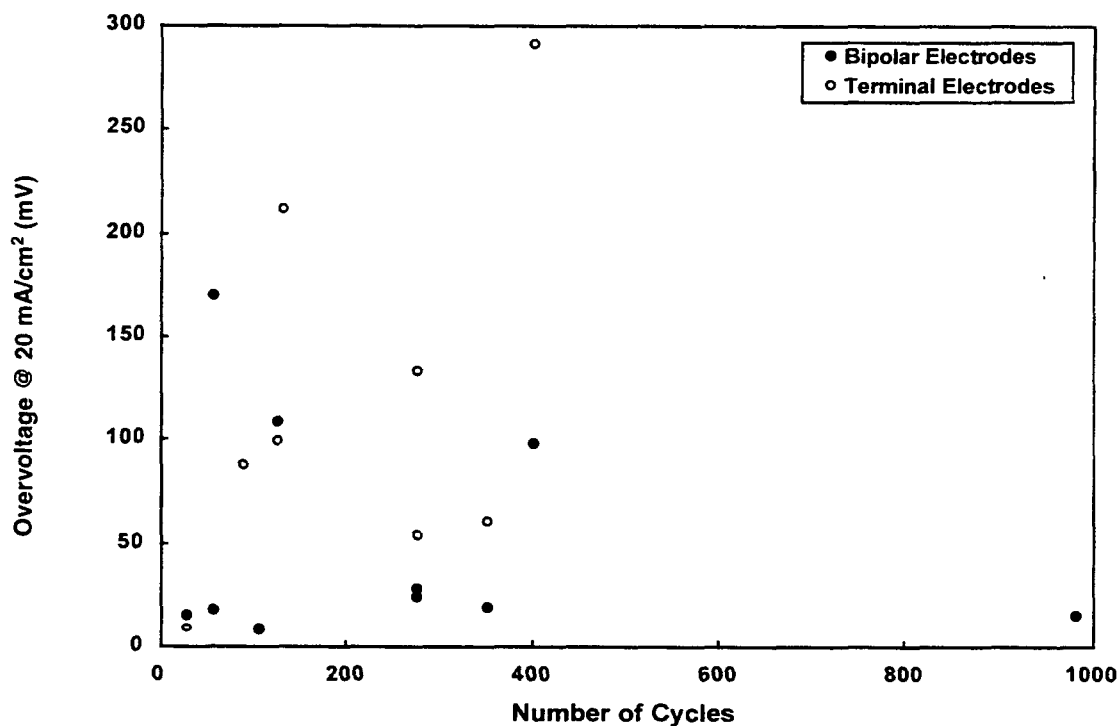


Figure 2-1. Overvoltage vs. Number of Cycles for Cycled Battery Electrodes.

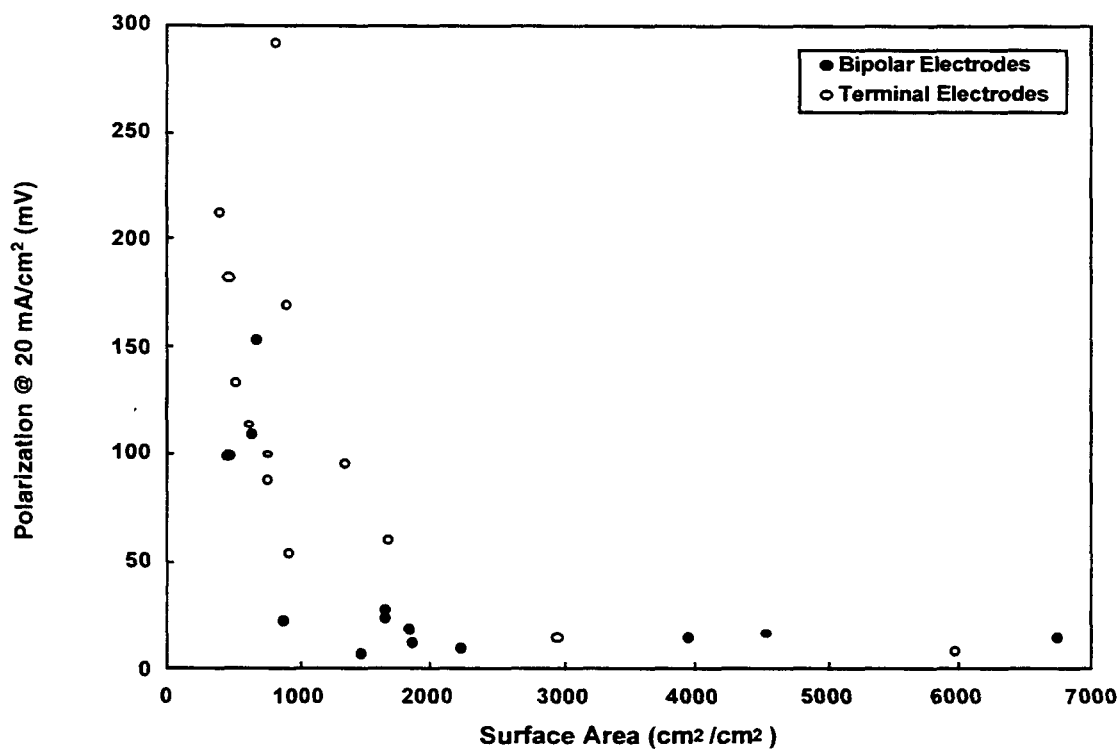


Figure 2-2. Overvoltage vs. Electrochemical Surface Area for Cycled Battery Electrodes.

**Table 2-2. Overvoltage and Surface Area
for Cycled and Uncycled Bromine Electrodes**

Battery Number	Number of Cycles	Bipolar Electrodes		Terminal Electrodes	
		Overvoltage @ 20 mA/cm ² (mV)	Surface Area (cm ² /cm ²)	Overvoltage @ 20 mA/cm ² (mV)	Surface Area
V1-64		21.8	892	13.5	2966
V1-66		153	686	113	635
V1-68	32	21.8 (5.5)	766 (1641)	20.5	2063
V1-73	171	36.5 (2.5)	1524 (3097)	151	860
V1-75	24	8.3 (2.5)	2625 (3097)	12.5	4141
V1-80	985	14	6753		
VL-17		10	2239	182	469
VL-18		11	1878	93.5	1375
VL-19	201	11.5	2031	11.5	5391
VL-20	201	11.8	1953	10.5	5657

Note: Overvoltage and surface area of bipolar electrodes before cycling are in parentheses.

the data that cycled battery electrodes with lower surface areas (<1500 cm²/cm²) tend to give poor overvoltage results.

The electrodes with the highest surface area had the lowest surface overvoltage losses; conversely, those with the lowest surface area had the highest overvoltage losses. This indicates that the cathode should be made with as high a surface area as possible. Work was performed to optimize the heat-press process to produce high-surface-area cathodes that are also physically strong.

The results in Table 2-2 show that the overvoltage increases and the surface area decreases during cycling. Also, the electrodes with surface areas greater than about 1500 cm²/cm² (V1-75, VL-19 and VL-20) still have fairly low overvoltage.

Terminal Electrode Development

Terminal electrodes for 1170-cm² battery stacks were prepared by imbedding a metal screen into a carbon plastic substrate. The metal screen is necessary to uniformly distribute the current in the x-y plane of the terminal electrode. All terminal electrode development done during this program was for 1170-cm² terminal electrodes.

In the past, the resistance from the electrical connection to the face of the electrode was higher than predicted. Also, the resistance measured from the face of the terminal electrode to the stud was higher than the resistance from the front to the rear face. This higher resistance indicated that there was a significant resistance at the copper screen/carbon plastic interface. The working face has 0.075 in. of carbon plastic and the entire part measures 0.100 in. A new method of preparing terminal electrodes was developed that reduced the resistance from the copper stud connection to the face of the electrode by 50%, from 0.5 Ω to 0.25 Ω. This reduc-

tion in terminal electrode resistance resulted in approximately a 2% increase in battery stack voltaic efficiency.

Test plaques were prepared by sandwiching two pieces of copper screen separated by two layers of Lot 08 carbon plastic. The first part was molded with bare Lot 08 carbon plastic. The second part was molded with plastic that had been specially coated. The resistances are shown in Table 2-3.

The coated plastic was also used to mold terminal electrodes. All samples were made with two sheets of Lot 08 plastic and two sheets of Lot 11 plastic. The Lot 11 carbon plastic was much more conductive than the Lot 08 plastic, but delamination occurred if multiple sheets of Lot 11 plastic were pressed together without Lot 08 plastic between them. TE-1 (TE = terminal electrode) used all uncoated Lot 11 plastic, while both TE-2 and TE-3 were made with sheets of coated Lot 11 plastic. Resistance results are given in Table 2-4 for terminal electrodes made with coated and uncoated carbon plastics.

The results in Table 2-4 show that the coating reduced the face-to-stud resistance of the terminal electrode by about 33%.

Separator Development

The zinc/bromine battery separator provides a barrier between the two sides of the electrochemical cell. It is necessary to allow the exchange of ions from one side of the cell to the other with minimal transport of bromine from the cathode to the anode. The characteristic parameters for the separator are the electrical resistivity and the rate of bromine diffusion. In the past, a tradeoff between the two properties was observed, but a large amount of effort has been made to minimize both of these separator characteristics.

The resistivity is measured in 0% state-of-charge electrolyte using a cell with known electrode dimensions. It is calculated by the difference between measurements made with and without the separator in place. The bromine diffusion is a measure of the amount of bromine transferred from one side of a diffusion cell to the other over a given period of time. In a diffusion cell, one side contains a simulated 100% state-of-charge catholyte while the other side contains a simulated 100% state-of-charge anolyte that is completely free of bromine.

The goal of the separator development work was to obtain a material with better properties than the standard material. Resistivity and bromine diffusion of labora-

Table 2-3. Resistance of Carbon Plastic Test Samples

Plaque Number	Variable	Resistance
1	none	36.5 mΩ
2	coated plastic	16.3 mΩ

Table 2-4. Resistance of Terminal Electrode Samples

Sample Number	Plastic Used	Resistance Face-to-Stud (Ω)
TE-1	Uncoated	0.65
TE-2	Coated	0.44
TE-3	Coated	0.46

tory-prepared separator samples containing various types of additives were compared to the standard zinc/bromine separator in Table 2-5. Sample No. 115-A contains no additives, while the others contain from 0.15-1.5% of additives that could improve certain properties of the separator. Table 2-5 shows that most of the experimental separators gave results that are similar to or slightly better than Asahi SF-600, particularly in resistivity.

After the lab trials, a series of compression-molded polyethylene compositions was prepared by a materials vendor. The results shown in Table 2-6 indicate higher than expected bromine diffusion. In particular, earlier samples made with the same composition as Material D in Table 2-6 had bromine transport of about 80% that of the Asahi separator and resistivity of about 67% that of the Asahi separator. The reason for the discrepancies in results is not known.

A large number of separator materials were manufactured by a separator vendor and tested for resistivity and bromine diffusion. The properties of the two most promising experimental battery separators are compared to the standard zinc/bromine battery separator in Table 2-7. Each of these samples was extruded on production-scale equipment. Both experimental samples had better properties than the standard separator material. To examine the electrochemical performance, 8-cell battery stacks were manufactured from each production material. Battery V1-84 was manufactured with separator 9502-10TA, and Batteries V1-85 and V1-86 were made with separator 95064-TA. Reasonably good performance was achieved for each of these battery stacks, as discussed in Chapter 4 under "8-Cell, 1170-cm², 1-kWh Battery Testing." Battery V1-86 achieved the highest efficiencies of any battery to date.

The transport of bromine through the separator in a zinc/bromine battery can be attributed to two possible mechanisms. One possible mechanism is the separator being wetted by the bromine complex, allowing elemental bromine to transfer from one side of the separator to the other. A second possible mechanism is bromine that is in equilibrium with the aqueous-phase diffusing through the separator. To estimate the contributions from these two forms of transport, two different diffusion tests were run. The first experiment was run with a combination of complexed-phase bromine and aqueous-phase catholyte. The second used only aqueous-phase catholyte with no complexed-phase. The aqueous-phase had previously been in equilibrium with the complexed-phase, and then the two phases were allowed to separate. The results of these diffusion tests are given in Table 2-8.

Both mechanisms contribute significantly to the bromine diffusion. The contribution from the aqueous-phase is 45-70% of the total amount of bromine that diffuses through the separator. Also, the samples that gave the lowest bromine transport in the presence of complexed-phase (9502-10TA and ISFS-TA) had a higher percentage of bromine transported from the aqueous-phase.

Quaternary Complexing Agents

Baseline cycle results for load-leveling electrolyte containing an experimental quaternary complexing agent are compared to standard load-leveling electrolyte results in Table 2-9. This particular quaternary compound contained an iodide ion form as opposed to the usual bromide ion form because the iodide form was commercially available. Also included in the table are

Table 2-5. Properties of Experimental Separator Materials

Sample Number	Resistivity (Ω -cm)	Bromine Diffusion (Mole-cm/sec/cm ²)
115-A	18.2	2.06E-10
115-B	18.1	1.44E-10
115-C	19.5	1.81E-10
115-D	17.4	2.74E-10
115-E	17.3	2.15E-10
Standard	23.1	1.97E-10

Table 2-6. Properties of Vendor-prepared Separator Compositions

Sample Number	Thickness (mm)	R ($\Omega\text{-cm}^2$)	Thickness (mm)	Br ₂ Diffusion (mole/sec/cm ²)	Normalized to Asahi
A-1	0.52	1.19	0.55	3.47E-10	1.95
A-2	0.51	1.17	0.50	2.5E-10	1.41
A-3	0.50	1.17			
B-1	0.51	1.24	0.53	3.45E-10	1.94
B-2	0.51	1.23	0.50	3.05E-10	1.72
B-3	0.51	1.23			
C-1	0.54	1.07	0.52	3.74E-10	2.10
C-2	0.52	1.02	0.55	3.47E-10	1.95
C-3	0.54	1.00			
D-1	0.52	0.75	0.50	3.55E-10	1.99
D-2	0.52	0.81	0.49	3.43E-10	1.92
D-3	0.49	0.82			
Standard	0.58	1.21	0.58	1.77E-10	1.00
	0.58	1.18	0.58	1.80E-10	
	0.58	1.14	0.58	1.87E-10	
	0.57	1.28			
	0.57	1.27			
	0.57	1.26			

Table 2-7. Experimental Separator Results

Separator Type	Thickness (mils)	Resistivity ($\Omega\text{-cm}$)	Bromine Diffusion (mole-cm/sec/cm ²)
9502 - 10TA	27.0	17.6	1.30×10^{-10}
95064 - TA	23.0	17.5	1.39×10^{-10}
Standard	23.5	23-25	1.97×10^{-10}

Table 2-8. Bromine Diffusion for Experimental Separators—Contribution from Complex and Aqueous Phases

Separator Sample	Bromine Diffusion (Aqueous and Complex) (mole-cm/sec/cm ²)	Bromine Diffusion (Aqueous Only) (mole-cm/sec/cm ²)	Ratio Aqueous/Complex
9502-102T	4.69 x 10 ⁻¹⁰	2.63 x 10 ⁻¹⁰	0.56
9502-10TA	1.40 x 10 ⁻¹⁰	9.86 x 10 ⁻¹¹	0.70
ISFS-T	4.85 x 10 ⁻¹⁰	2.20 x 10 ⁻¹⁰	0.45
ISFS-TA	1.41 x 10 ⁻¹⁰	8.56 x 10 ⁻¹¹	0.61
Standard	2.13 x 10 ⁻¹⁰	1.13 x 10 ⁻¹⁰	0.53

Table 2-9. Quaternary Complexing Agent Comparison

Electrolyte Type	Coulombic Efficiency (%)	Voltaic Efficiency (%)	Energy Efficiency (%)
Standard	86.1	84.7	72.9
Experimental Quat	84.5	76.0	64.2
Standard with 0.2M KI	75.8	82.9	62.9

results for load-leveling electrolyte containing standard quat with the addition of 0.2 M potassium iodide (KI), to show the effect of iodide ions on efficiencies. The information in Table 2-9 indicates that the lower efficiencies for the experimental complexing agent may be caused by the presence of iodide ions in the electrolyte, as opposed to the complexing agent itself. Following these tests, only the bromide forms of the complexing agents were considered for use in a battery.

Bromine Distribution and Evaporation Study

A series of synthetic catholyte solutions was prepared using load-leveling electrolyte components. The objective was to measure the bromine in the aqueous-phase and oily-phase. In making these samples, it was assumed that nearly all the quaternary ions from the anolyte would shift to the catholyte during charge.

The volume of second-phase increases as the state of charge increases, but extrapolates to above zero at low states of charge, as seen in Figure 2-3. The oily-phase in the 10% state-of-charge sample did not form right away, but separated out after standing overnight. The concentration of bromine in the oily-phase was calculated from the amount of bromine added and the volume of oily-phase seen. The bromine concentration also increased with the state of charge, as shown in Figure 2-4. For this calculation, it was assumed that the amount of bromine transferred to the aqueous-phase was negligible. The concentration of bromine in the aqueous-phase was directly titrated and is shown in Figure 2-5. The bromine concentration is higher at low state of charge because the bromide ion concentration is higher.

Quaternary salts with improved complexing capabilities can enhance the battery system's performance in two ways. The self-discharge of the battery will be

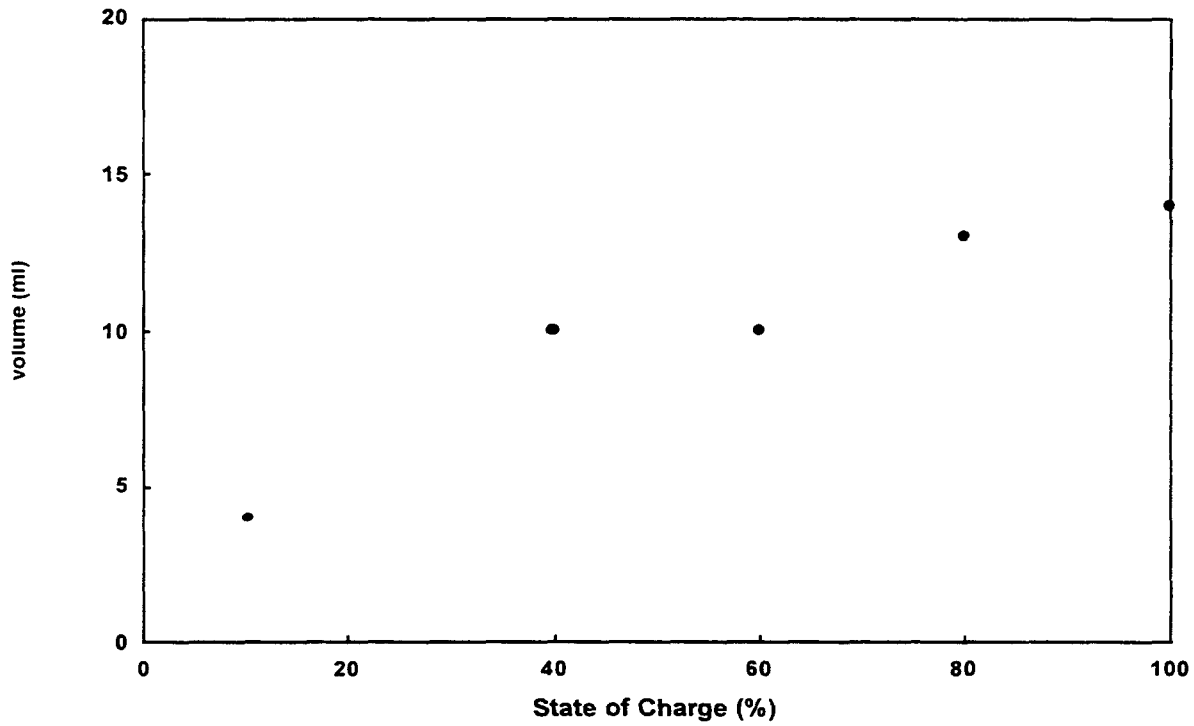


Figure 2-3. Volume of Second-phase in Load-leveling Electrolyte.

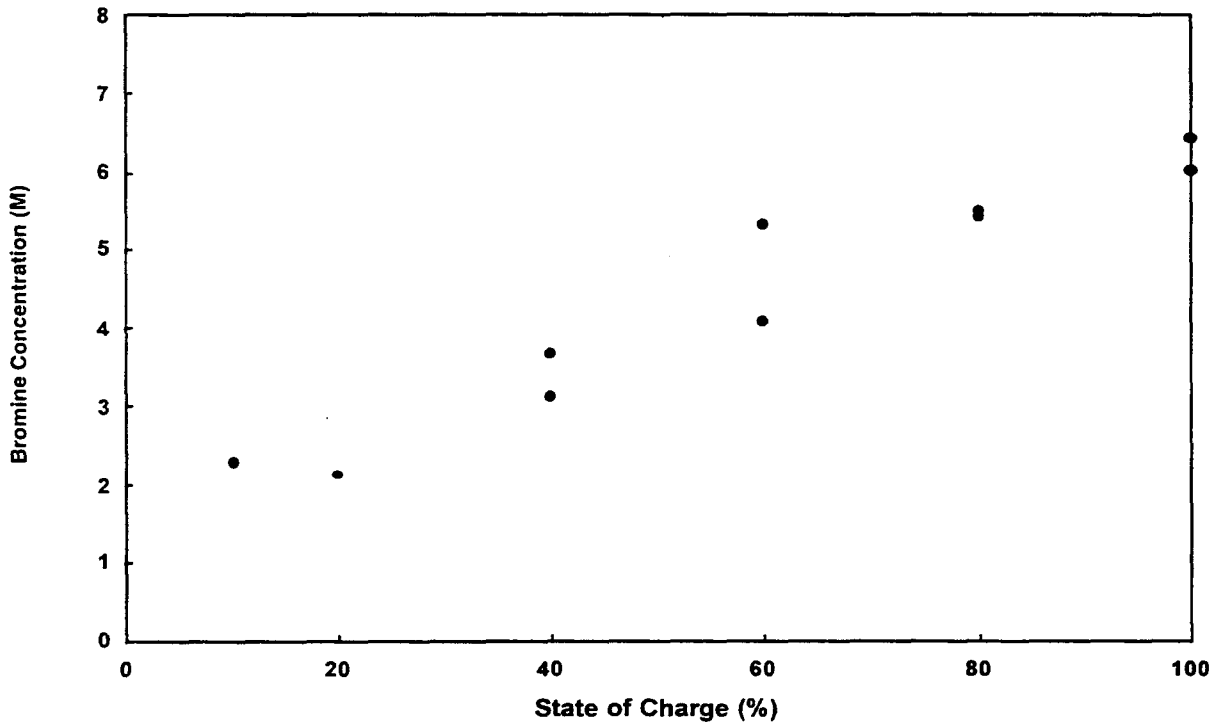


Figure 2-4. Bromine Concentration in Second-phase for Load-leveling Electrolyte.

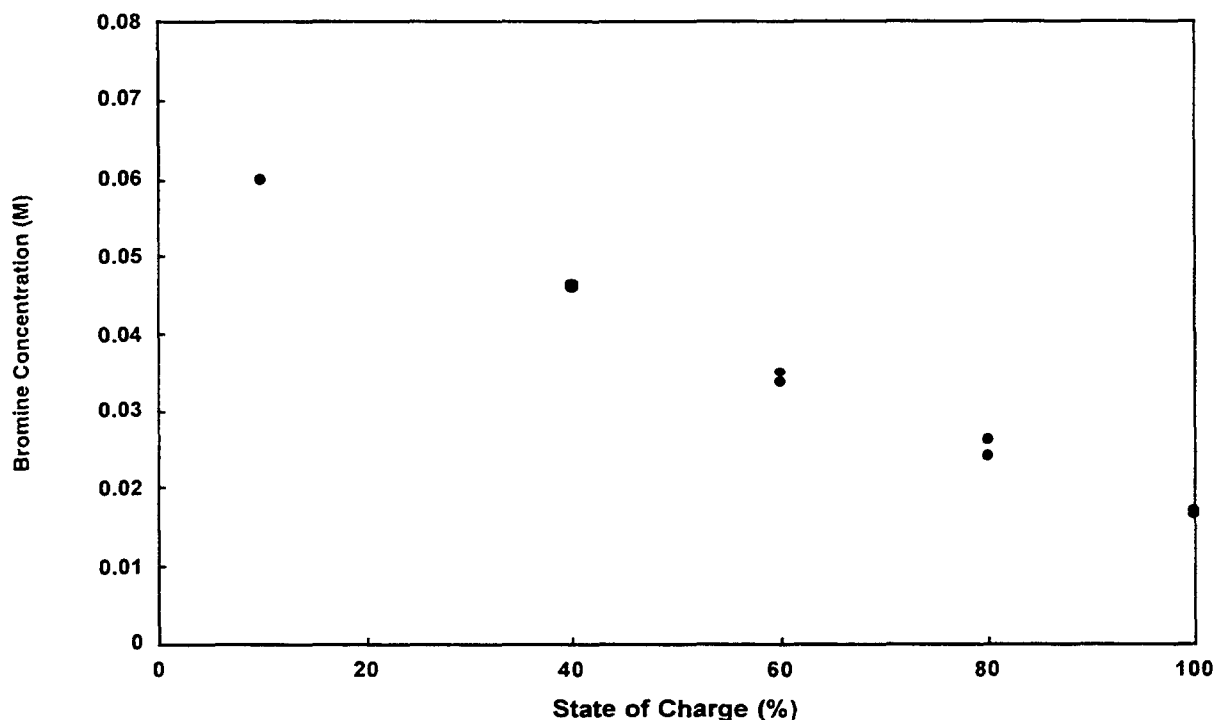


Figure 2-5. Bromine Concentration in Catholyte Aqueous Layer for Load-leveling Electrolyte.

reduced because of a lower aqueous bromine concentration, and the safety of the system will be improved because of reduced bromine vapor pressure.

Experimental Complexing Agent

Single-cell battery efficiencies for load-leveling electrolyte with experimental quats are compared to the standard electrolyte in Table 2-10. The electrolyte with one experimental quat (B) was slightly more resistive than the standard ($16.2 \Omega\text{-cm}$ as opposed to $14.2 \Omega\text{-cm}$), which is indicated by the lower voltaic efficiency. Additionally, the coulombic efficiency for the experimental quat is significantly higher than for the standard, while the energy efficiencies are essentially the same at a 20 mA/cm^2 charge/discharge rate. At a lower rate of 15 mA/cm^2 , the energy efficiency for the new quat is higher than for the standard, primarily because of the reduced transport losses.

Another experimental quat (C) had even lower bromine evaporation rates than Quat B, but gave much lower energy efficiencies (50%) than the other two quats. Most of the inefficiency (27%) was because of residual losses. Decreasing the quaternary salt concentration by 50–75% did not significantly improve the performance of the battery. Even a blend of Quat C with

the standard quat gave only about 60% energy efficiency, whereas electrolyte made with the standard quat or Quat B gave about 73% energy efficiency. It is believed that the experimental Quat C forms a very strong complex with bromine, causing a large amount of unreacted bromine to remain at the end of discharge.

Beaker-scale tests were run to determine if the electrode overvoltage is influenced by the type of complexing agent in the electrolyte. Previous tests indicated that three experimental complexing agents have stronger bromine complexing ability than the standard according to the relative order $C > G > B > \text{Standard}$, as shown in Table 2-11. Based on the improved complexing ability of these experimental quats, battery performance was expected to increase because of reduced bromine concentration in the aqueous-phase catholyte, which in turn reduces self-discharge. However, cycles run in single-cell batteries have shown that the experimental complexing agents caused a decrease in battery voltaic performance, which prevented any gains in overall energy efficiencies.

The overvoltage tests showed that the experimental quats caused an increase in electrode overvoltage to a degree consistent with their complexing ability (that is, $C > G > B > \text{Standard}$), as seen in Figure 2-6. This was

Table 2-10. Single-Cell Battery Efficiencies for Experimental Quaternary Complexing Agents

Quat Type	Current Density	Coulombic Efficiency (%)	Voltaic Efficiency (%)	Energy Efficiency (%)	Transport Inefficiency (%)	Residual Inefficiency (%)
Standard	20 mA/cm ²	87.8	83.1	73.0	7.2	5.1
Quat B	20 mA/cm ²	91.5	79.9	73.1	4.9	3.6
Quat C	20 mA/cm ²	64.5	77.2	49.7	8.6	27.0
Standard	15 mA/cm ²	86.1	86.3	74.3	10.9	3.0
Quat B	15 mA/cm ²	91.7	83.7	76.8	5.2	3.0

Table 2-11. Aqueous Bromine Concentration and Evaporation Rates for Experimental Quaternary Complexing Agents

Quat Type	Aqueous Br ₂ (Mole/Liter)	Br ₂ Evaporation (mg/cm ² -min.)
MEP	0.024	33.0
Quat B	0.010	17.6
Quat C	0.0037	11.0
Quat G	0.006	13.0

anticipated because it should take more energy to break the stronger complex, and thus the electrode overvoltage would be higher. Figure 2-7 shows that the overvoltage of the electrodes in each of the electrolytes decreases as the temperature increases. Not only was the electrode overvoltage higher with the experimental quats, but the resistances of electrolytes were also higher. The trend toward increased resistance follows the order B > G > C > Standard. The combination of increased electrode overvoltage and increased resistance of the experimental quats as compared to the standard quat appears to explain the poor performance observed when cycling the batteries with these complexing agents.

Zinc Plating

Electrolytes from two poorly performing battery stacks, when cycled in a minicell, yielded zinc deposits

that had a poor, mossy appearance compared to normal-looking zinc deposits. Samples of smooth and mossy zinc deposits were analyzed by (1) leaching in nitric acid and testing for total oxidizable carbon, and (2) chloroform leaching followed by infrared spectroscopy. The results indicated that the poor zinc deposits had higher carbon content and that an oily material was present in them. The source of these impurities was not investigated.

Electrolyte pH is considered to have an important effect on zinc plating quality and may be a factor in the mossy zinc observed. It has been reported that as the pH of the electrolyte approaches 4.0, mossy zinc may appear.² The pH was measured for electrolytes taken from recently failed batteries and showed that the batteries that had mossy zinc plating also had a higher pH than the other batteries.

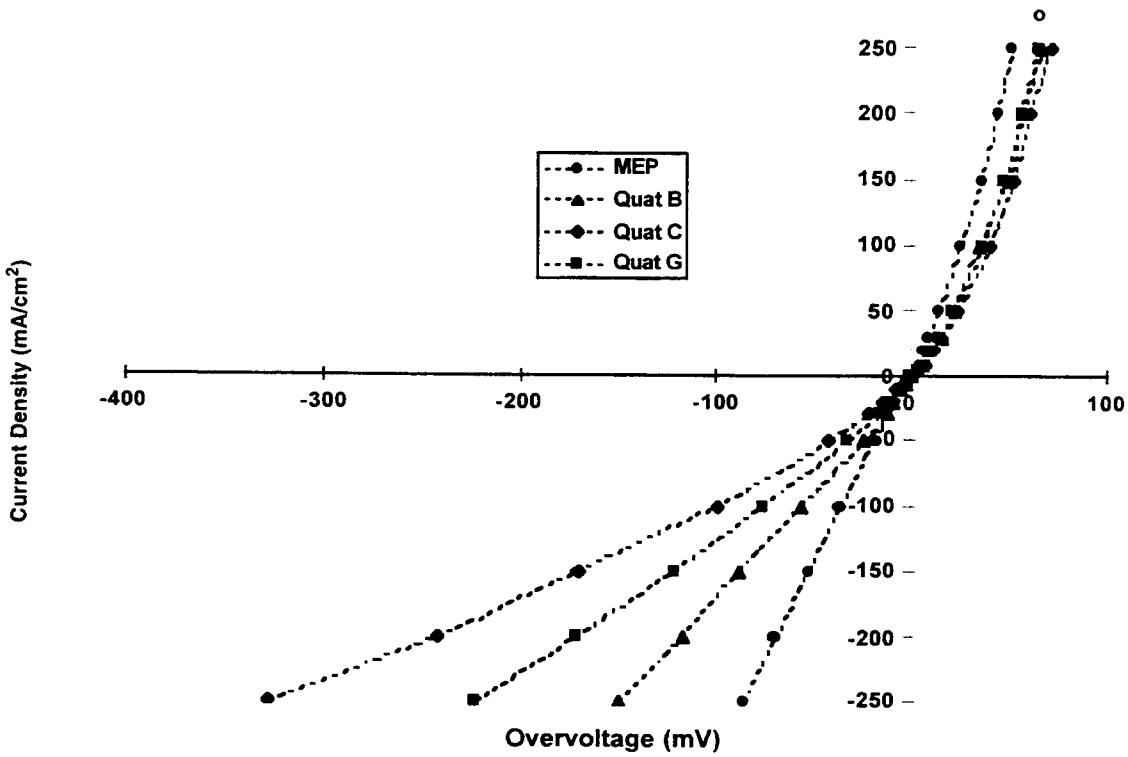


Figure 2-6. Beaker-scale Overvoltage Curves for Bromine Electrodes at 30°C.

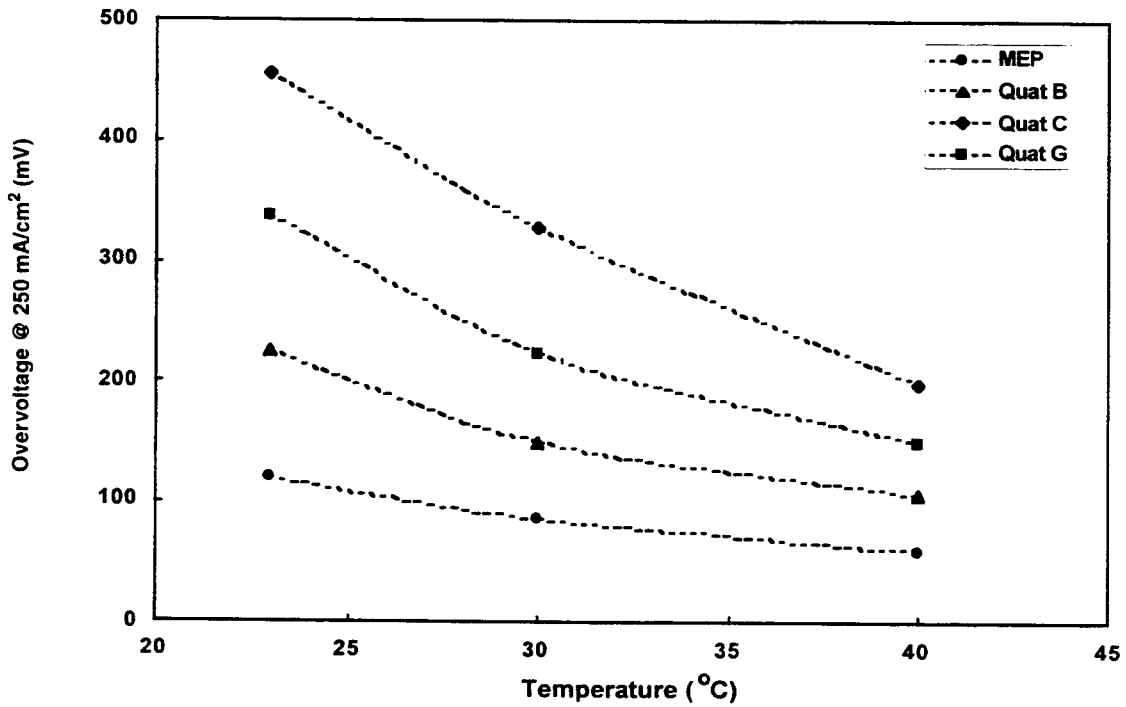


Figure 2-7. Effect of Temperature on Overvoltage of Bromine Electrodes for Various Complexing Agents.

3. Battery Design, Fabrication, and Qualification

Battery Design

The zinc/bromine battery is composed of three parts: the cell stack, the reservoirs, and the electrolyte circulation system. The electrode reactions take place in the cell stack. The battery starts each cycle with the same composition $ZnBr_2$ electrolyte in each reservoir. The two electrolytes are continuously pumped in separate circulation loops through the anode and cathode chambers in the stack. During charge, zinc is plated on the anode side of a bipolar electrode, while bromine is formed on the cathode side. The bromine instantly forms a complex with quaternary ammonium ions in the electrolyte, and this complex separates from the aqueous solution forming a second, denser liquid phase. Depleted aqueous electrolyte and second-phase flow continuously from the stack and are replaced by fresh electrolyte from the reservoirs. The newly produced second-phase falls to the bottom of the catholyte reservoir because it is denser than the aqueous solution. The second-phase remains in the catholyte reservoir throughout the charge period. Then, during discharge, an emulsion of second-phase and aqueous solution is circulated through the cathode chamber. The bromine, complexed in the second-phase and to a lesser extent dissolved in the water, reacts at the cathode surface to form bromide ions. In the anolyte, the plated zinc metal oxidizes to form zinc ions.

Stack and Battery Assembly

Each cell stack is composed of a number of bipolar electrodes and cell separators with terminal electrodes on either end. The electrodes are made from electrically conducting carbon plastic and are thermally welded into a nonconducting plastic flow frame. The flow frame contains the channels and openings used to conduct the electrolyte to and from the electrodes. The same flow-frame design is used for both electrodes and separators. The flow frames are vibrationally welded together to form the body of the cell stack. Rigid endblocks are placed outside the terminal electrodes to resist outward bending forces that are present when electrolyte is pumped through the stack.

During Phase 1, 25 8-cell and 7 larger cell stacks were produced in the effort to refine the assembly process and to collect operating data. Some of the more

significant changes in the production process included: a new injection mold for the flow frame that had a more uniform electrolyte flow pattern, changes in the vibration weld surfaces and process, modified tooling on the welding machines, and a change to a different welding machine.

During Phase 2, the cell-stack manufacturing process underwent continuous improvements. Some of these improvements included better fixturing methods (during the welding process), improvements in electrode manufacturing, changes in separator cleaning, and a refinement of the thermal welding parameters. A larger welding machine for the 2500-cm² battery stacks was installed, and the welding process was transferred to it. An automated data collection system that records the assembly parameters was initiated as part of long-term quality control.

Because one of the goals of the project was to demonstrate leak-free battery stacks, burst testing was used to evaluate the strength and integrity of the welds. Each time a change was made in the welding process (for example, adding more weld beads, using a different size of weld beads, etc.), cells manufactured using that process were filled with pressurized air until the welds began to fail. (When welds fail, they make a "popping" sound.) Under normal operating conditions, the pressure of the flowing electrolyte is between 6 and 8 psi. The goal was to obtain a safety factor of about 3 for the welds. In other words, cells should be able to withstand around 24 psi before bursting (weld failure). Cells that burst at low pressure were opened to determine where the failure(s) occurred. The results of the burst tests were used to refine the manufacturing process. Once a given manufacturing technique demonstrated consistent welds, cells were manufactured for life-cycle testing.

Before beginning life-cycle testing, water (rather than electrolyte) was circulated in the cells to ensure that there were no obvious leaks. The presence of electrolyte crossflow, which could indicate ripped or cracked separator material, was also checked during water testing. Cells that successfully passed water testing were filled with electrolyte and began life-cycle testing.

When a manufacturing process was developed that could consistently produce leak-free, 2500-cm² cells stacks, attention shifted to improving other subsystems of the battery system. Specifically, the heavy AC motors

used to run the circulation pumps were replaced by brushless DC motors. The motor revolutions per minute (rpm) are controlled by a pulsewidth modulator circuit,

which allows efficient adjustment of the flow rate. This simplified the electrolyte circuit because valves were no longer needed to adjust the pump output.

4. Battery Testing

8-cell, 1170-cm², 1-kWh Battery Testing

The 1170-cm² vibration-welded (V-design) battery stacks were originally developed to demonstrate the feasibility of the vibration welding process for sealing battery stacks. These stacks are currently being used for cycle-life testing of battery components and for demonstrating new testing procedures.

The standard cycle used for gathering baseline data consists of a 4.5-hour charge at 20 mA/cm² followed by a discharge at the same current to a cutoff voltage of 1.0 V/cell. The battery is then fully discharged, or stripped, through a resistor to 0 V. Battery efficiencies are calculated from the amp-hours (coulombic) and watt-hours (energy) removed from the battery until the cutoff of 1.0 V/cell is reached. The voltaic efficiency is the ratio of the average discharge voltage and the average charge voltage. Any capacity left in the battery after the 1.0-V/cell cutoff (unevenly deposited zinc and bromine retained in the cathode activation layer) is considered as residual losses. Transport losses, which include diffusion of bromine across the separator and shunt currents, can also occur during cycling.

The performance and cycle life of 1170-cm² vibration-welded batteries have improved significantly since the beginning of Phase 1 of the contract, as seen in Table 4-1. The end of life is considered to be a 10% decline from the peak energy efficiency for the battery stack.

Batteries V1-53 through V1-57 were manufactured and tested during Phase 1 of the contract and averaged 71.8% energy efficiency over an average of 290 baseline cycles.

A lower-resistance carbon plastic electrode material was developed and tested in Batteries V1-72 through V1-77. Low-resistance terminal electrodes allowed Battery V1-76 to achieve slightly higher energy efficiency than the other batteries. This series of batteries achieved an average cycle life of 447 cycles and an average energy efficiency of 74.6%.

Optimized cathode-layer pressing parameters were used to manufacture Battery V1-79. This battery completed 1036 baseline cycles before the energy efficiency declined by 10% from the peak value of 76.0%. Testing

of this battery stack continued until the performance declined by 20% from the peak.

Battery V1-80 was manufactured using low-resistance terminal electrodes and a very-high-surface-area cathode activation layer. The terminal electrodes were about 50% lower in resistance than previously prepared electrodes, and the cathode layer had about three times the surface area of the electrodes used in Battery V1-79. The improvements incorporated into Battery V1-80 have resulted in higher energy efficiencies and should extend the life of the battery.

Batteries V1-84 through V1-86 were manufactured using experimental separator materials. The separators demonstrated about 25% lower resistance and 30% lower bromine transport than the standard zinc/bromine battery separator. Battery V1-86 achieved over 80% energy efficiency on baseline cycles.

Table 4-2 gives an overview of the performance and failure modes for all 8-cell, 1170-cm², V-design battery stacks tested during Phase 2 of this contract. Testing performed on each individual battery stack is described in more detail below.

Battery V1-67 (1 kWh)

This battery was used primarily for no-strip cycling tests. The results for these tests are shown in Table 4-3. As expected, the results demonstrate that no-strip cycle regimes afforded a significant increase in efficiency by reducing residual losses.

After completing 105 cycles, testing of Battery V1-67 was suspended so that other batteries could be cycled. The battery was cycled again after being off test for nine months. The additional cycles showed no degradation in performance during the time that the battery was not being tested. A total of 110 cycles were run on this battery stack. Figure 4-1 shows a plot of the cycle efficiencies for the battery.

Battery V1-68

Initial testing of Battery V1-68 gave respectable efficiency levels such as 89.7% coulombic efficiency, 81.4% voltaic efficiency, and 73.0% energy efficiency. Early tests for this battery included some high-power tests with supported electrolyte during

Table 4-1. V-Design Battery Stack Performance

Battery Number	Manufacture Date	Cycles Completed	Average Energy Efficiency	Peak Energy Efficiency
V1-53	3/91	325	72.6%	74.6%
V1-54	4/91	218	71.0%	74.4%
V1-55	4/91	366	71.7%	74.2%
<u>V1-57</u> (Avg.)	4/91	<u>250</u> 290	<u>71.4%</u> 71.8%	75.9%
V1-72	10/92	504	73.3%	75.3%
V1-76	1/93	325	76.4%	77.9%
<u>V1-77</u> (Avg.)	3/93	<u>513</u> 447	<u>74.7%</u> 74.6%	76.7%
V1-79*	6/93	1500 (1036)	71.7% (73.5%)	76.0% (10% degradation)
V1-80	2/94	985	76.8%	79.0%
V1-84	5/95	25	74.4%	77.7%
V1-85	5/95	20	72.5%	75.1%
V1-86	6/95	34	78.3%	80.2%

* See text to explain parenthetical values.

Cycles 5 through 7. After running these tests, the electrolyte was changed to the baseline electrolyte.

Different electrolytes were studied in an attempt to decrease the bromine vapor pressure and increase the life expectancy of the cathode activation layer. The mixtures studied did not produce favorable results under baseline test conditions. The first experimental electrolyte was installed after 15 cycles were run on the battery. The battery voltage increased significantly after about 1.5 hours of charge and, some time before this, a precipitate began to settle out in the anolyte reservoir. About 2.5 hours into charge, the increase in voltage stopped, and the precipitate was no longer present. After 2.9 hours of charge, the voltage started to drop as if the battery had developed a short. Additionally, a great deal of gas was generated at the anode during the entire cycle. Performance on this cycle was 47.6% coulombic efficiency, 77.4% voltaic efficiency, and 36.8% energy efficiency, with 32.5% transport inefficiency and 19.9% residual inefficiency. Following this cycle, the electro-

lyte was replaced with the standard load-leveling formulation, and performance returned to normal.

Another electrolyte mixture was tested in this battery at Cycle 27. This solution had previously been tested in a mini-cell with favorable results. In this 8-cell battery, the performance of the new electrolyte mixture was similar to that of the other experimental electrolyte. After three cycles were run with this electrolyte, standard load-leveling electrolyte was returned to the battery, but the battery's performance did not recover. A significant amount of internal leakage became evident when large amounts of complexed-phase bromine in the anolyte were observed early in discharge. Figure 4-2 shows cycle efficiencies for Battery V1-68.

When torn down, the battery exhibited signs of localized heating in a small portion of one of the cells. The electrode, separator, and spacing mesh also showed some degree of melting. Adjacent cells had heat damage in the same area but to a lesser extent. Although no

Table 4-2. Overview of 8-cell, V-Design Battery Testing

Battery Number	Number of Cycles	Peak Coulombic Efficiency (%)	Peak Voltaic Efficiency (%)	Peak Energy Efficiency (%)	Additional Information/ Failure Mode
V1-67	110	88.6	82.9	73.4	Used for no-strip cycling. Showed no decline in performance after open circuit stand for 9 months.
V1-68	31	89.7	81.0	72.7	Experimental electrolytes tested. May have caused failure of battery. Localized heating caused holes in separator.
V1-69	52	91.9	80.7	74.2	Battery was taken off test to make room for newer builds. Showed minimal decline in performance after open circuit stand for 9 months.
V1-70	—	—	—	—	Never tested because of leak.
V1-71	195	89.6	82.2	73.6	Baseline cycling. Used for modified utility cycling regime. Failure caused by leak between vibration welds.
V1-72	504	88.4	85.2	75.3	Baseline cycling. Used to test reconditioning process. Failure caused by leak.
V1-73	171	90.0	86.2	77.6	Baseline cycling. Some no-strip. Failure caused by high overvoltage.
V1-74	262	90.0	85.8	77.2	Experimental electrode material. No-strip cycling. Failure caused by high overvoltage.
V1-75	24	90.0	86.9	78.2	Experimental cathode layer. Internal leak suspected, but not located.
V1-76	414	89.7	86.9	77.9	Baseline cycling. First battery tested for reconditioning process. Failure caused by high overvoltage.
V1-77	517	89.4	85.8	76.7	Baseline cycling. Tested reconditioning process before 10% degradation. Failure caused by high overvoltage.
V1-78	21	89.8	85.7	76.9	Tested as SNL deliverable. Retested after more than one year. Failure caused by cracked separators.
V1-79	1500	89.4	85.1	76.0	Baseline cycling. Ran reconditioning process regularly. Failure caused by high overvoltage. Tested to 20% degradation from peak.
V1-80	985	90.3	87.7	79.0	Baseline cycling. Ran reconditioning process regularly. Failure caused by leak.
V1-81	343	89.5	85.5	76.5	Baseline cycling. Apparent internal weld failure.
V1-82	—	—	—	—	Not used for this program.
V1-83	77	87.8	83.2	73.1	Experimental battery separator. Baseline cycles run.
V1-84	25	89.1	87.2	77.7	Experimental battery separator. Baseline cycles run. Some poor cycles resulting from insufficient second-phase.
V1-85	20	85.5	87.9	75.1	Experimental battery separator. Baseline cycles run. Some poor cycles resulting from faulty solenoid valve.
V1-86	34	90.9	88.2	80.2	Experimental battery separator. Baseline cycles run.

Table 4-3. Cycle Efficiencies for Battery V1-67

Cycle Type	Coulombic Efficiency (%)	Voltaic Efficiency (%)	Energy Efficiency (%)	Transport Inefficiency (%)	Residual Inefficiency (%)
Baseline Cycle	88.1	80.1	70.6	6.0	5.9
No-Strip Cycles 47-52	92.7	79.6	73.7	5.8	1.5
No-Strip Cycles 53-58	93.1	79.5	74.1	5.3	1.6
No-Strip Cycles 59-64	92.7	79.4	73.5	5.7	1.6

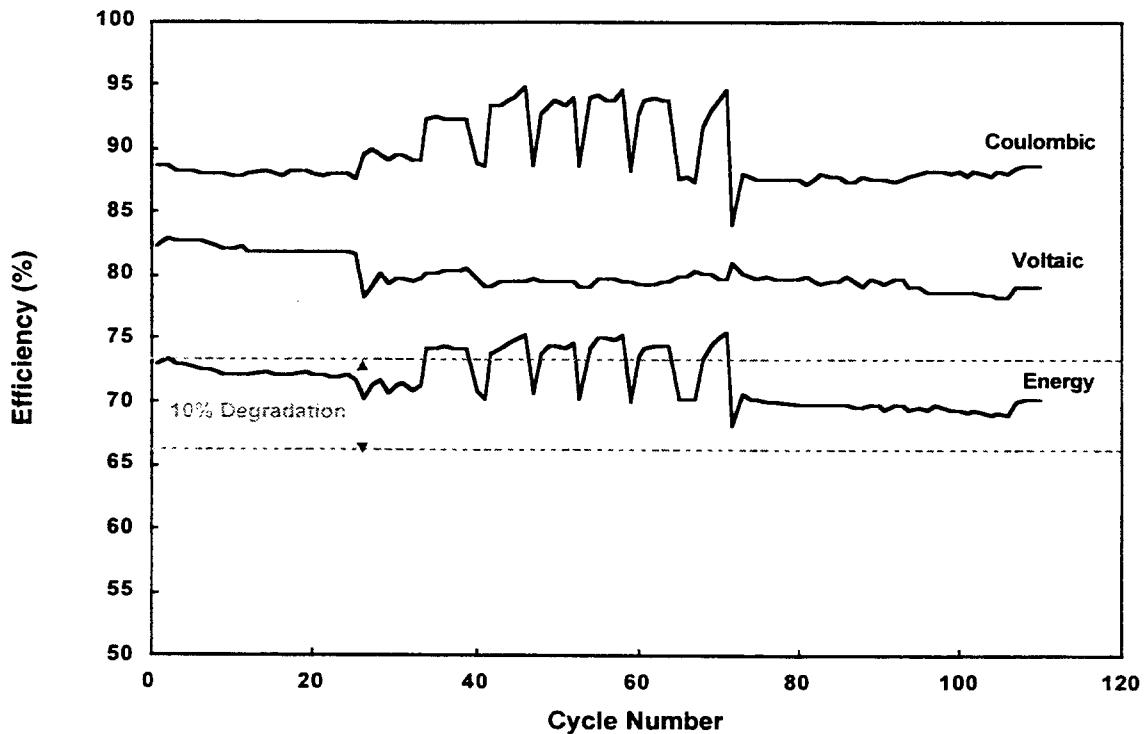


Figure 4-1. Cycle Efficiencies for Battery V1-67 (Includes Baseline and No-strip Cycles).

dendrites were observed, it appeared that some short dendrites might have formed when the experimental electrolyte was used, leading to localized overheating.

Battery V1-69

Battery V1-69 completed the first 39 cycles with a peak performance of 89.1% coulombic efficiency,

83.2% voltaic efficiency, 74.2% energy efficiency, 5.2% transport inefficiency, and 5.7% residual inefficiency. Because this battery had low energy efficiency compared to batteries built later, it was taken off test after 39 cycles so that other batteries could be tested. The battery was placed back on test after being on the shelf for nine months. The performance declined slightly during this time, but it declined by less than 10% from the peak performance. The battery was cycled for a total of

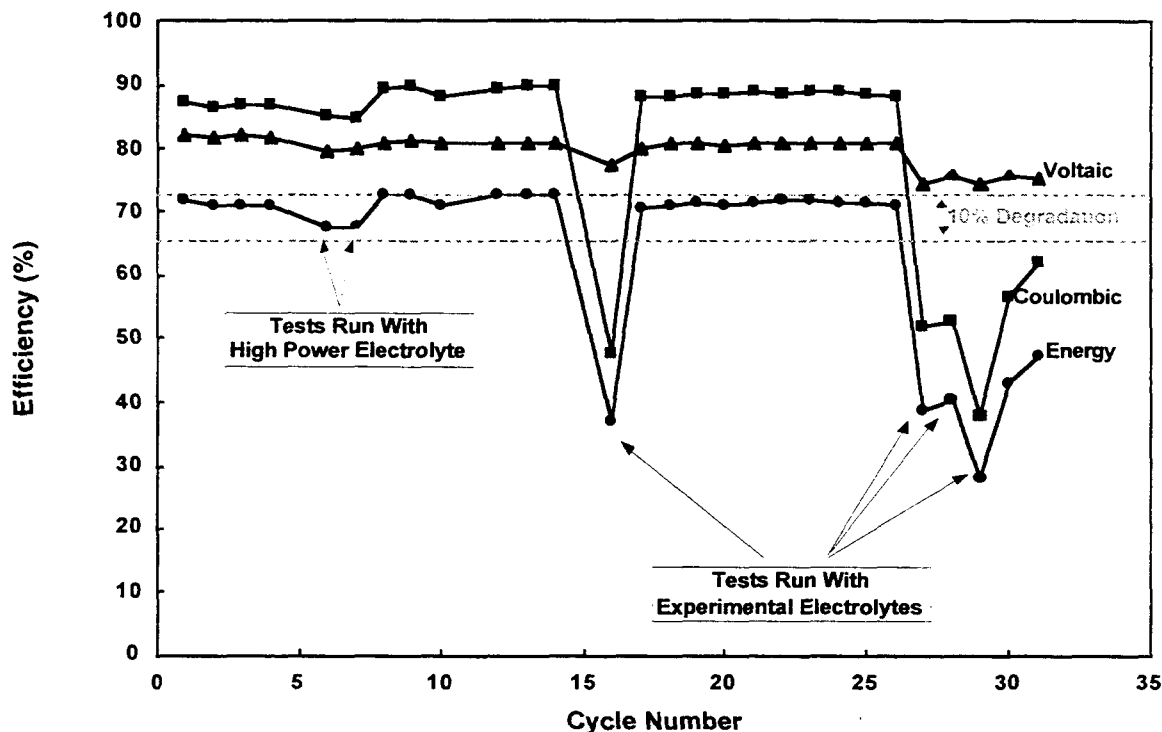


Figure 4-2. Baseline Cycle Efficiencies for Battery V1-68.

52 cycles, with the final cycle giving 88.0% coulombic efficiency, 79.6% voltaic efficiency, and 70.0% energy efficiency. Figure 4-3 is a cycle efficiency plot for Battery V1-69.

Battery V1-70

This battery was not tested because of a leak at the right anode stud (right stud if facing the anode side) that was observed during water testing.

Battery V1-71

The energy efficiency for Battery V1-71 decreased by more than 10% from the peak after 195 cycles, as seen in Figure 4-4. At this point the performance had declined to 83.5% coulombic efficiency, 74.4% voltaic efficiency, and 62.1% energy efficiency, with 6.6% transport inefficiency and 10.0% residual inefficiency. The peak performance for this battery stack was obtained on the first baseline cycle. It achieved 89.6% coulombic efficiency, 82.2% voltaic efficiency, and 73.6% energy efficiency with 5.3% transport inefficiency and 5.1% residual inefficiency.

After the battery's performance had declined by more than 10% from the peak, the stack was used to investigate a modified utility-type cycling regime. The modified cycles consisted of a charge for 4.5 hours at 20 mA/cm² followed by a repetitive sequence of 60-minute discharges at 21 mA/cm² and 65-minute charges at 20 mA/cm². The charge steps were longer than the discharge steps to compensate for transport losses and the difference between charge and discharge rates. It was also important that the battery was always at 100% state of charge at the start of each short cycle. The short charge/discharge steps continued until the voltage on discharge fell below 1.0 V/cell.

The final trial completed under the short charge/discharge cycle regime terminated at 78 cycles. Previous runs of this test reached 52, 56, and 69 cycles. During the last test, Battery V1-71 developed a slow but steady leak and was therefore removed from test. A total of 551 cycles (including both baseline and short cycles) were completed. When the battery was torn down, it was found to have a leak between vibration welds on the bottom surface of the battery stack.

4. BATTERY TESTING
8-cell, 1170-cm², 1-kWh Battery Testing

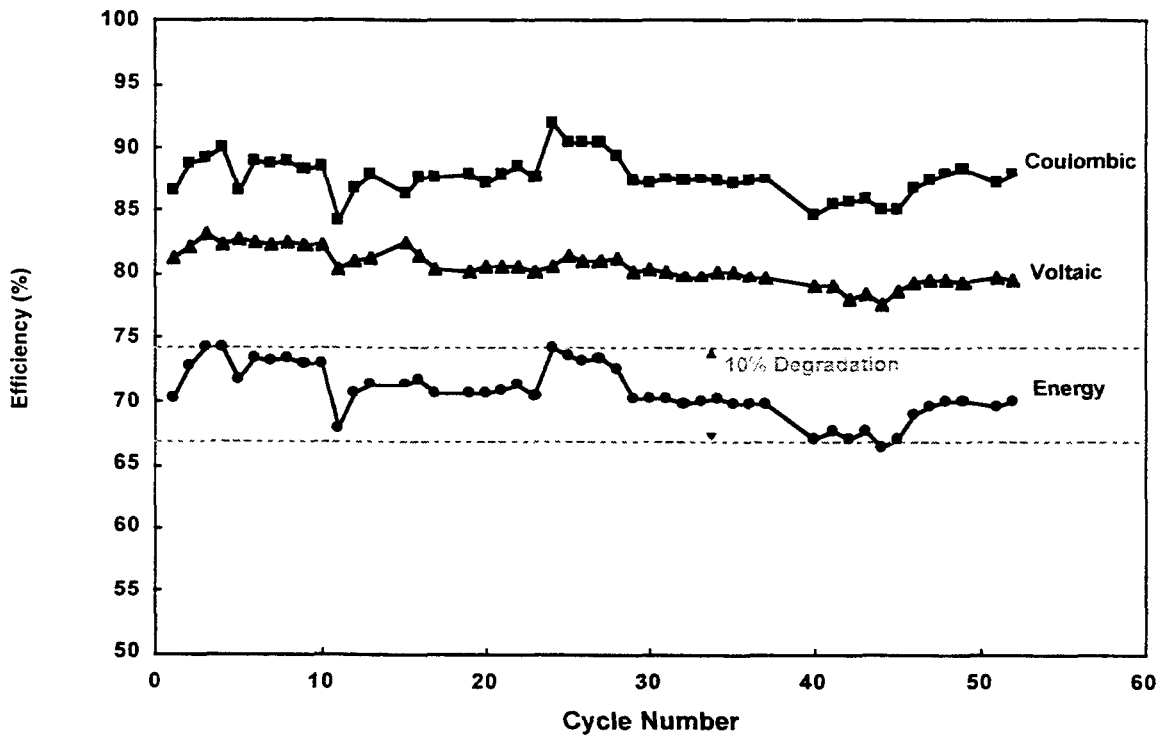


Figure 4-3. Baseline Cycle Efficiencies for Battery V1-69.

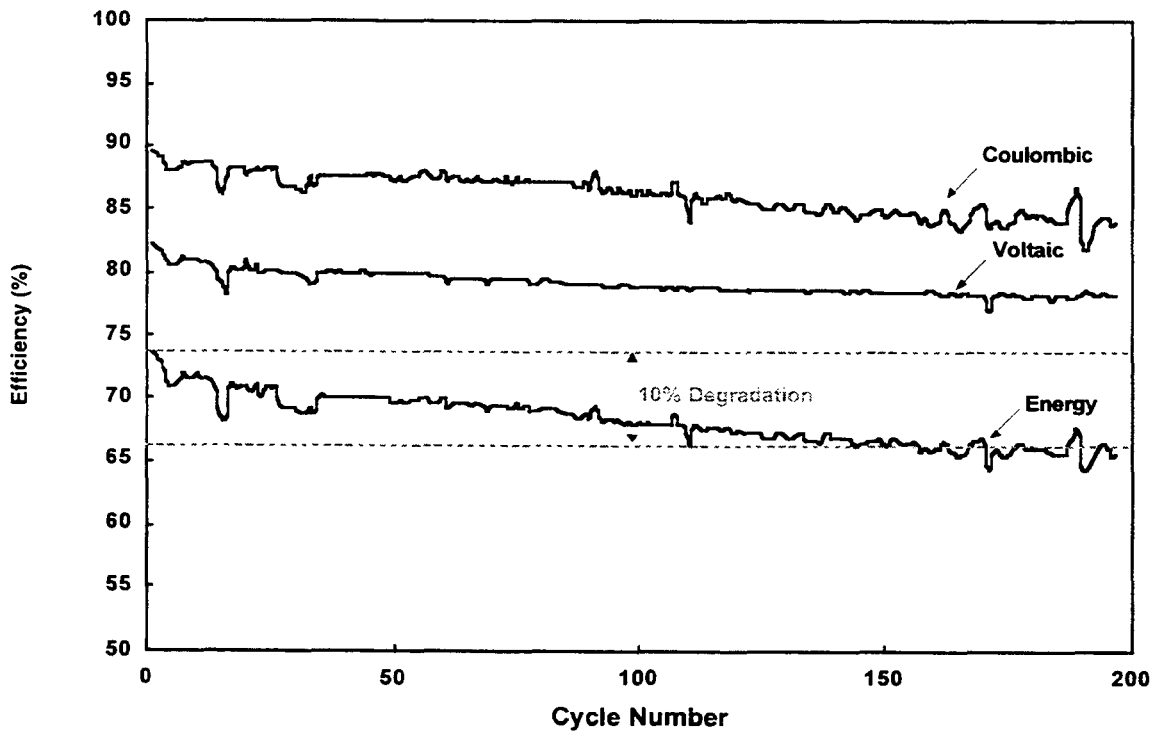


Figure 4-4. Baseline Cycle Efficiencies for Battery V1-71.

Battery V1-72

Battery V1-72 leaked during water testing. The leak was from the seam of the endblock cover near the catholyte inlet port. This problem had also been observed on several earlier battery stacks. The leak was attributed to porosity in the endblock material caused by high concentrations of blowing agent. The leak was repaired, and cycling of the battery was initiated.

After Cycle 8, the battery had to be put on a new test station because one of the pump heads had cracked. This did not affect battery performance.

During Cycle 458, a circuit that ran the pumps for the battery failed. The cycling unit continued to charge and discharge the battery without the pumps running. At this point in the cycle life, the battery performance started to decline fairly rapidly. It is not known whether the outage, and the subsequent pump failure, contributed to the decline. The pumps were out only during one cycle, but the outage happened during charge, and the upper voltage limit of the battery was reached during this cycle.

By Cycle 460, the performance of this battery had declined by more than 10% from the peak energy effi-

ciency of 75%. The efficiencies at that time were 84.4% coulombic, 79.7% voltaic, and 67.3% energy, with 7.3% transport and 8.2% residual inefficiencies. At this point, an electrode reconditioning process was run. The reconditioning significantly improved efficiencies on the subsequent cycles, as seen in Figure 4-5. The decline in performance of the battery can be associated with a corresponding increase in overvoltage, represented by the filled circles in the figure. The overvoltage is a measure of the battery's inability to perform the desired reactions. Figure 4-5 shows that following the reconditioning cycle, the overvoltage decreased, causing the performance of the battery to improve.

A split between vibration welds on the end of the battery stack occurred during Cycle 472. A C-clamp was placed on the battery stack to hold the weld together so that the battery could continue cycling. Battery V1-72 continued cycling for a total of 504 cycles. The efficiencies at the end of testing were 88.4% coulombic, 79.1% voltaic, and 70.0% energy, with 5.5% transport and 6.1% residual inefficiencies.

After Cycle 504, the second-phase solenoid valve became inoperable during a series of six consecutive baseline cycles. Because the valve remained closed, only aqueous-phase electrolyte was circulated during

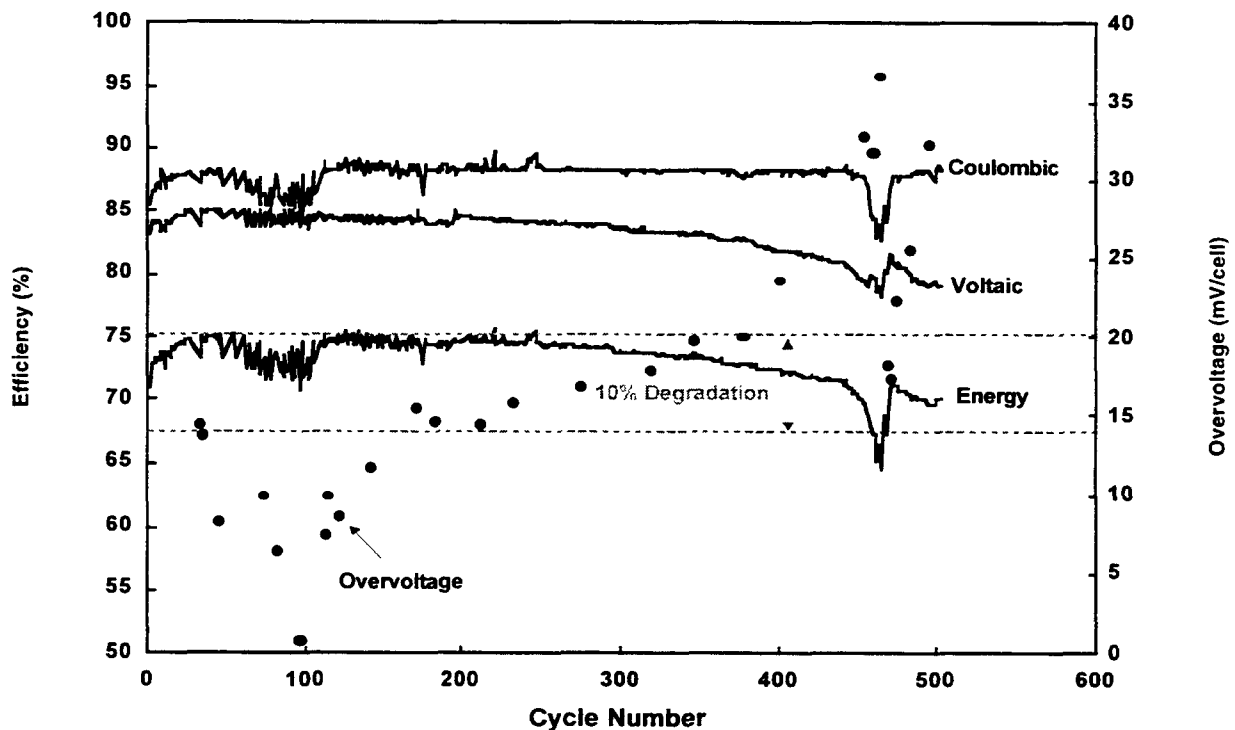


Figure 4-5. Baseline Cycle Efficiencies for Battery V1-72.

4. BATTERY TESTING
 8-cell, 1170-cm², 1-kWh Battery Testing

the discharge portion of the cycle. The battery became severely overcharged because it could be only partially discharged during each of the six cycles. It was taken off test because a small leak developed from the anode terminal stud connection.

Battery V1-73

Battery V1-73 was run primarily under the standard baseline cycling regime. A set of no-strip cycles was started, but it was stopped when it was observed that the solenoid valve that delivers complexed-phase bromine to the battery stack during discharge never opened. The valve failure was observed at Cycle 62. Because no complexed-phase bromine was fed to the battery, it did not completely discharge on the first cycle of the set of no-strip cycles, which caused the battery to be significantly overcharged (about 60%) on the subsequent cycle. The performance did not decline on the following baseline cycle, so the overcharge did not appear to damage the battery in the short term, but it may have caused some permanent damage that lowered the life of the battery.

The energy efficiency of this battery had dropped 10% from the peak value by 146 cycles, as seen in Figure 4-6. Testing for crossflow in the cell stack indicated

no internal leakage. However, the overvoltage had increased starting at about Cycle 110, which corresponded to a decline in the voltaic efficiency. The battery teardown showed moderately rough zinc plating and some indication that dendrite activity had occurred.

Another potential cause for the battery failure is that the electrolyte was slightly contaminated with nickel. The contamination may have come from cracked pump impellers, which were discovered after cycling was completed.

Battery V1-74

Battery V1-74 was manufactured using an experimental carbon-plastic electrode material. The material was more difficult to work with than the standard material and did not significantly lower the resistance of the battery, so it was not used in any other batteries.

The testing regime for Battery V1-74 during the first 230 cycles consisted primarily of consecutive sets of six no-strip cycles. After 240 cycles, the energy efficiency had declined by 10% from the peak values (see Figure 4-7). This battery was torn down at a full state of charge after completing a total of 264 cycles. The terminal anodes generally had uniform plating, but there were

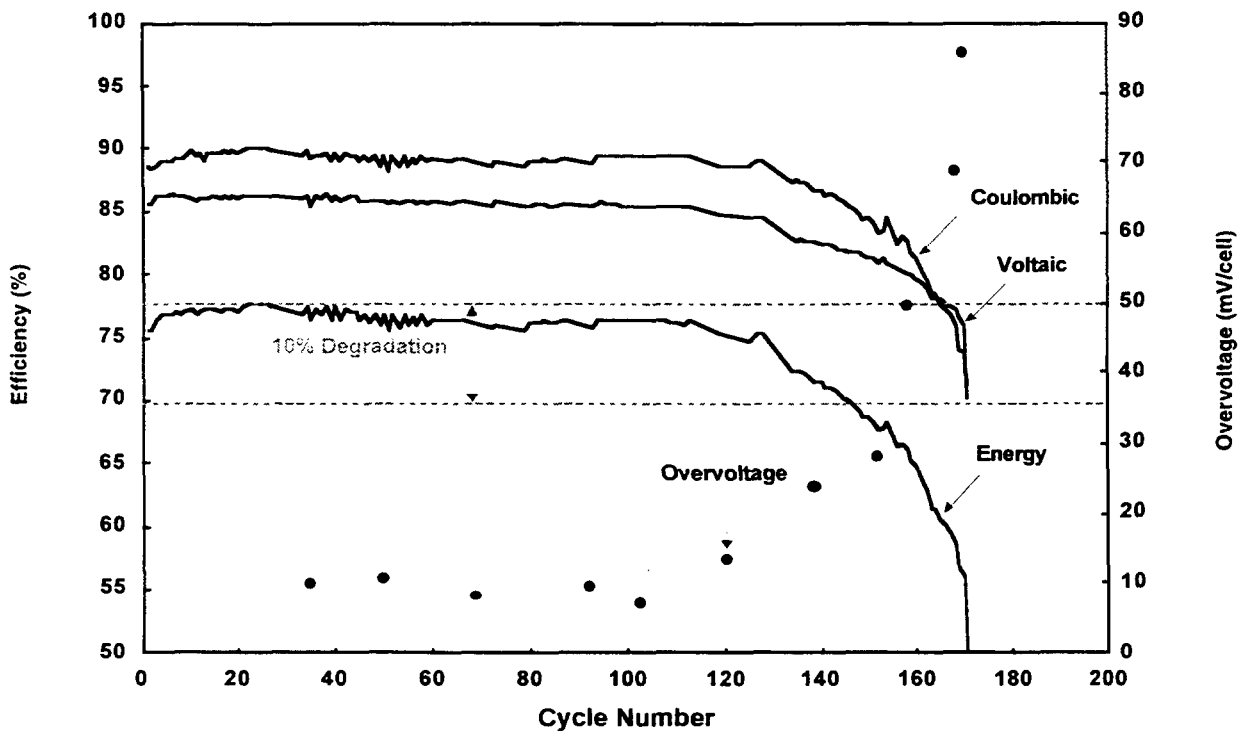


Figure 4-6. Baseline Cycle Efficiencies for Battery V1-73.

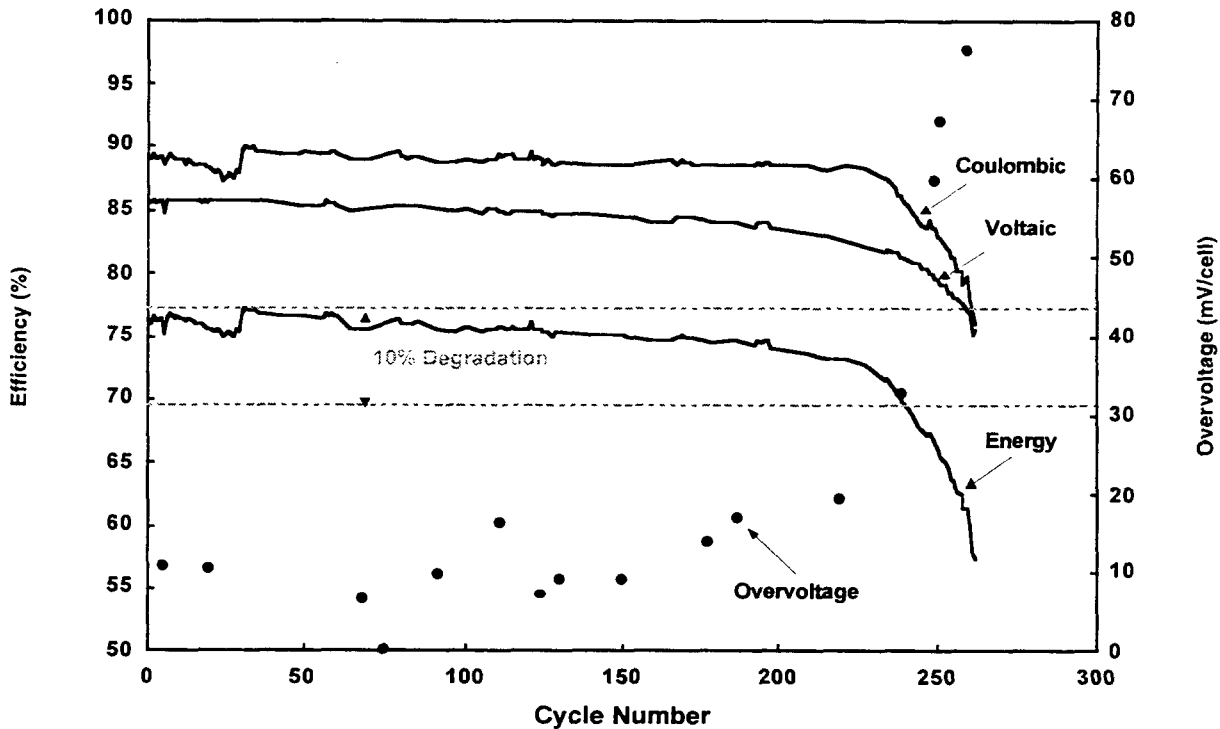


Figure 4-7. Baseline Cycle Efficiencies for Battery V1-74.

a few rough areas. On the right anode terminal a small section of dendritic plating had grown into the adjacent separator. Moderate to severe blistering on the cathode side was present on a number of the separators, apparently caused by previous zinc penetration on the anode side. On the right side of the stack, the sixth and seventh bipolar electrodes were severely warped, which caused rough plating that had grown into the adjacent separators. Similar warpage and zinc plating were observed on the seventh left bipolar electrode. Other than several isolated areas, the zinc plating was uniform and fairly smooth. The warpage of the remaining bipolar electrodes was typical.

Battery V1-75

Battery V1-75 was manufactured with bipolar electrodes in which the cathode activation layer was applied during the carbon-plastic extrusion process. The activation layer was applied to the terminal electrodes in the same way as had been done with the previous battery stacks.

A sudden decline in performance was observed at Cycle 16, as seen in Figure 4-8. By the last cycle (Cycle 24), the coulombic efficiency had fallen to 78.7%

and the energy efficiency to 65.9%, and some red bromine complex was observed in the anolyte reservoir. The battery was torn down at a full state of charge, and a bad cell was found. Six of the eight cells appeared to have normal zinc plating, separator integrity, and electrode warpage. In Cell 3, a 2-inch region of the separator was found to be heavily dendrited, and the adjacent anode in Cell 4 was bare of zinc at the same location. A specific cause for the problem was not found, but an internal leak near the center of the stack, possibly the result of a center-weld failure, was suspected.

Battery V1-76

The performance of Battery V1-76 declined by more than 10% after 325 cycles and continued to drop rapidly through Cycle 341. The residual inefficiency increased 100% during this decline. See Figure 4-9 for a graph of the cycle performance. Figure 4-9 also shows a dramatic increase in overvoltage, which appears to be the primary reason for the declining efficiencies. This rapid increase in overvoltage also occurred in Battery V1-73, which was found (during postmortem evaluation) to have a severely degraded cathode layer.

4. BATTERY TESTING
8-cell, 1170-cm², 1-kWh Battery Testing

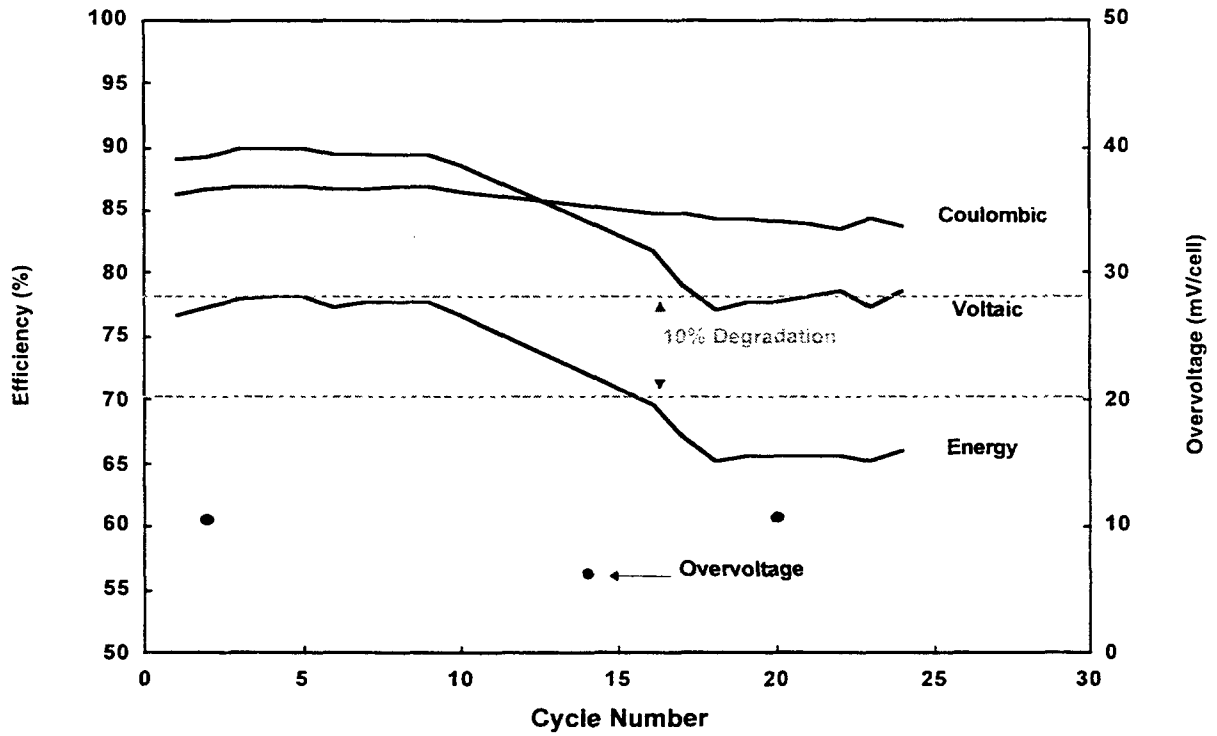


Figure 4-8. Baseline Cycle Efficiencies for Battery V1-75.

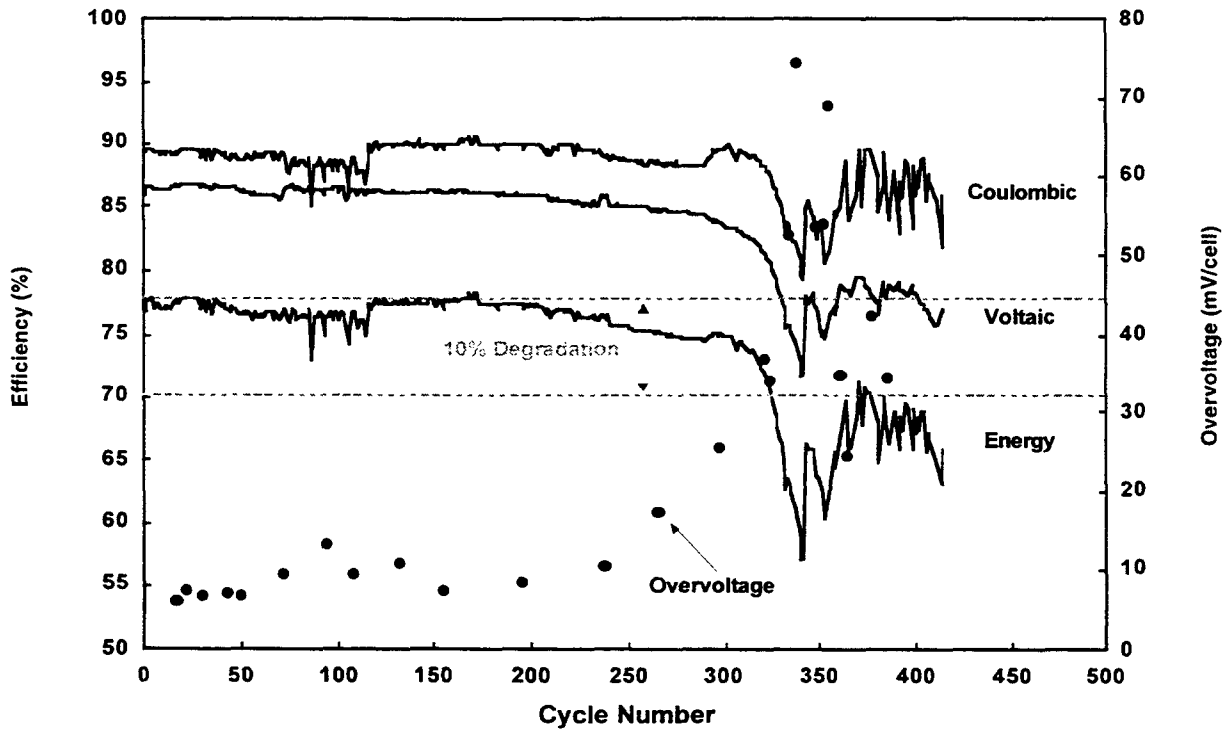


Figure 4-9. Baseline Cycle Efficiencies for Battery V1-76.

The battery was taken off test after completing 414 cycles. Efficiencies were 85.9% coulombic, 76.8% voltaic, and 66.0% energy, with 7.3% transport and 6.7% residual inefficiencies. A number of attempts to recondition the electrodes were made without bringing the performance back into the 10% degradation range. After the battery underwent the reconditioning process, its performance improved dramatically, but the improvement did not last for more than a couple of cycles. It appears that the electrode reconditioning process is more successful if it is done before the performance of the battery has degraded significantly. The battery failed because of high electrochemical overvoltage and an increase in the battery's internal resistance.

Battery V1-77

Battery V1-77 had completed 350 baseline cycles, but the efficiencies were decreasing fairly rapidly, as seen in Figure 4-10. The cycle performance was at 86.4% coulombic efficiency, 81.4% voltaic efficiency, and 70.3% energy efficiency, with 6.2% transport and 7.4% residual inefficiencies when an attempt was made to recondition the electrodes. Following one reconditioning cycle, the efficiencies increased to 90.0% coulombic efficiency, 83.3% voltaic efficiency, and 75.0% energy efficiency, 83.3% voltaic efficiency, and 75.0%

energy efficiency. This was the third battery to realize a significant improvement in performance following the electrode reconditioning process.

The electrode reconditioning process was performed a number of times on this battery. Each time the process was performed, a significant increase in performance was observed after the reconditioning cycle. The increases in efficiencies in Figure 4-10 reveal where the reconditioning process was performed. As indicated by the plot, the electrodes needed to be reconditioned after about 25 baseline cycles.

During the charge portion of Cycle 454, a cooling-water line broke and filled the spill-containment tray, completely submerging the pumps. The pumps became inoperable, and the battery remained partially charged until the stack could be drained and transferred to another test station. This pump failure did not appear to irreversibly damage the battery, but it may have caused the battery performance to deteriorate more rapidly than it would have otherwise.

After 517 cycles, the performance of the battery had declined by more than 10% from the peak energy efficiency of 76.7%. The final cycle gave 84.0% coulombic efficiency, 80.6% voltaic efficiency, and 67.7% energy

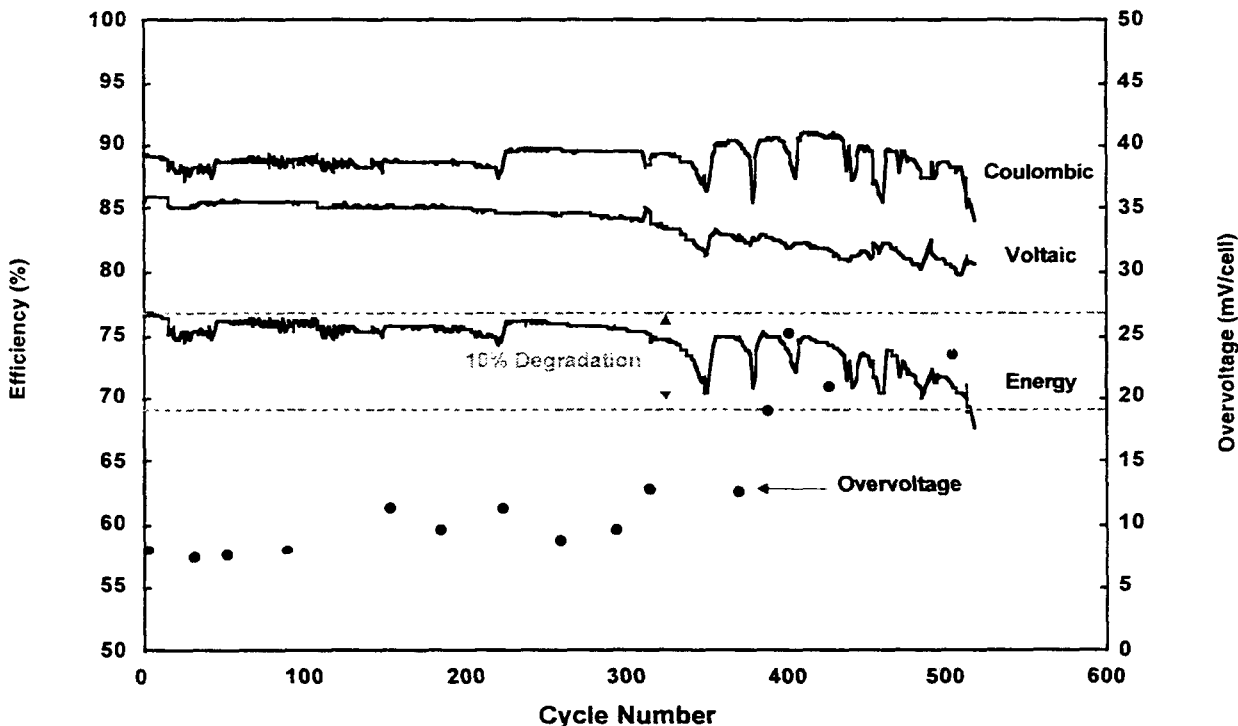


Figure 4-10. Baseline Cycle Efficiencies for Battery V1-77.

4. BATTERY TESTING
8-cell, 1170-cm², 1-kWh Battery Testing

efficiency. This battery failed as a result of high electrochemical overvoltage and an increase in internal resistance.

Battery V1-78

Battery V1-78 was built using a new, more conductive carbon plastic electrode material. Twenty-one baseline cycles were run with very consistent results. The cycle efficiencies averaged 89.6% coulombic, 85.6% voltaic, and 76.7% energy, with 5.4% transport and 5.0% residual inefficiencies. The battery was removed from test after the 21 baseline cycles and was going to be sent to SNL for additional testing. Figure 4-11 is a graph of the cycle efficiencies for this battery.

The battery was never sent to SNL, so it was placed back on test after being on the shelf for more than a year. A lower-cost electrolyte was to have been tested, but the battery gave poor performance. The battery was taken off test after only 4 cycles. When the battery was torn down, cracks on some of the separators were visible near the bottom of the stack. It appears that the separators may have dried out and cracked while the battery was not in operation, which probably caused the poor performance.

Battery V1-79

Battery V1-79 was the first V-design battery stack to complete 1000 baseline cycles with no leaks and less than 10% degradation in performance. The electrode reconditioning process was performed on this battery stack about every 50 cycles, starting at about Cycle 250, which indicates that overall life of the battery can be increased significantly if the reconditioning process is performed fairly regularly. Electrode reconditioning should be part of a standard maintenance schedule.

The battery completed 1036 cycles before the energy efficiency declined to 90% of the peak value (76.0%). Baseline cycling was continued on this battery stack until the performance declined by 20% from the peak. Figure 4-12 shows that a total of 1500 cycles were run on the battery. It achieved only 79.0% coulombic efficiency, 63.1% voltaic efficiency, and 49.8% energy efficiency on the final cycle. The battery was taken off test because the performance had dropped by more than 20% from the peak energy efficiency.

Battery V1-80

Battery V1-80 was prepared using improved manufacturing techniques to obtain low-resistance terminal electrodes and a cathode activation layer with a high

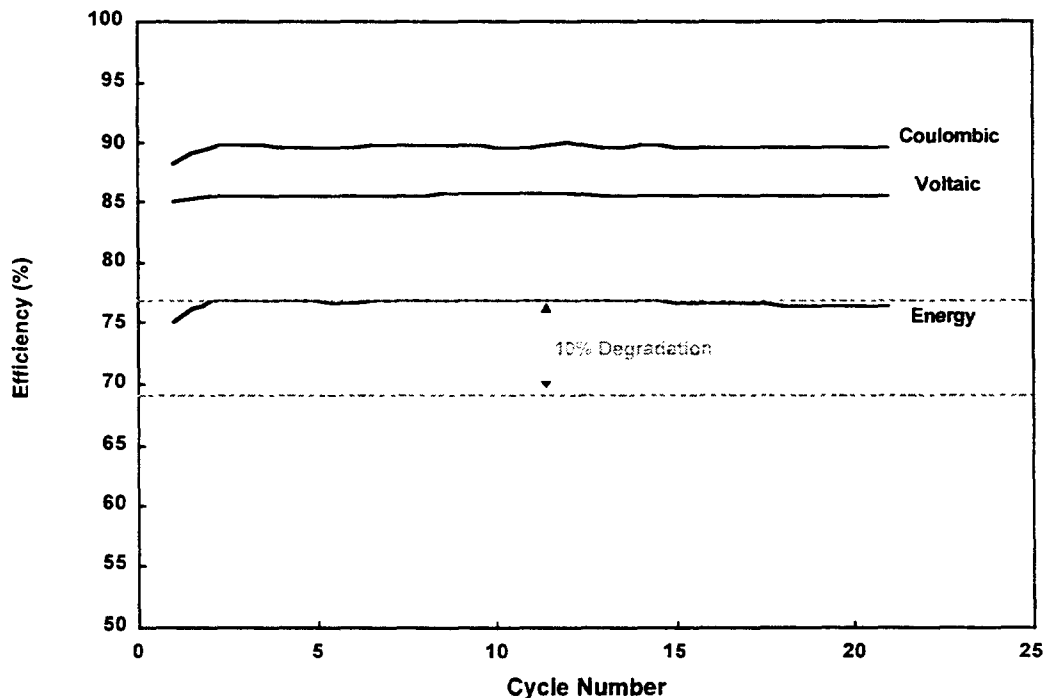


Figure 4-11. Baseline Cycle Efficiencies for Battery V1-78.

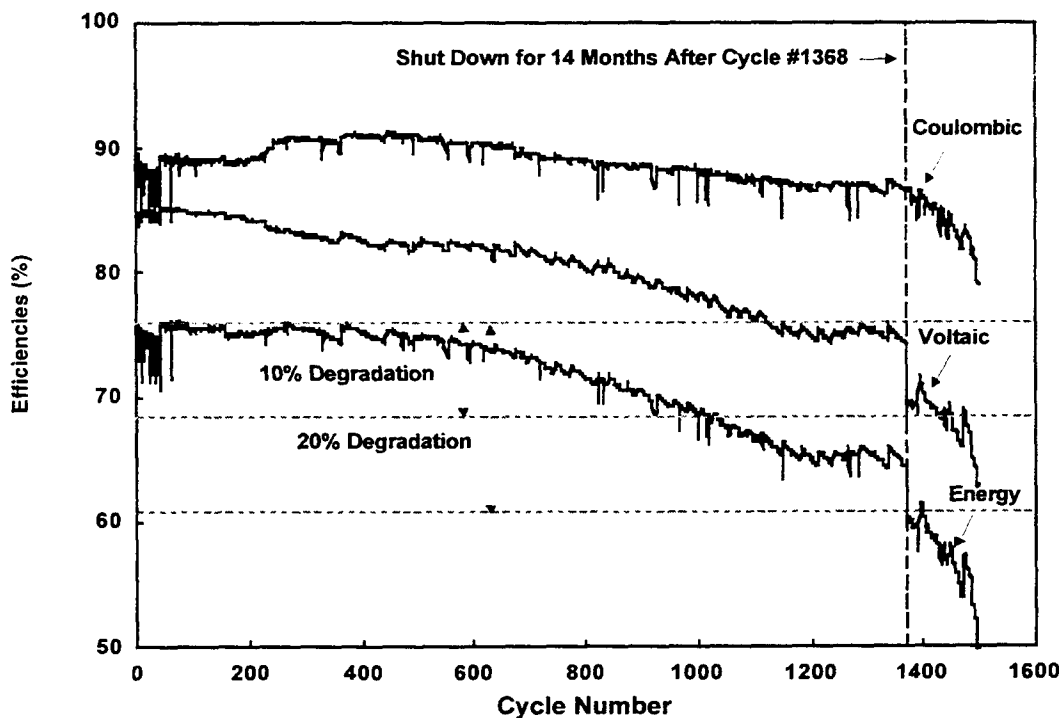


Figure 4-12. Baseline Cycle Efficiencies for Battery V1-79.

electrochemical surface area. The performance over the first 80 cycles was inconsistent because of an insufficient amount of bromine in the electrolyte. Because of the large-surface-area cathode layer, additional bromine needed to be supplied so that the concentration in the electrolyte was sufficient to maintain consistent cycling.

Battery V1-80 completed 985 baseline cycles with the last cycle giving 87.4% coulombic efficiency, 79.8% voltaic efficiency, and 68.9% energy efficiency (see Figure 4-13). After running a series of six consecutive cycles over a weekend, the anolyte reservoir was discovered to be nearly empty on Monday morning. From the data, it appeared that something happened either during the second cycle on Saturday or the first cycle on Sunday. The reservoir was not wet on top, so it did not overflow. The battery was taken off test and was found to have a split on the edge that was toward the back of the hood (the right edge while looking at the cathode). The split in the battery was clamped to prevent leakage; the battery was then rinsed and torn down. This battery was still performing reasonably well when it began leaking. No major problems were observed during the teardown. Failure of this battery was caused by a split between vibration welds, which caused a leak external to the battery stack.

Battery V1-81

Battery V1-81 was assembled to qualify an experimental manufacturing technique. The bipolar electrodes were the same as those used in Battery V1-80, but the terminal electrodes were prepared using the original manufacturing technique, which gives higher resistance. The battery had completed 334 cycles with very little decline in efficiencies, but the following cycle showed a rapid decline in coulombic efficiency, as seen in Figure 4-14. The battery completed a total of 343 cycles with the final cycle giving 79.9% coulombic, 82.0% voltaic, and 65.6% energy efficiencies, with 11.1% transport and 9.0% residual inefficiencies. Teardown of this battery stack showed rough plating on the anode terminal electrode, but no sign of any internal weld failures. The poor plating indicates probable poor electrolyte flow distribution in the anode terminal electrode. Evidence from later batteries indicates that this may have resulted from a center weld failure causing a small tear in the separator.

4. BATTERY TESTING
 8-cell, 1170-cm², 1-kWh Battery Testing

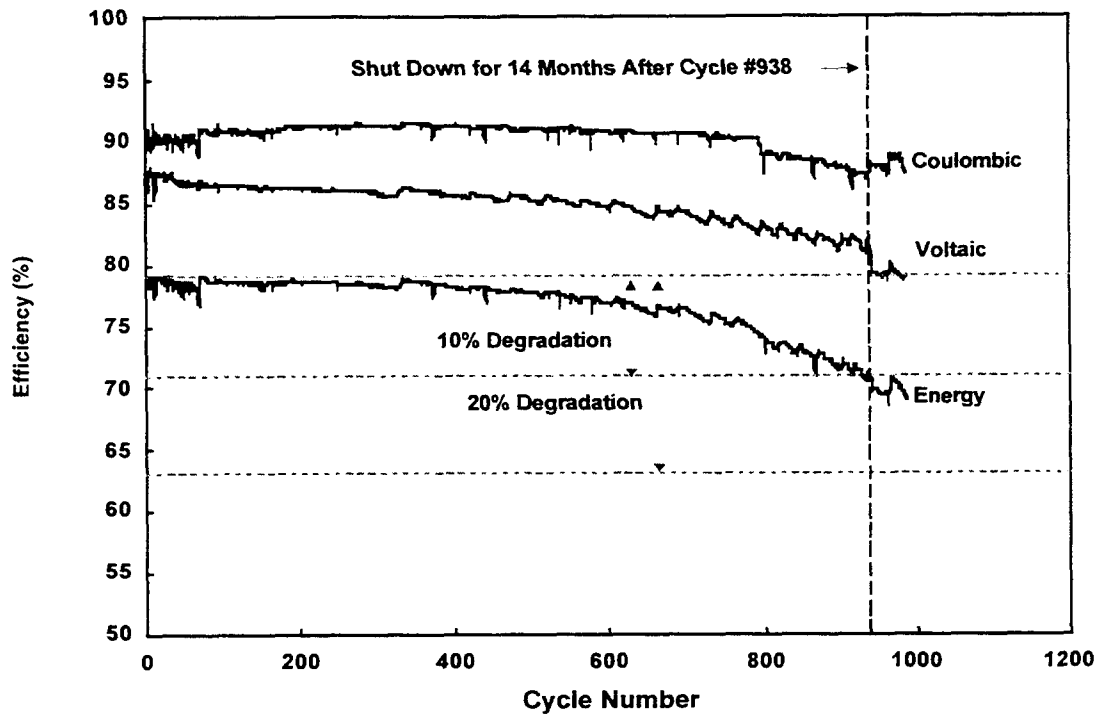


Figure 4-13. Baseline Cycle Efficiencies for Battery V1-80.

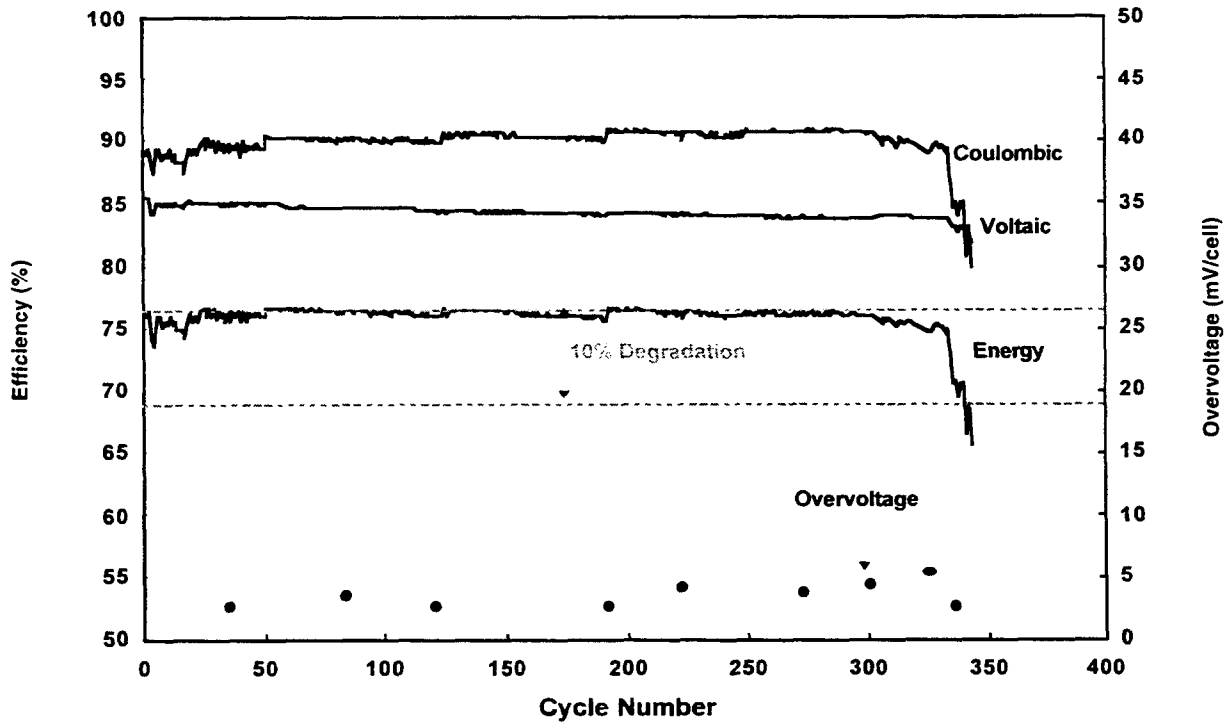


Figure 4-14. Baseline Cycle Efficiencies for Battery V1-81.

Battery V1-83

Battery V1-83 was manufactured to verify the performance of an experimental battery separator material. The separator used in this battery stack was higher in resistance and bromine transport than the standard material. The energy efficiency was about 5% lower than for Battery V1-80, which corresponds closely to a computer simulation based on the properties of the separator. The battery completed 77 baseline cycles, with the most recent cycle giving 84.7% coulombic efficiency, 83.0% voltaic efficiency, and 70.3% energy efficiency. Figure 4-15 shows the baseline cycle performance for the battery. Because of the relatively poor performance, this battery was removed from test to make room for other batteries.

Battery V1-84

Battery V1-84 was manufactured with an experimental separator that had previously demonstrated good properties in beaker-scale separator testing. The battery completed 25 cycles with somewhat inconsistent results, as seen in Figure 4-16. The battery achieved 77.7% energy efficiency, but the bromine transport appeared to be sensitive to the rate of complexed-phase bromine circulated during discharge. Efficiencies varied from 77.7% to 71.6% depending on the amount of bromine

circulated. Batteries manufactured with the standard separator were not as sensitive to bromine flow rate. The variations were probably caused by a high rate of crossflow from one side of the cell to the other. The separator material used in this stack was warped and difficult to weld into the flow frames because it was hand-extracted.

The battery exhibited very low coulombic efficiency on Cycle 17, but this was caused by an insufficient amount of complexed-phase bromine circulated during discharge. The valve was set at the same position as during the previous seven cycles, but the complexed-phase bromine flow was cut off during Cycle 17. The last cycle achieved 82.3% coulombic efficiency, 86.6% voltaic efficiency, and 71.3% energy efficiency. The voltaic efficiency for this battery stack was very good, but the coulombic efficiency was inconsistent. The stack was taken off test to make room for later battery builds.

Battery V1-85

Battery V1-85 was manufactured with another experimental separator that also demonstrated good properties in beaker-scale separator testing. This separator material had a different internal structure than the material used in Battery V1-84, and the oil extraction

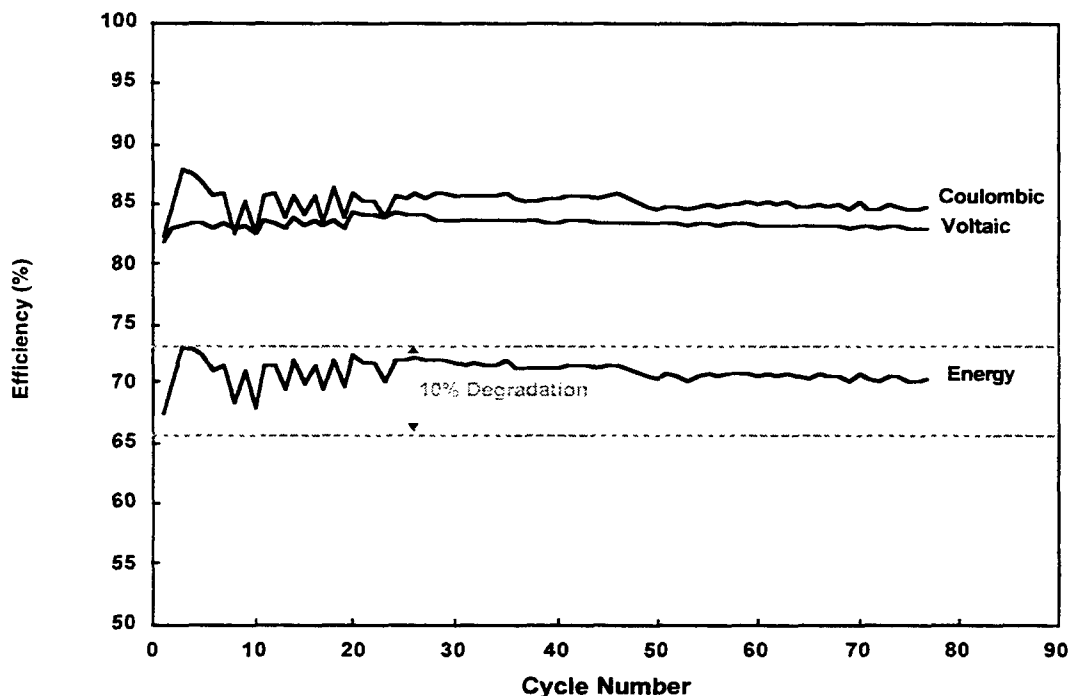


Figure 4-15. Baseline Cycle Efficiencies for Battery V1-83.

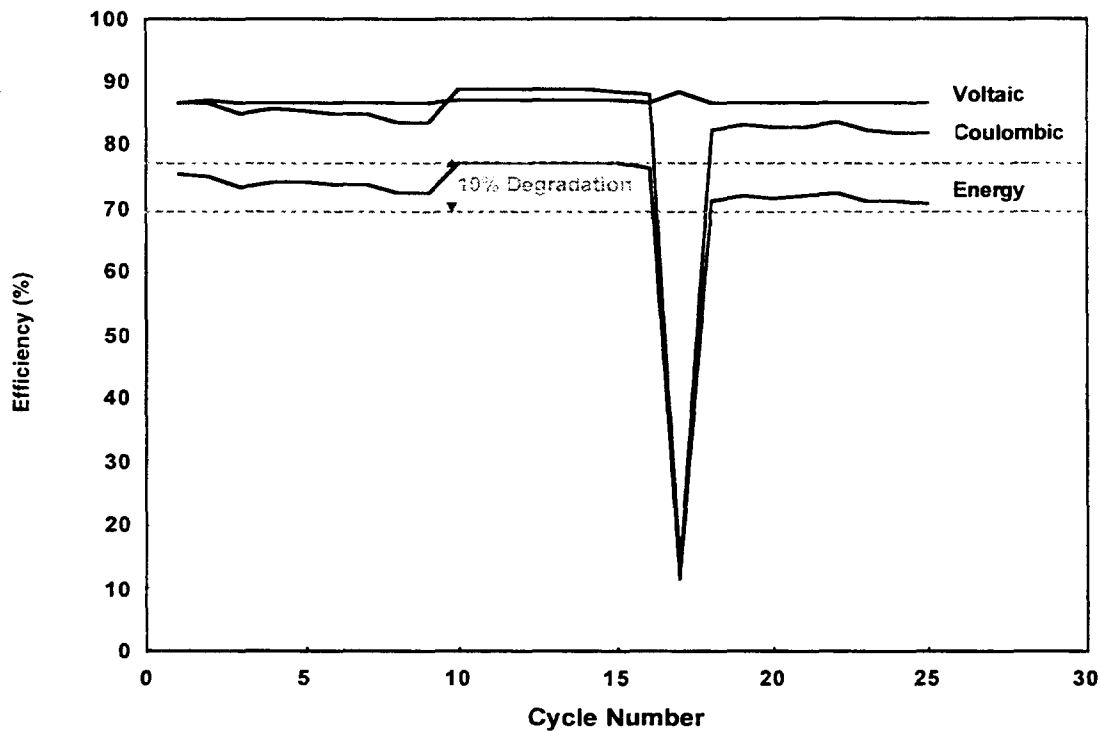


Figure 4-16. Baseline Cycle Efficiencies for Battery V1-84.

was performed on production-scale equipment. The separator was flat and relatively easy to weld into the flow frames.

This battery completed 20 cycles with inconsistent results, as seen in Figure 4-17. The last cycle gave 86.0% coulombic efficiency, 86.3% voltaic efficiency, and 74.2% energy efficiency. The inconsistent performance of this stack was caused by the lack of flow of complexed-phase bromine during discharge. The complexed-phase bromine valve became plugged on a number of occasions, causing incomplete discharge of the battery. It is probable that the solenoid valve, which was used for testing other battery stacks, was corroded and incapable of opening completely.

Battery V1-86

Battery V1-86 was manufactured using the same separator as that used in Battery V1-85, but a post-treatment was used on the separator after the manufacturing process. The battery completed 34 cycles, with the last cycle achieving 89.5% coulombic efficiency, 87.5% voltaic efficiency, and 78.3% energy efficiency with 6.3% transport and 4.2% residual inefficiencies, as seen in Figure 4-18. This battery achieved a peak energy effi-

ciency of 80.2% on baseline cycling and 81.2% on cycles without stripping. This is the highest efficiency obtained for a battery stack with this design.

8-cell, 2500-cm², 2-kWh Battery Stacks

The 2500-cm² series battery stacks were developed as the building block for large utility battery systems. For utility applications, the active area of the battery stack was increased from 1170 cm² to 2500 cm² to reduce the part count and to lower the manufacturing cost of the battery system. The channels and diverters of the 2500-cm² flow frame were designed to minimize shunt currents and to improve the flow of electrolyte across the face of the electrodes. The new design used a patented glass-filled plastic endblock to maintain dimensional stability, which eliminated the need for metal inserts and improved the recyclability of the battery stack.

Initially, 8-cell battery stacks were manufactured to demonstrate the design of the larger flow frames and manufacturability of the stacks. A number of flow-frame and endblock design iterations were completed

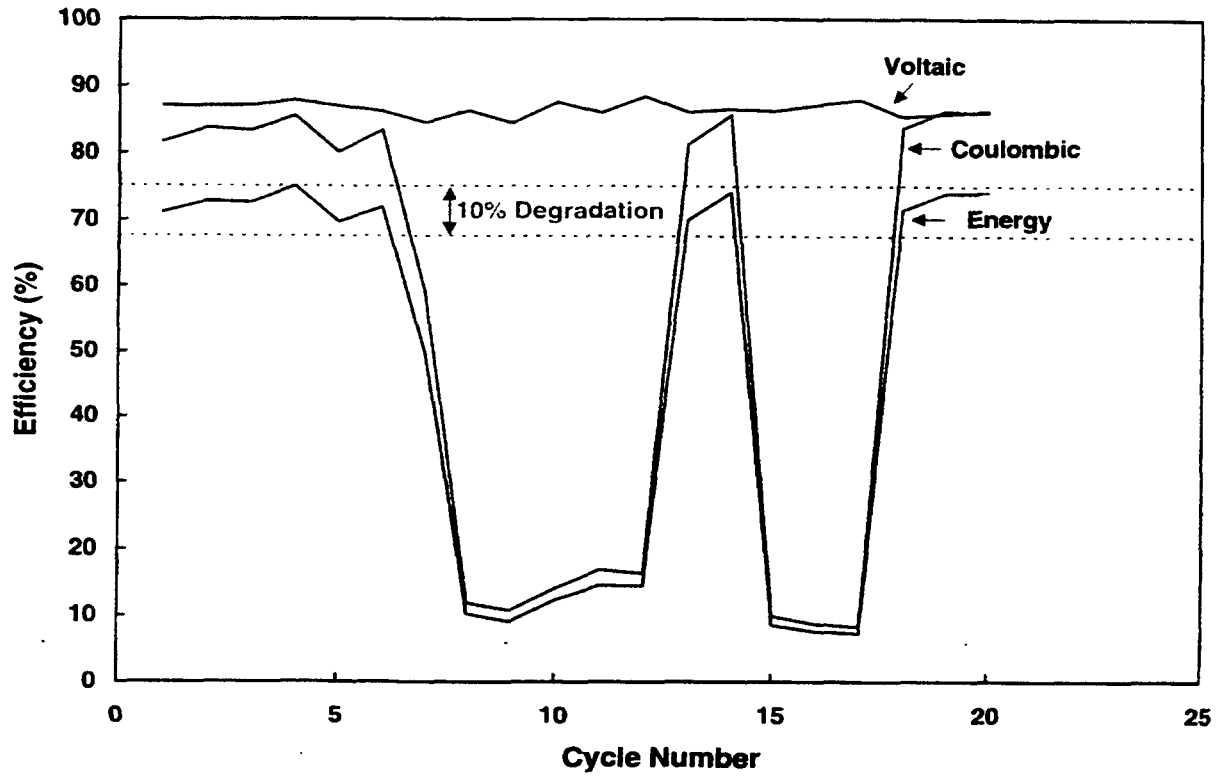


Figure 4-17. Baseline Cycle Efficiencies for Battery V1-85.

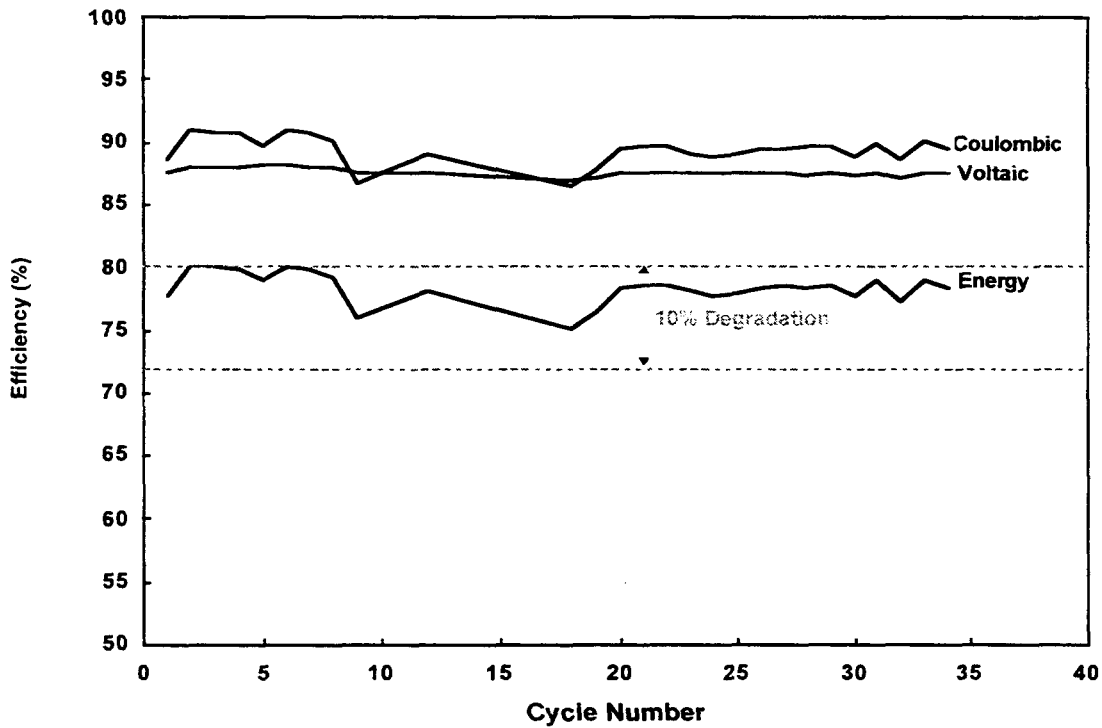


Figure 4-18. Baseline Cycle Efficiencies for Battery V1-86.

4. BATTERY TESTING

8-cell, 2500-cm², 2-kWh Battery Stacks

over a seven-month period. Once adequate performance was achieved from 8-cell stacks, production of 60-cell stacks began.

Several problems were discovered after the post-mortem analysis of the first 2500-cm² batteries. Complexed-phase bromine was not being evenly distributed over the face of the electrodes; the complexed-phase bromine had a tendency to transfer into the anolyte side of the cell, and some external leakage was observed. One problem was that some of the diverters and flow channels were not forming a complete weld with the adjacent frame. Additional seals were added to the diverters and vanes, and the heights of existing seals were increased to improve the distribution of second-phase. The leakage problem was minimized by reduc-

ing sink marks during the injection molding process. The quality of the welds in areas where weld beads cross a flow channel on the adjacent frame was improved by adding additional weld beads in this area.

Scaling up from 8-cell stacks to 60-cell stacks revealed that the endblock tended to slip while in the vibration welding machine. The endblock tooling for the welder was modified to minimize the slippage. Minor problems with the vibration welder also surfaced during development, but modifications were made to eliminate the errors and to improve the consistency of the process.

Table 4-4 gives an overview of the testing and modes of failure for 8-cell, 2500-cm² battery stacks tested during this program. Batteries with battery num-

Table 4-4. Overview of 8-cell, 2500-cm² Battery Testing

Battery Number	Number of Cycles	Peak Coulombic Efficiency (%)	Peak Voltaic Efficiency (%)	Peak Energy Efficiency (%)	Additional Information/ Failure Mode
V25-01-08	10	79.5	81.7	64.9	Baseline cycling. Failure caused by external leak. Poor distribution of second-phase.
V25-02-08	9	88.3	86.2	76.1	Baseline cycling. Small external leaks. Some incomplete welds on inside.
V25-04-08	20	87.7	85.0	74.6	Baseline cycling. Tested on SNL deliverable station.
V25-05-08	12	87.8	86.4	75.8	Baseline cycling. Center weld failure.
V25-06-08	30	90.0	85.7	77.1	Baseline cycling. Cracked reservoir caused electrolyte to leak out while cycling. Appeared to cause battery to fail.
V25-07-08	14	90.1	85.8	77.4	Baseline and no-strip cycling. Center weld failure.
V25-10-08	24	89.5	86.3	77.3	Baseline cycling. Used as SNL 2-kWh deliverable battery.
V25-12-08	7	88.1	80.3	70.7	Baseline cycling. Failure caused by restricted flow in first flow cell.
V25-13-08	23	90.6	86.5	78.3	Baseline cycling. Tested experimental complexing agent. Failure caused by bromine stain, indicating internal weld failed.
V25-27-08	10	85.7	89.5	76.7	Baseline cycling. Incomplete weld caused external leak.
V25-30-08	16	86.3	89.1	76.8	Baseline cycling. Used for burst test.
V25-32-08	19	79.7	87.9	70.0	Baseline cycling. Used for burst test.
V25-33-08	127	82.2	86.5	71.1	Baseline cycling. Used for qualification of experimental cathode layer.
V25-37-08	9	75.0	86.3	64.8	Baseline cycling. Tested at SNL. Center weld failure.

bers not listed sequentially in the table were either not tested or were 60-cell battery stacks, which are listed in Table 4-5 under "60-cell, 2500-cm² Battery Stack Qualification." Test results for individual 8-cell battery stacks are described in more detail below.

Battery V25-01-08

Battery V25-01-08 was cycled 10 times and demonstrated inconsistent performance, as seen in Figure 4-19. The energy efficiencies for this battery ranged from 10.7% to 64.9%. Some of the charge cycles had voltages below the open-circuit voltage of the battery, indicating a probable internal short.

Two leaks were observed in the battery stack. One was on the top near the center of the stack. The other was at the bottom left side near the anode terminal electrode. The reason for the leaks appeared to be sink marks that were later eliminated during the injection-molding process.

The zinc plating was very smooth; therefore, the poor performance of this battery indicated poor flow of the catholyte second-phase across the face of the electrodes. Cross sections of the flow channels showed that some of the vanes were not completely welded. This would cause an uneven distribution of the catholyte

across the electrode surface. The flow frames were modified to eliminate this problem.

Battery V25-02-08

Battery V25-02-08 declined by more than 10% in energy efficiency after only seven cycles, as seen in Figure 4-20. Initially the battery performed at 76.1% energy efficiency, but the efficiencies after nine cycles were 74.2% coulombic, 84.6% voltaic, and 62.8% energy. Small leaks were observed from both the bottom and the top of the stack. The leaks appeared to be coming from between the first frame and the endblock. Also, by the end of cycling, a small amount of complexed-phase bromine was observed in the anolyte reservoir, indicating a probable internal weld failure.

The battery was torn down at 80% depth of discharge. The terminal anode on the left side of the stack had very little zinc, indicating that complexed bromine was getting into this cell. The flow channels, especially near the manifolds, showed some incomplete welds. These appeared to be in regions of the flow frame where the plastic was thin. The welding process deforms these areas slightly, causing incomplete contact of the weld beads. A solution to this problem was identified, and new flow frames and endblocks were produced.

Table 4-5. Performance of 60-cell, 2500-cm² Stacks

Battery Number	Number of Cycles	Peak Energy Efficiency	Average Energy Efficiency
V25-08-60	Never Cycled		
V25-09-60	4	73.0%	70.0%
V25-11-60	10	77.0%	76.2%
V25-14-60	7	72.0%	71.3%
V25-15-60	12	78.1%	73.8%
V25-16-60	5	76.8%	75.7%
V25-19-60	6	75.2%	73.0%
V25-20-60	4	76.4%	75.3%
V25-21-60	7	74.1%	73.2%
V25-22-60	6	75.4%	73.1%
V25-23-60	11	75.4%	73.1%
V25-24-60	9	73.0%	71.6%
V25-25-60	5	75.5%	74.0%
V25-34-60	Never Cycled		

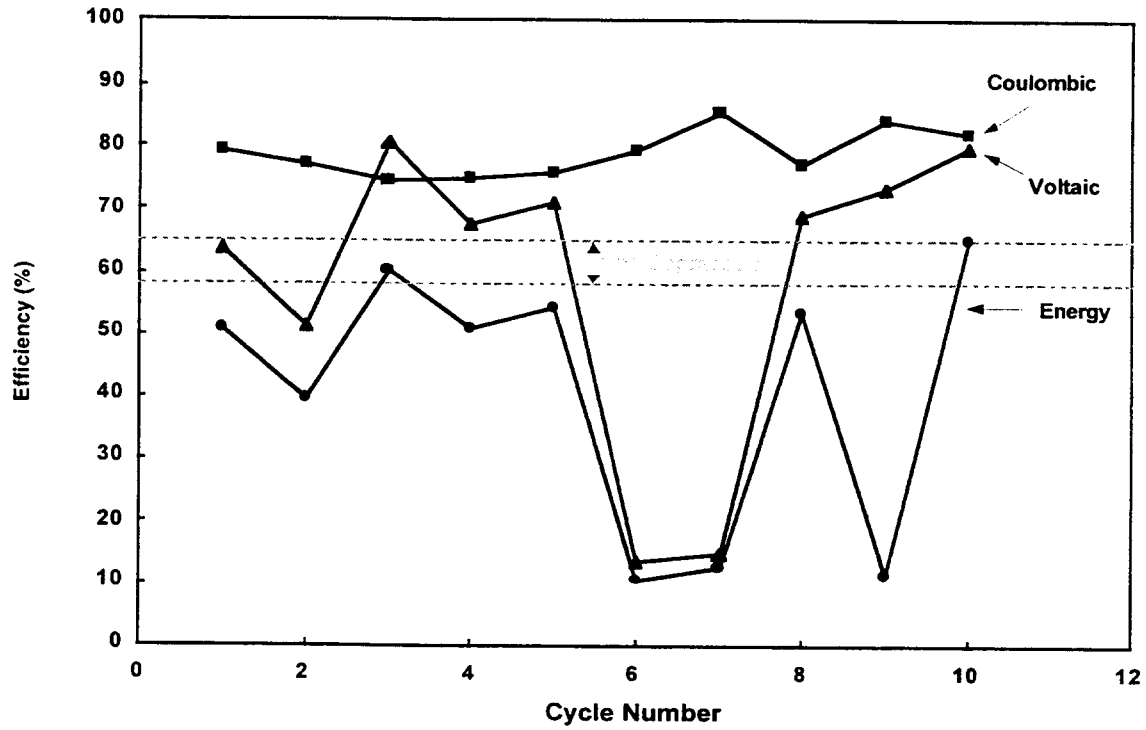


Figure 4-19. Baseline Cycle Efficiencies for Battery V25-01-08.

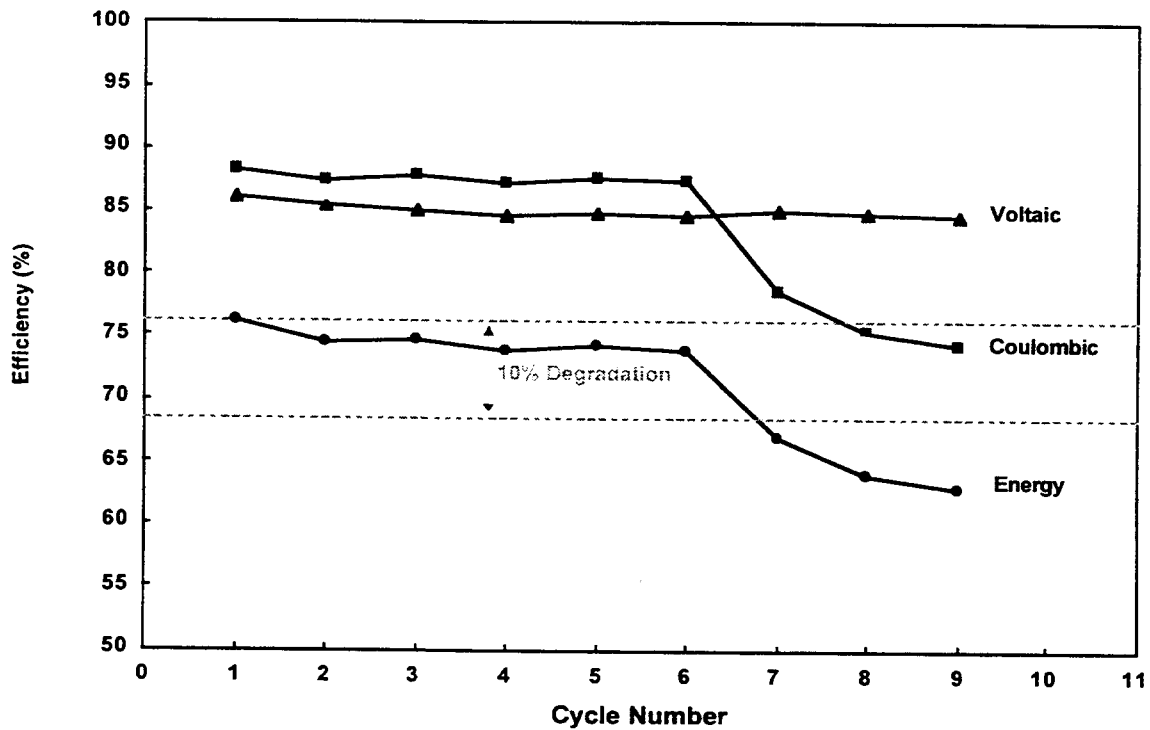


Figure 4-20. Baseline Cycle Efficiencies for Battery V25-02-08.

Battery V25-03-08

Battery V25-03-08 had some external leaks when the battery was water-tested. Because of this, it was never cycled with electrolyte.

Battery V25-04-08

Battery V25-04-08 gave consistent performance with about 74.5% energy efficiency over the first 10 cycles, as seen in Figure 4-21. It was then placed on a 2-kWh control station to demonstrate the controller and station design. The performance of the stack on this station was fairly good, about 89.5% coulombic efficiency, but the voltaic efficiency was low, about 82-83%, which was attributed to a problem with the cycling unit. This battery was tested on the station until 20 cycles were completed. The control station is described in more detail in Chapter 7 under "2-kWh Control Station."

Battery V25-05-08

Figure 4-22 illustrates that battery V25-05-08 had consistent performance until the coulombic efficiency dropped dramatically during Cycle 11. Teardown of this battery showed a failure of the center weld between the

endblock and the first flow frame. The failure was attributed to warpage of the endblock, which caused a weak weld at the center of the stack. Additional gates were added to the endblock injection mold, which reduced warpage and improved the quality of the center weld.

Battery V25-06-08

Problems with the first 2500-series battery stacks included poor distribution of complexed-phase bromine over the face of the electrode and electrolyte crossing over between flow frames. Battery V25-06-08 was the first 2500-series battery stack to be manufactured using flow frames that were modified to eliminate these problems.

The flow rates needed to obtain optimum performance for the 2500-cm² battery stacks were determined using this battery. The battery consistently performed at about 76-77% energy efficiency over the first 26 cycles, as seen in Figure 4-23. During a set of six consecutive baseline cycles, the anolyte reservoir cracked, causing all of the electrolyte to drain from the reservoir. The battery probably became severely overcharged because insufficient reactants would have been available to charge the battery. A cycle was run after replacing the

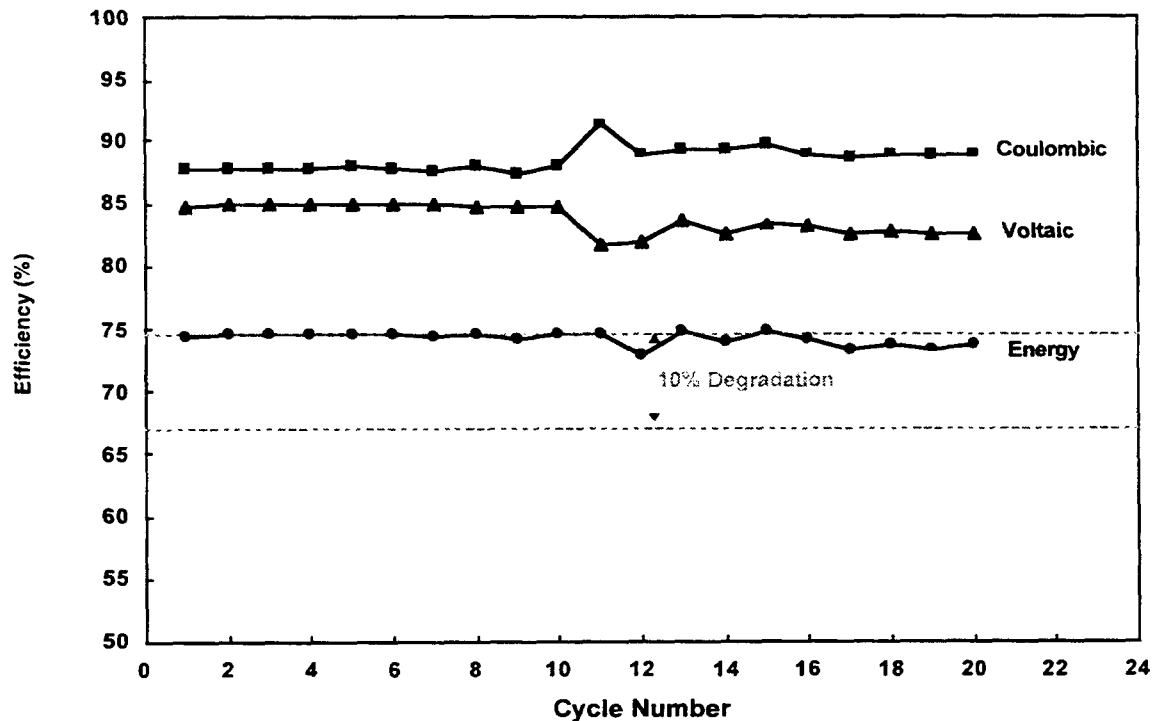


Figure 4-21. Baseline Cycle Efficiencies for Battery V25-04-08.

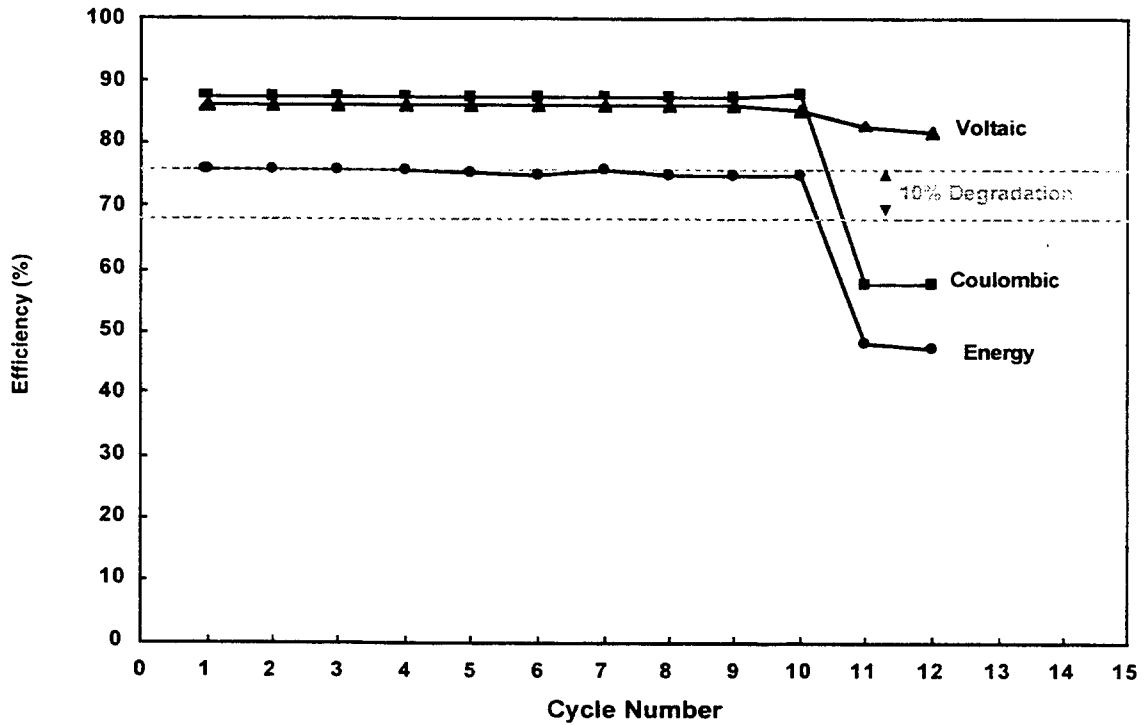


Figure 4-22. Baseline Cycle Efficiencies for Battery V25-05-08.

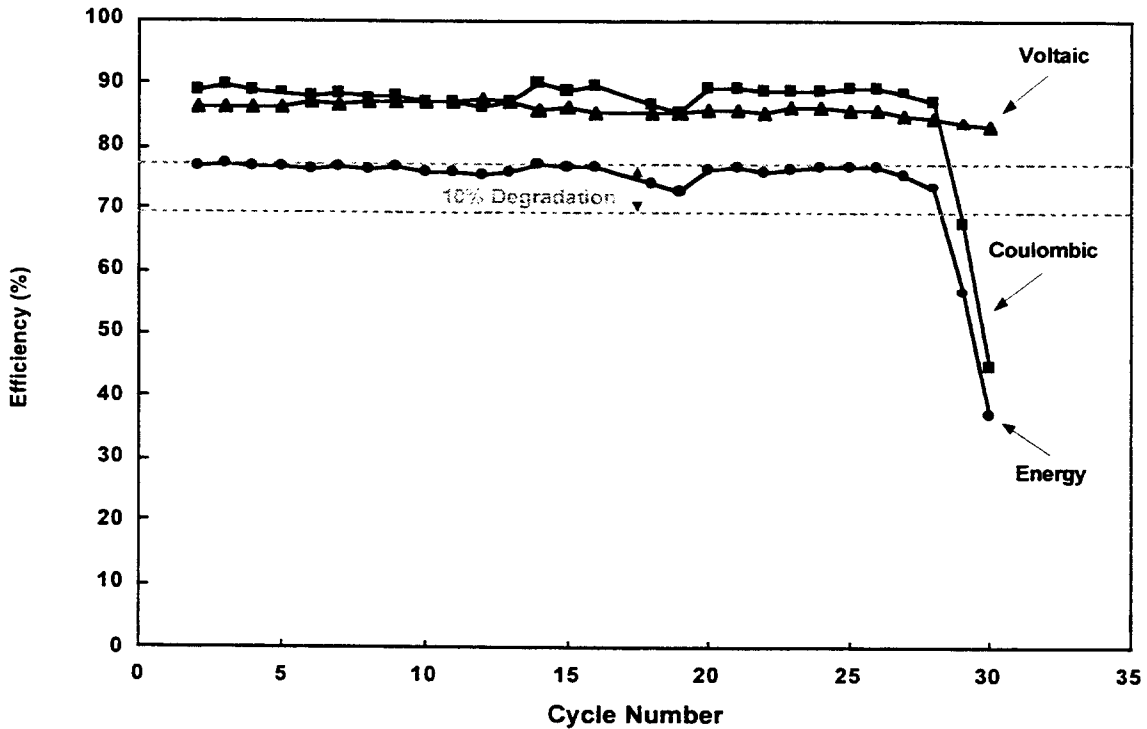


Figure 4-23. Baseline Cycle Efficiencies for Battery V25-06-08.

reservoir, but complexed-phase bromine was observed in the anolyte, indicating an internal leak. The battery was taken off test.

Battery V25-07-08

Several welding problems were encountered during the manufacture of Battery V25-07-08. Initial results gave greater than 77% energy efficiency, but the performance varied considerably from one cycle to the next, as seen in Figure 4-24. This battery was used for no-strip cycle testing, which is described in Chapter 5 under "No-strip Cycling."

During Cycle 18, complexed-phase bromine was observed in the anolyte reservoir, indicating crossflow between cells. Teardown of this stack showed that the center weld between the cathode endblock and the first frame had failed, which is the probable reason for the inconsistent performance of this battery. Changes implemented to reduce the warpage of the endblock appear to have eliminated the problem.

Battery V25-10-08

Battery V25-10-08 completed 20 cycles with very consistent performance. The last cycle gave efficiencies of 89.2% coulombic, 85.8% voltaic, and 76.5% energy. This stack was then tested at SNL on the 2-kWh control station. Figure 4-25 is a plot of cycle efficiencies for Battery V25-10-08. The last four cycles are the results of testing on the 2-kWh control station at SNL. Some problems were encountered while running this battery on the 2-kWh control station. It was decided to discontinue testing of this battery and focus on the manufacture and testing of the 100-kWh battery system.

Battery V25-12-08

Battery V25-12-08 was cycled seven times with inconsistent results, as seen in Figure 4-26. The battery was torn down at 50% depth of discharge and was found to have good zinc plating except for the first bipolar electrode next to the cathode terminal electrode. This electrode had a large bare area with no zinc and other areas with a large number of dendrites. This electrode frame was severely overwelded, which apparently restricted the flow in the first cell.

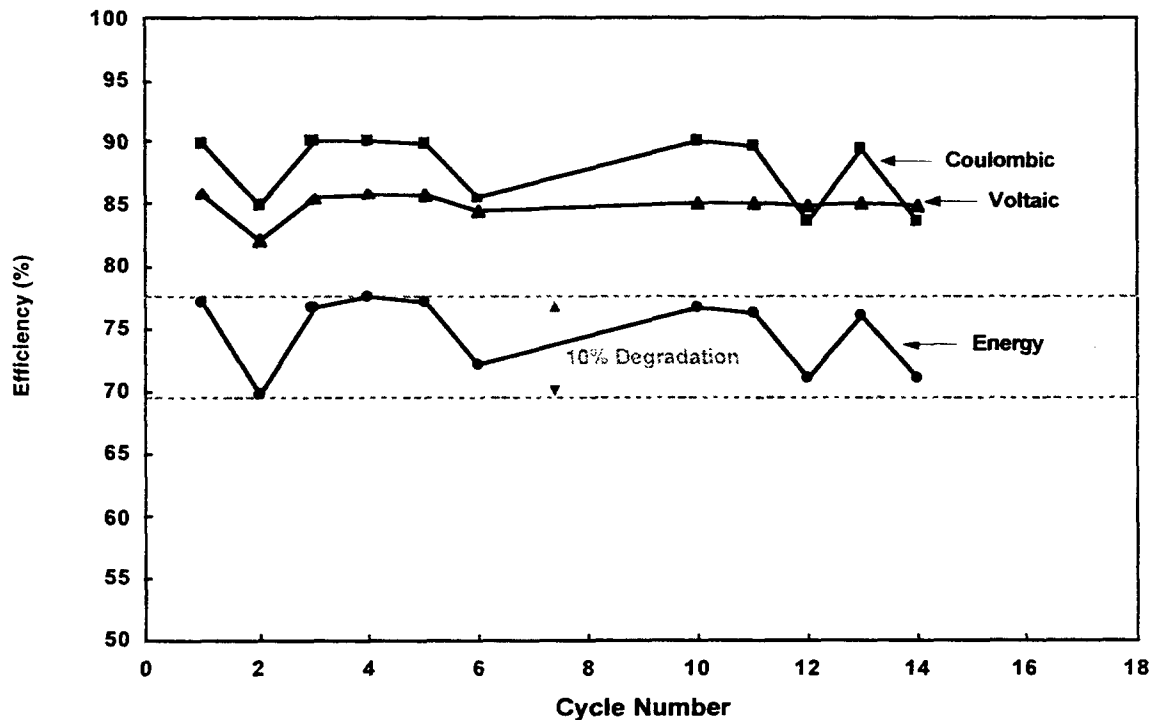


Figure 4-24. Baseline Cycle Efficiencies for Battery V25-07-08.

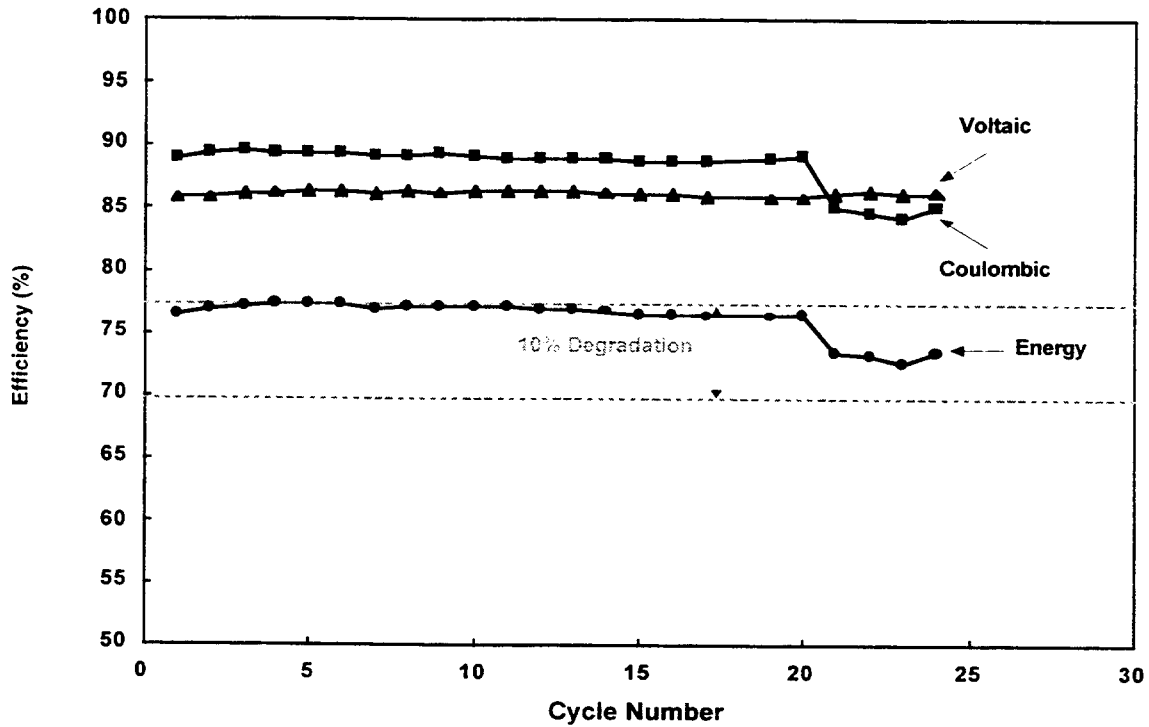


Figure 4-25. Baseline Cycle Efficiencies for Battery V25-10-08.

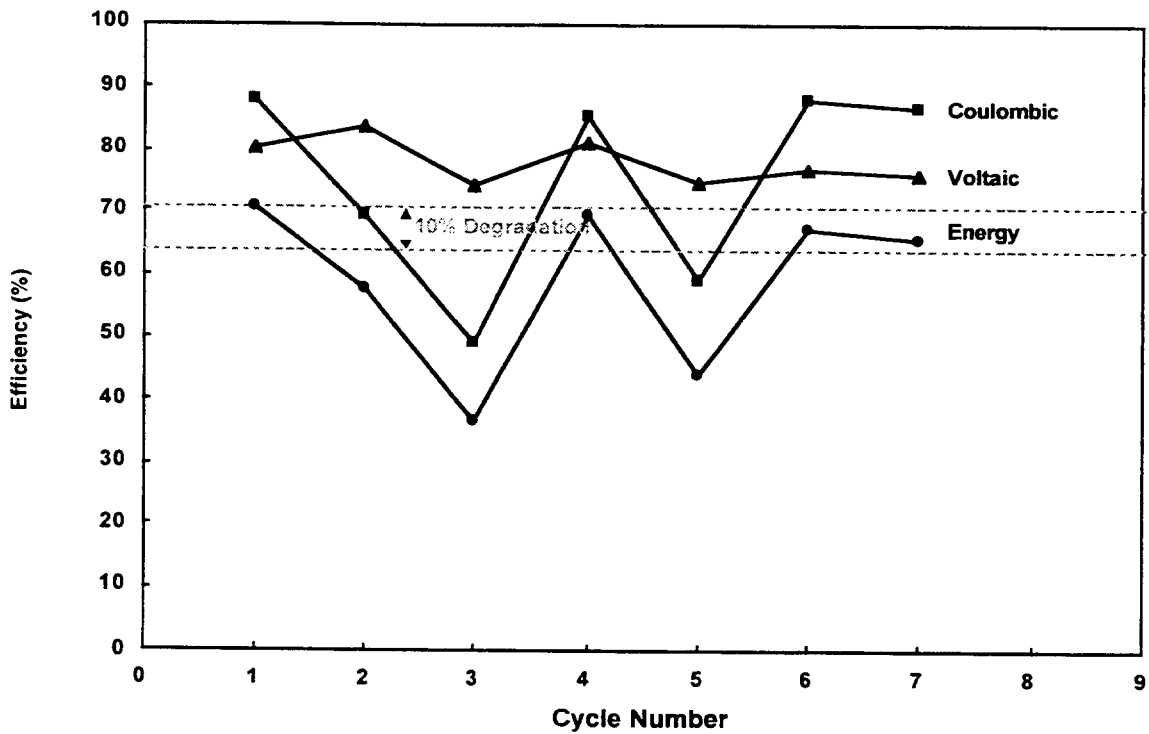


Figure 4-26. Baseline Cycle Efficiencies for Battery V25-12-08.

Battery V25-13-08

Battery V25-13-08 performed consistently over the first 20 cycles with energy efficiencies of about 78%, as seen in Figure 4-27. This battery was taken off test as a potential deliverable battery when a bromine stain on the bottom of the battery was observed. Because the battery was performing well, it was then used to compare bromine complexing agents. Results of the complexing agent testing are given in Chapter 2 under "Quarternary Complexing Agents."

Following cycling, the stack was milled apart to locate the source of the leak. One frame near the center of the stack had an incomplete weld near the catholyte manifold that allowed the bromine to escape from the flow channel to a dead space near the outside of the stack (at the site of the bromine stain). The problem did not appear to adversely affect the performance of the battery.

Battery V25-27-08

Battery V25-27-08 was cycled 10 times before a small leak was observed on the top of the stack. The

battery was performing consistently at about 76.6% energy efficiency, as seen in Figure 4-28. The battery had an incomplete weld that was most probably caused by the taper of the endblocks or the welding parameters. Following this battery build, more uniform endblocks were obtained, and burst tests were performed to examine welding parameters.

Battery V25-30-08

Battery V25-30-08 was manufactured using a new vibration-welding technique. The battery performed consistently for 12 cycles before the second-phase valve was accidentally closed during a set of four consecutive baseline cycles over the weekend. The performance declined dramatically because only the aqueous portion of the catholyte was allowed to circulate during discharge. The second-phase valve was opened, and the battery was completely stripped before resuming baseline cycling. The performance on Cycle 16 returned to the original efficiencies, as seen in Figure 4-29, indicating that the battery was not permanently damaged by cycling with the second-phase valve closed. This battery was taken off test and burst tested to inspect the integrity of the vibration welds.

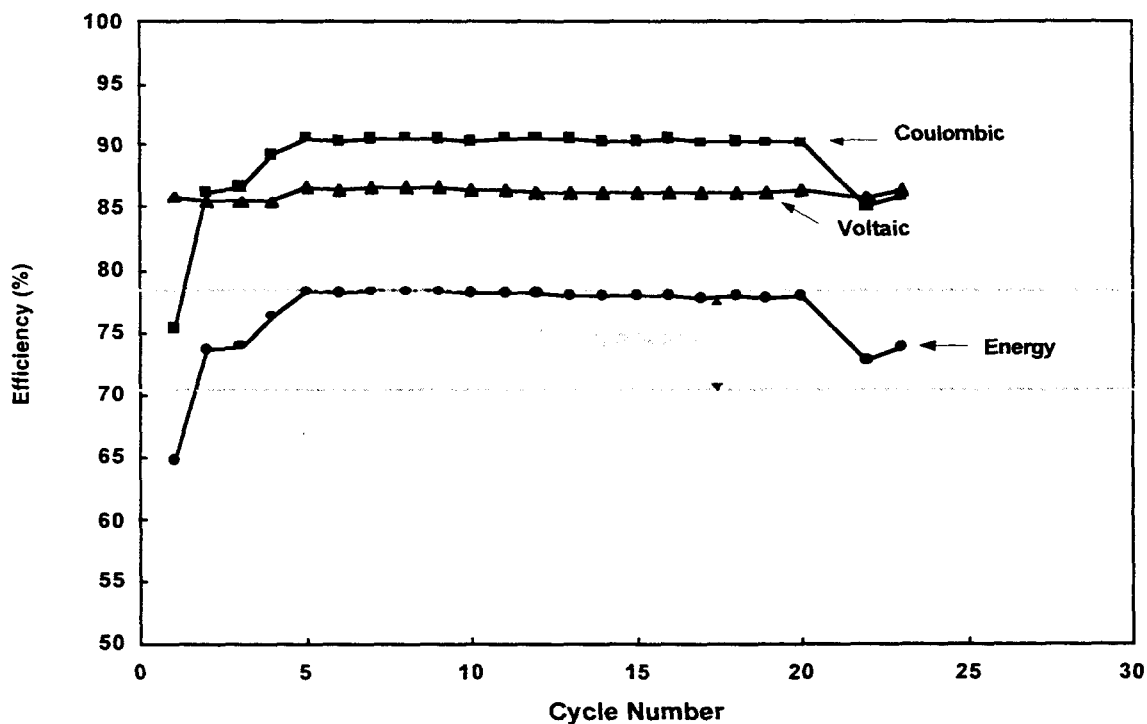


Figure 4-27. Baseline Cycle Efficiencies for Battery V25-13-08.

4. BATTERY TESTING
 8-cell, 2500-cm², 2-kWh Battery Stacks

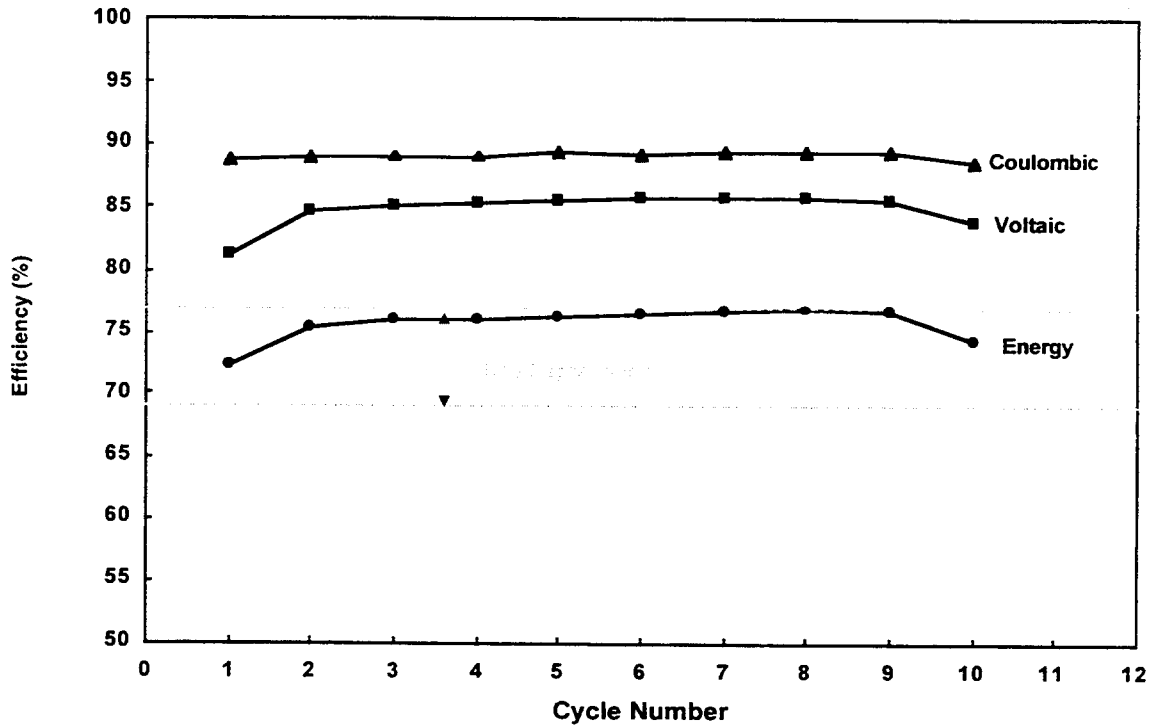


Figure 4-28. Baseline Cycle Efficiencies for Battery V25-27-08.

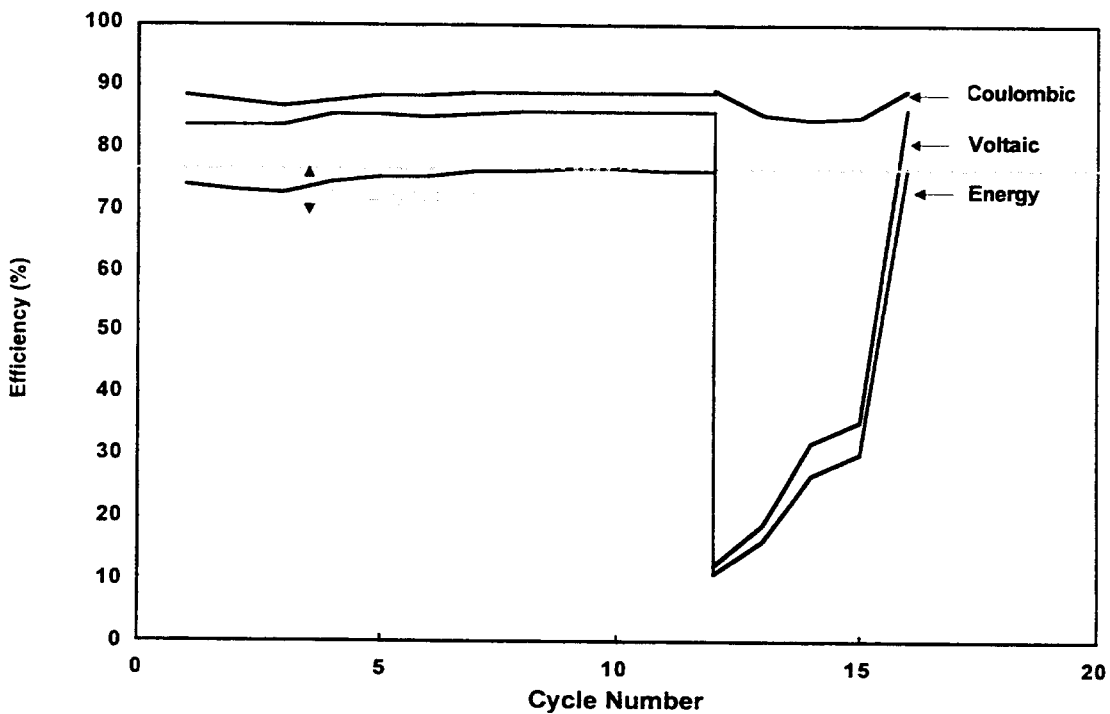


Figure 4-29. Baseline Cycle Efficiencies for Battery V25-30-08.

Battery V25-32-08

Battery V25-32-08 was manufactured using different vibration-welding parameters than those used for Battery V25-30-08. It completed 20 baseline cycles, with the last baseline cycle achieving 79.7% coulombic efficiency, 87.9% voltaic efficiency, and 70.0% energy efficiency, as seen in Figure 4-30. This battery was manufactured with the same separator material used in Battery V1-83, which was found to give lower efficiencies than the standard separator material. The primary objective of this testing was to examine the integrity of the vibration welds using the new manufacturing technique. Burst tests were performed on both V25-30-08 and V25-32-08 to compare the strength of the welds. The results of these tests are given in Chapter 7 under "Battery Stack Manufacturing."

Battery V25-33-08

Battery V25-33-08 was manufactured to allow investigation of an alternative adhesive for the cathode activation layer. The battery stack contained the same experimental battery separator as that used in Battery V25-32-08. It performed consistently over the first 127 baseline cycles, as seen in Figure 4-31, with the

last cycle giving 81.8% coulombic efficiency, 86.0% voltaic efficiency, and 70.3% energy efficiency. The performance did decline slightly at Cycle 17 because of a faulty solenoid valve that caused the heat exchanger to remain on during the entire cycle. This valve was fixed, and cycling of the battery was resumed. This battery was used for no-strip cycling and to examine the cycle life of the alternative adhesive.

Battery V25-37-08

Battery V25-37-08 was sent to SNL for testing on the 2-kWh control station. The battery never performed very well, with a peak energy efficiency of 64.7% during the first cycle, as seen in Figure 4-32. The coulombic efficiency declined significantly from the first to the ninth cycle, and complexed-phase bromine was observed in the anolyte reservoir during the last several cycles, which indicated an internal leak.

The battery was returned to ZBB and was cut apart. It was found that the center weld between the cathode endblock and the first separator frame had split. The center weld appeared to be very weak in the middle, which probably failed first, after which the entire weld gave way. It was also observed that the first separator and electrode frames tore at the center bottom right of

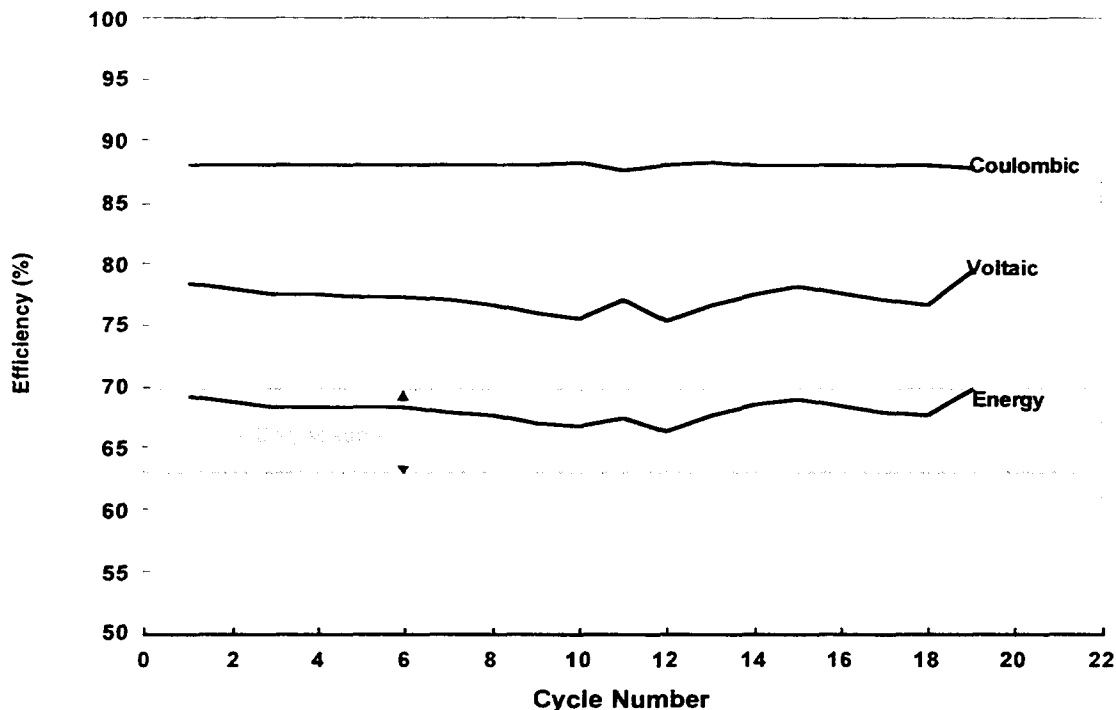


Figure 4-30. Baseline Cycle Efficiencies for Battery V25-32-08.

4. BATTERY TESTING
 8-cell, 2500-cm², 2-kWh Battery Stacks

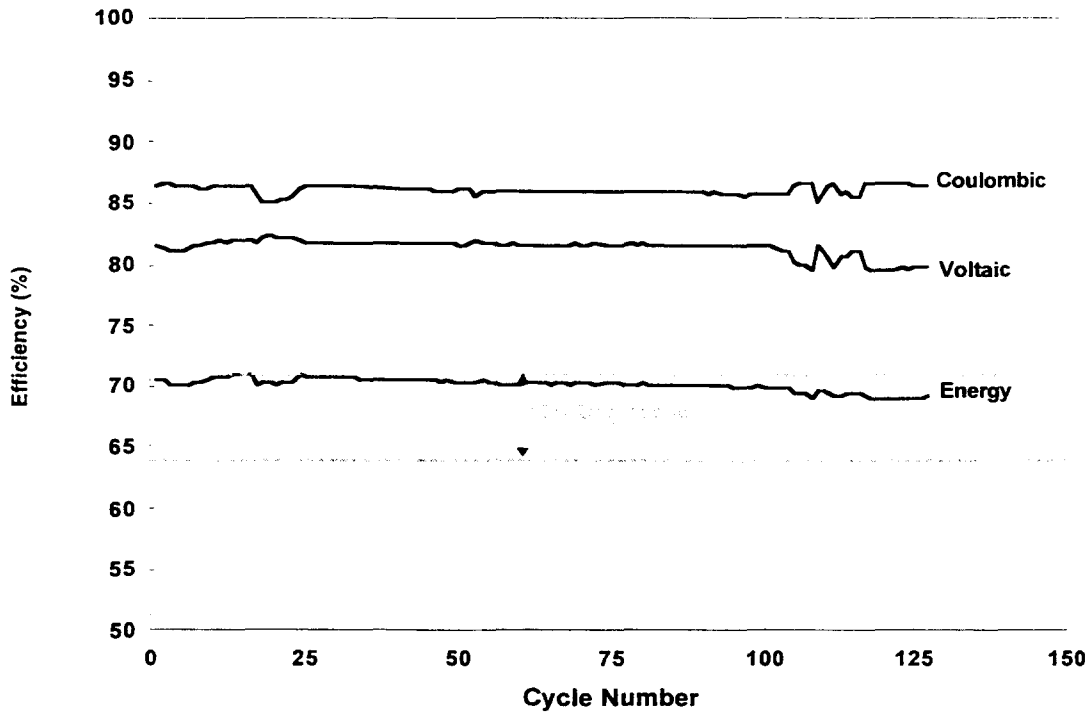


Figure 4-31. Baseline Cycle Efficiencies for Battery V25-33-08.

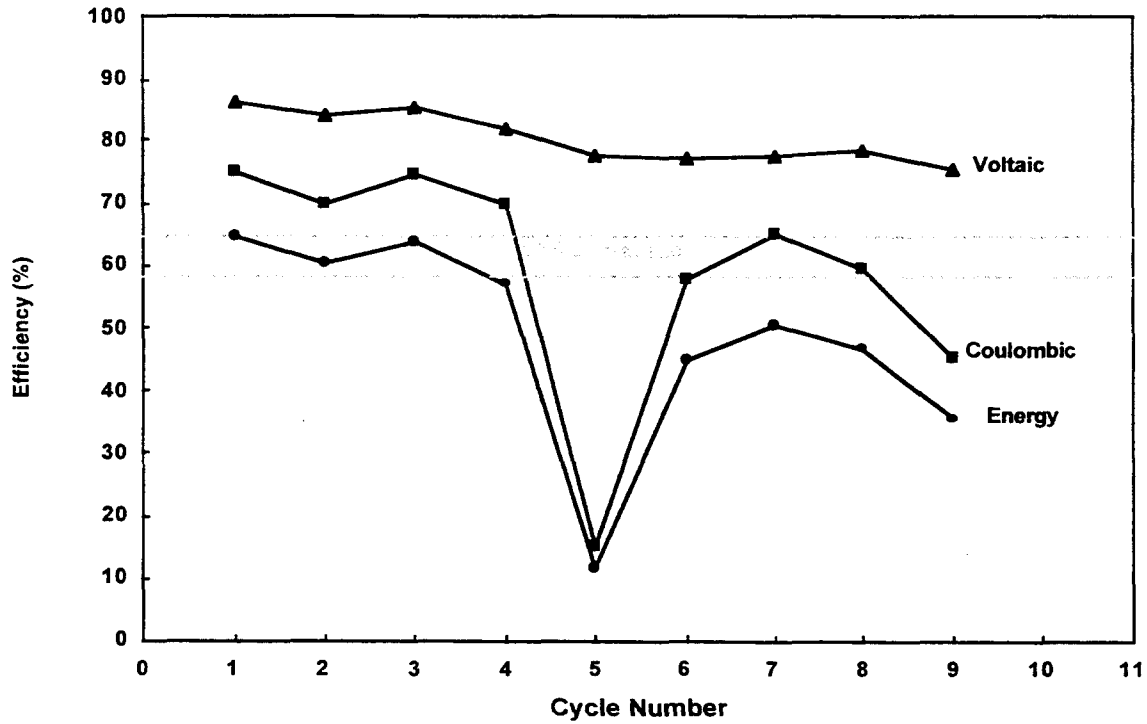


Figure 4-32. Baseline Cycle Efficiencies for Battery V25-37-08.

the center weld. These tears appeared to be caused by the center weld failure. This section is a very thin piece of plastic that probably got bent when the weld gave out and eventually caused a split in the frames. The split would be the reason for the high crossflow from one cell to the other. Overall, no damage was done to the separator or the infrared welds. The failure of this battery stack appeared to be caused by the incomplete center weld.

60-cell, 2500-cm² Battery Stack Qualification

The 60-cell, 2500-series battery stack will be the building block of large utility battery systems. A 100-kWh deliverable battery contains six of these battery stacks. Battery stacks were qualified by running 5 to 10 baseline cycles on each stack. The stacks were then taken off test until the modules for the 100-kWh deliverable battery were completed. The peak and average energy efficiencies for each stack are given in Table 4-5.

Batteries Delivered for Testing at SNL

SNL518 (8-cell, 1-kWh)

Battery V1-57 was tested at SNL under the designation SNL518. After performing well for about 260 cycles, the battery's efficiencies declined and the battery was returned to JCBGI. The electrolyte was removed and tested in a minicell; testing indicated that the quality of the zinc deposit was good. With fresh electrolyte, the efficiencies of the 8-cell stack improved only slightly.

The average values of the last five cycles at SNL are compared to those of the five cycles run at JCBGI in Table 4-6. The plots of the efficiencies versus cycle number are shown in Figure 4-33.

After a total of 278 cycles, the cell stack was torn down at 100% state of charge with the assistance of visiting SNL personnel. A normal amount of warping was found in the bipolar electrodes. On both of the electrode panels in one cell, a few dendrites had penetrated the separator. However, there was no indication that the dendrites had reached the cathode to complete an electrical short. The zinc plating was completely absent from one corner of the sixth and seventh bipolar electrodes. Corresponding to this corner, the separator was severely blistered. Based on the battery performance and the evidence from the teardown, it was concluded that the cycle life was compromised by high electrode overvoltage.

SNL526 (50-cell, 15-kWh)

Two 50-cell stacks, VL-19 and VL-20, were delivered on February 5, 1992, to SNL as a 15-kWh battery. They were designated SNL526. Before delivery, the battery was qualified by the performance of 20 baseline cycles at JCBGI. At SNL, some initial delays were caused by problems with the cycling equipment and fume hood. After testing began, the catholyte reservoir was observed to partially collapse during some cycles. Originally this reservoir was sealed, while the anolyte reservoir was open to the atmosphere through a vent. The problem was overcome by adding a tube from the top of one reservoir to the top of the other, which allowed fluid transfer between the reservoirs.

SNL526 completed 200 cycles with final baseline efficiencies of 86.6% coulombic, 82.6% voltaic, and 71.5% energy. The transport inefficiency was about

Table 4-6. Final Average Efficiencies of Battery SNL518

	Coulombic Efficiency (%)	Voltaic Efficiency (%)	Energy Efficiency (%)	Transport Inefficiency (%)	Residual Inefficiency (%)
At SNL	77.3	74.1	57.3	11.4	9.8
At JCBGI*	83.7	70.5	59.0	7.2	9.1

* with fresh electrolyte

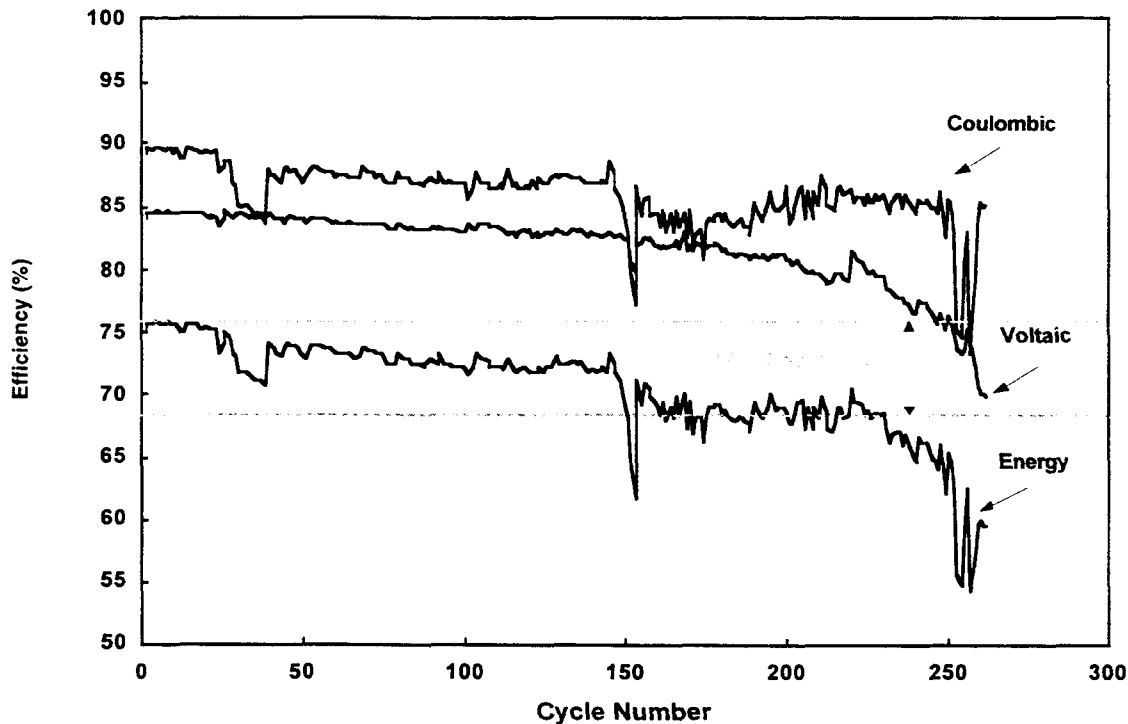


Figure 4-33. Baseline Cycle Efficiencies for Battery SNL518.

7.4% and the residual inefficiency 6.0%. The testing regime at SNL for the majority of these cycles was a repetition of six consecutive no-strip cycles. After three sets of no-strip cycles, a baseline cycle was performed for comparison. Cycle efficiencies are shown in Figure 4-34.

On August 20, 1992, during Cycle 201, Battery SNL526 was damaged as the result of a brief power outage. Because the controller for the pumps had to be manually reset, the pumps remained off when the power resumed. The cycler, however, was not interrupted by the power outage because it had a backup power source. When the pumps stopped, the battery was three hours into discharge. The cycler had been programmed to run a series of full-discharge cycles without strip, and the cycler continued to apply current to the disabled battery. The voltage increased during charge, which should have triggered a high-voltage shutdown. The system was set to shut down when the battery voltage reached 105 V (2.1 V/cell); unfortunately, the power supply used for charging was limited to 104 V, and then the setpoint drifted downwards. Therefore, the battery potential never reached 105 V, and the cycler continued despite the noncirculating condition of the battery. Two cycles

were performed before the testing apparatus was turned off by SNL personnel.

During each of the cycles, charge current was applied for 4.5 hours, but the battery was unable to support any discharge, and the voltage fell rapidly to the cutoff in each cycle. The episode resulted in elevated stack temperatures and a small loss of electrolyte from the system. Because the electrolyte was not circulating, only the reactants in the battery stack were available during charge. Consequently, the battery was severely overcharged, which caused irreversible damage to the battery stacks.

SNL526 (VL-19/VL-20) was dismantled at 0% state of charge with the assistance of SNL personnel. All of the separators in the two stacks were cracked and brittle. Many of the cells showed the effects of localized heating, indicated by melting of the screen, separator, and bipolar electrodes. Several cells had holes through the electrodes. Many of the bipolar electrodes were grossly wrinkled or warped due apparently to high temperature. Some separators also had a characteristic dendrite rash. The conclusion from the teardown is that excessive heating occurred while cycling took place in the absence of electrolyte flow, and this was the major cause of failure.

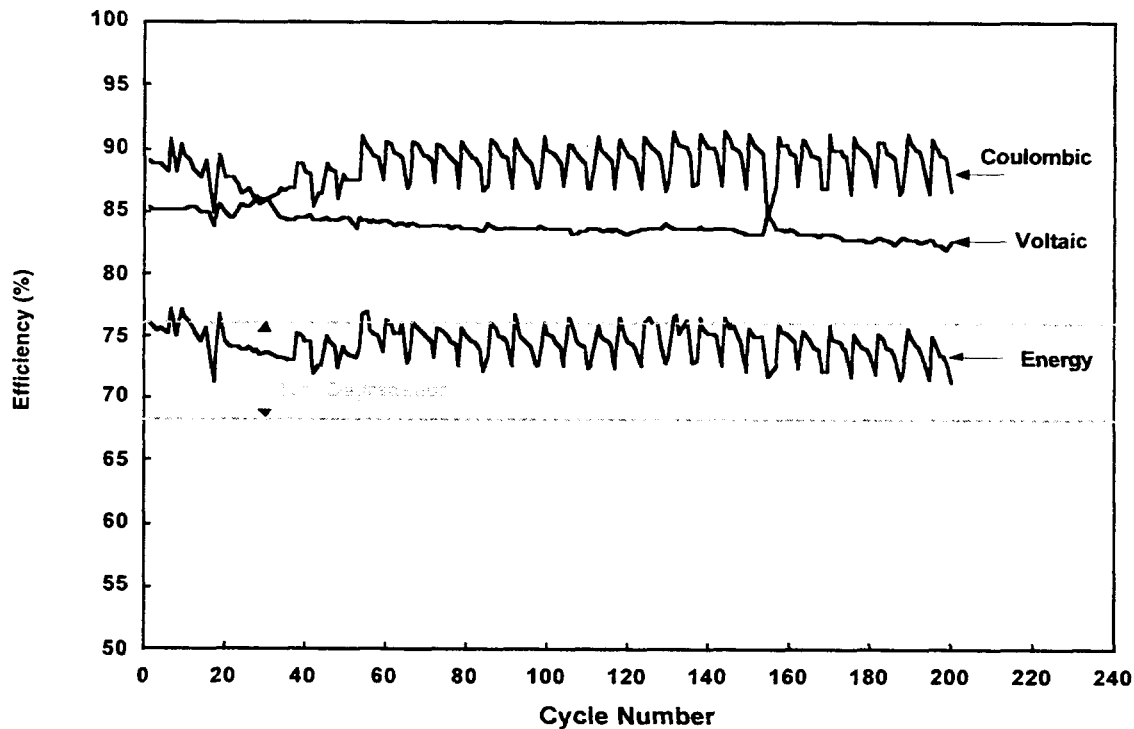


Figure 4-34. Baseline and No-strip Cycle Efficiencies for Battery SNL526.

Intentionally Left Blank

5. Additional Battery Testing

No-strip Cycling

After a zinc/bromine battery is discharged to 1.0 V/cell, it is usually completely stripped of any residual zinc by connecting the battery across a resistor. This is done to ensure that there is a smooth electrode surface for the deposition of zinc at the beginning of each cycle. It also simplifies the data collection procedure for the zinc/bromine battery by making it possible to differentiate between transport and residual inefficiencies.

Although it is recommended, it is not necessary to strip the battery after every cycle. The time needed to completely strip the battery may not be available in all cases, and the capacity remaining in the battery before stripping can be utilized during the following cycle. For example, if 5 Ah remain at the end of discharge, then a loading of 105 Ah (90 mAh/cm² for an 1170-cm² battery) on top of this layer would be equivalent to a total of 110 Ah, or a 94-mAh/cm² loading. Subsequently, more capacity can be removed during a no-strip cycle, giving a higher efficiency than for a standard 90-mAh/cm² baseline cycle.

Battery V1-60 was operated over a number of full-discharge cycles without stripping. There was an immediate gain of 2.5–3% in energy efficiency when the strip was omitted, but the advantage decreased as more cycles were added between strips, as shown in Table 5-1. Even so, after 26 cycles, the efficiencies were still higher than baseline.

The results of six consecutive cycles without stripping are compared to baseline cycle efficiencies in Table 5-2 for Batteries V1-80 and V1-81. The average efficiencies did not increase as much as for earlier battery stacks, but the amount of residual losses observed during baseline cycling for these two battery stacks was also lower. Earlier battery stacks gave 5 to 6% residual losses on baseline cycling.

Another interesting characteristic of these two batteries is that the energy efficiencies increased on each cycle of the no-strip sequence up to the fifth cycle for V1-81 and the sixth for V1-80. Previous battery stacks achieved the maximum efficiencies on the second cycle of the set (the first no-strip cycle); efficiencies then declined on each successive cycle, as seen in Figure 5-1. The reason for this can be associated with a redesign of the flow frame, which improved the distribution of electrolyte across the face of the electrodes.

Results of no-strip cycling performed on three 2500-cm² battery stacks are given in Table 5-3. The second cycle of the no-strip set experienced an increase in coulombic efficiency for each battery stack, but the efficiencies dropped on each successive cycle. The coulombic efficiency for the first cycle without strip was initially higher because a portion of the zinc normally lost to stripping was retained in the battery.

The efficiencies for a good-performing battery stack should level off following the second cycle of a

Table 5-1. No-strip Cycle Efficiencies for Battery V1-60

Number of No-strip Cycles	Coulombic Efficiency (%)	Voltaic Efficiency (%)	Energy Efficiency (%)	Transport Inefficiency (%)	Residual Inefficiency (%)
None-Baseline (11-14)	90.1	85.9	77.4	5.9	4.0
6 cycles (15-21)	93.2	85.6	79.8	5.1	1.7
8 cycles (78-86)	92.4	85.7	79.2	5.6	2.0
11 cycles (43-54)	92.1	85.5	78.7	5.8	2.2
16 cycles (57-73)	91.8	85.8	78.8	6.1	2.1
26 cycles (88-114)	91.4	85.2	77.9	7.3	1.3

Table 5-2. Average of Six No-strip Cycles Compared to Baseline Cycle Results

Battery Number	Cycling Regime	Coulombic Efficiency (%)	Voltaic Efficiency (%)	Energy Efficiency (%)	Transport Inefficiency (%)	Residual Inefficiency (%)
V1-80	Baseline	90.7	86.5	78.5	6.1	3.2
V1-80	No-strip	91.9	86.8	79.8	6.4	1.7
V1-81	Baseline	90.3	84.8	76.6	5.8	3.9
V1-81	No-strip	91.6	85.3	78.6	6.6	1.8

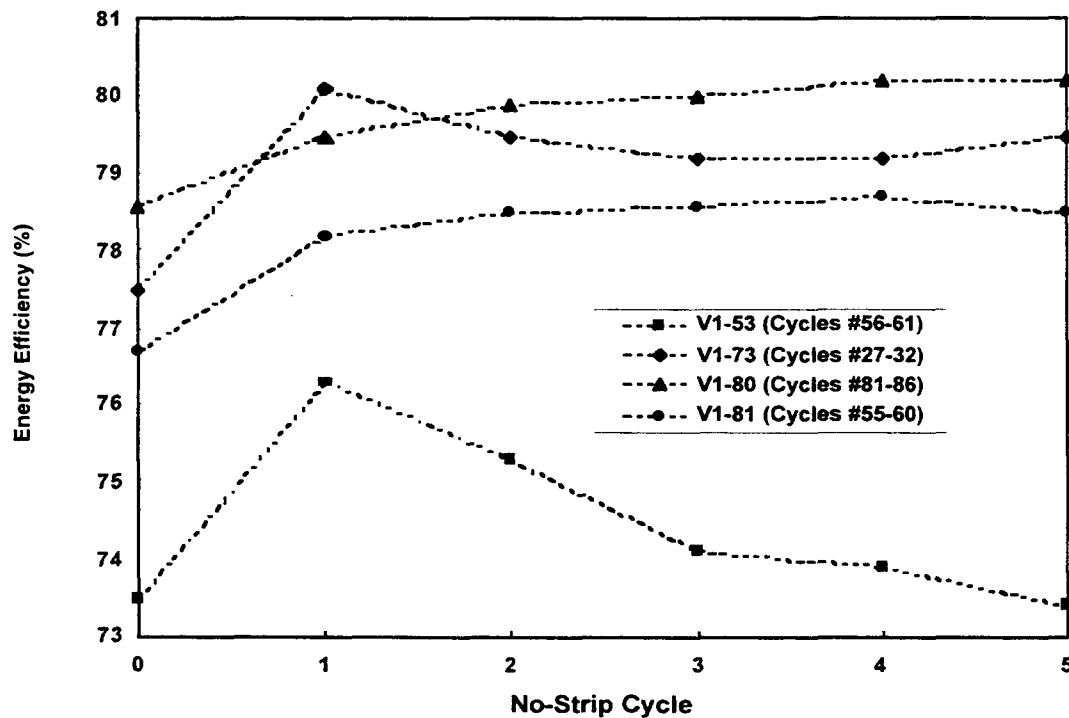


Figure 5-1. Energy Efficiency over a Set of Six Consecutive Cycles without Stripping.

no-strip sequence. The progressive decrease in efficiency indicates poor flow distribution, which results from an accumulation of zinc on the anodes, most likely in zones of lower activity. From observations made in earlier teardowns, these zones are located in the corners, away from the flow entry points and along the center rib. Warps in the electrode material can also create low-activity zones where the electrolyte gap is very thin.

The coulombic efficiency for Battery V25-07-08 declined much more rapidly than the coulombic efficiency for the other two battery stacks. Similar results were observed for early V-design 1170-cm² battery stacks, apparently because of poor electrolyte flow distribution. Teardown of this battery stack uncovered a center weld failure in one of the cells, which could have caused nonuniform flow of electrolyte over the face of the electrode in that cell.

**Table 5-3. Performance of Battery V25-07-08
 During Consecutive Cycles Without Stripping**

Battery Number	Cycle Number	Coulombic Efficiency (%)	Voltaic Efficiency (%)	Energy Efficiency (%)
V25-07-08	6	85.4	84.5	72.1
	7	88.0	84.3	74.2
	8	83.2	84.8	70.6
	9	81.6	85.3	69.6
V25-32-08	21	75.5	88.3	66.7
	22	83.2	88.3	73.5
	23	82.1	88.1	72.4
	24	82.4	87.6	72.1
V25-33-08	34	81.8	86.4	70.7
	35	83.7	86.8	72.6
	36	83.2	86.9	72.3
	37	82.7	87.0	71.9
	38	82.3	87.0	71.6
	39	82.1	87.0	71.4

Overvoltage and Internal Resistance (IR) Testing

Most of the 8-cell batteries tested during Phase 2 of the contract were monitored for overvoltage (also known as polarization) and internal resistance (IR) loss on a regular basis during the course of testing. A current-interrupt method, which allows a measurement of the IR-free overvoltage as well as the IR loss during discharge, was performed approximately every 50 cycles on several batteries to examine degradation. Also, on a more frequent schedule, rough measurements of the electrode overvoltage were made using only the AC resistance. After running tests on several batteries, it was determined that the two methods gave approximately the same results. After that, only the AC resistance test was performed because it was simpler to run.

Figures 5-2 and 5-3 show the overvoltage and IR drop for Battery V1-74 measured with the current-interrupt test procedure. Figure 5-2 shows a significant increase in overvoltage between Cycles 184 and 241, which suggests cathode-layer degradation. Figure 5-3 indicates that the resistance of the battery also gradually

increased during the life of this battery. Figure 4-7, which demonstrates results determined using AC resistance and baseline current density (21 mA/cm²), also shows that V1-74's overvoltage began to increase significantly after around 200 cycles. The normal value for the overvoltage is about 10 mV/cell for an 8-cell battery.

Overvoltage and IR losses measured by the AC resistance method are compared for several 8-cell, 1170-cm² battery stacks in Figures 5-4 and 5-5, respectively. Figure 5-4 shows that the overvoltage for earlier batteries (V1-54 and V1-76) began to increase rapidly at about 250 cycles, but not for the last battery builds. Battery V1-80 gave the lowest overvoltage over the first 900 cycles because of the development of a large-surface-area cathode activation layer and the development of an electrode reconditioning process.

Figure 5-5 shows that later battery builds are also much lower in resistance than earlier battery stacks (for example, V1-54). This lower resistance results from the development of a low-resistance carbon plastic electrode material. Batteries V1-76 and V1-80 gave very low IR losses as a result of the development of low-resistance terminal electrodes.

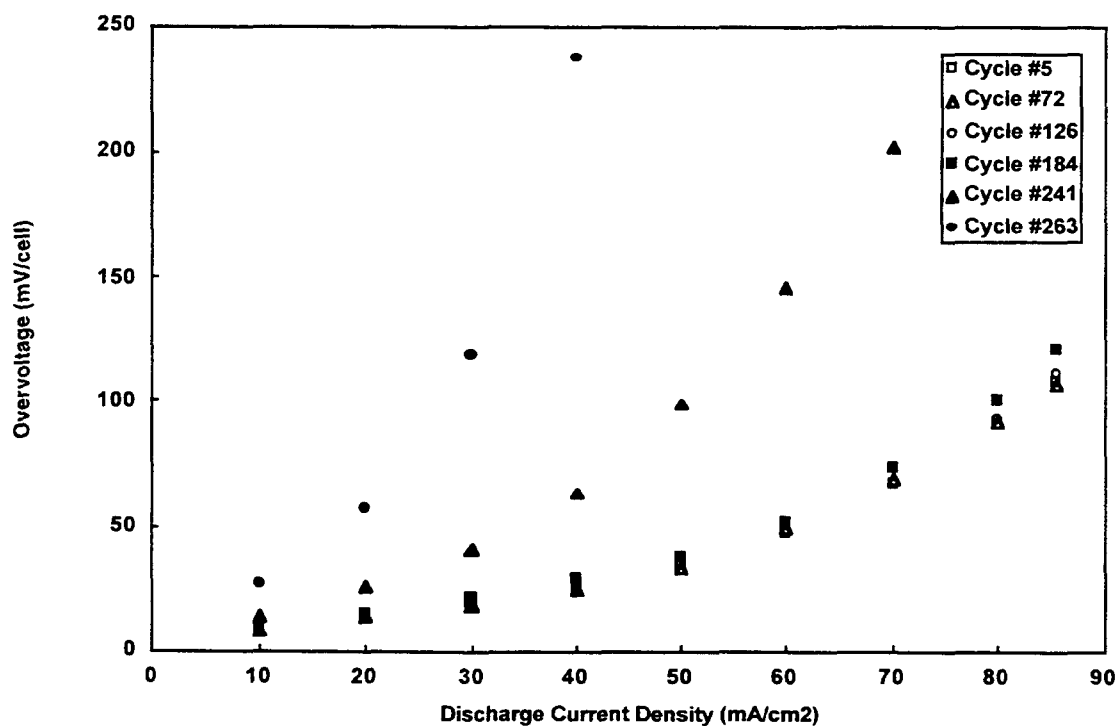


Figure 5-2. Overvoltage Losses for Battery V1-74 Measured by the Current-interrupt Method.

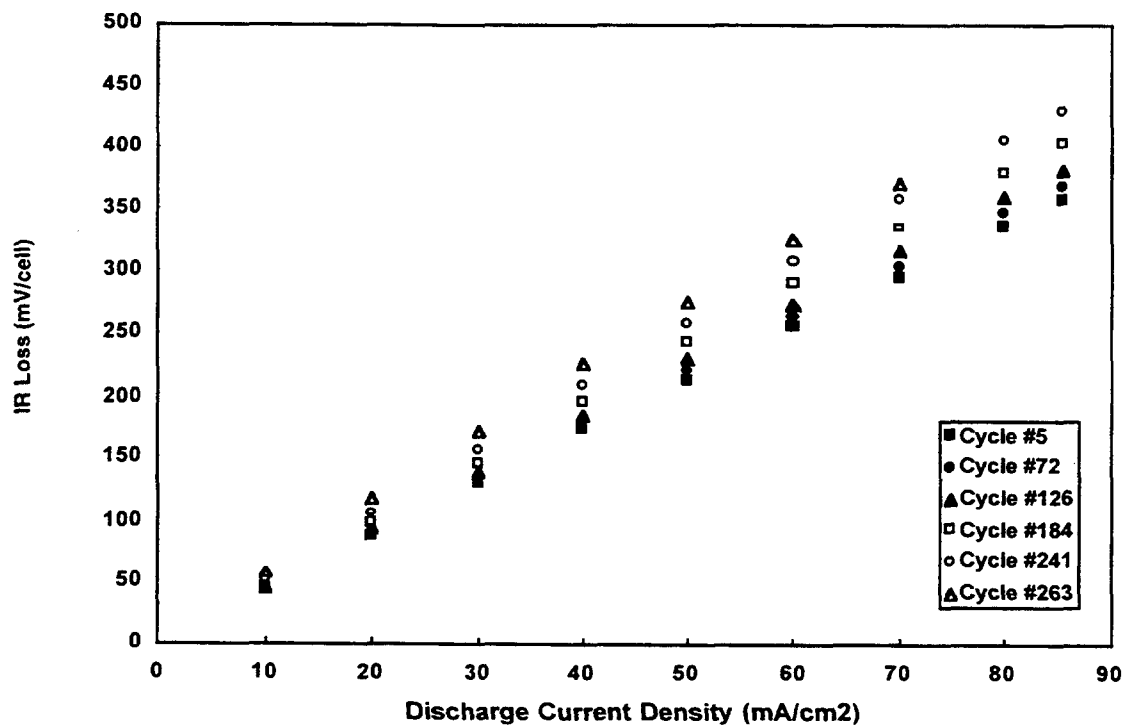


Figure 5-3. IR Losses for Battery V1-74 Measured by the Current-interrupt Method.

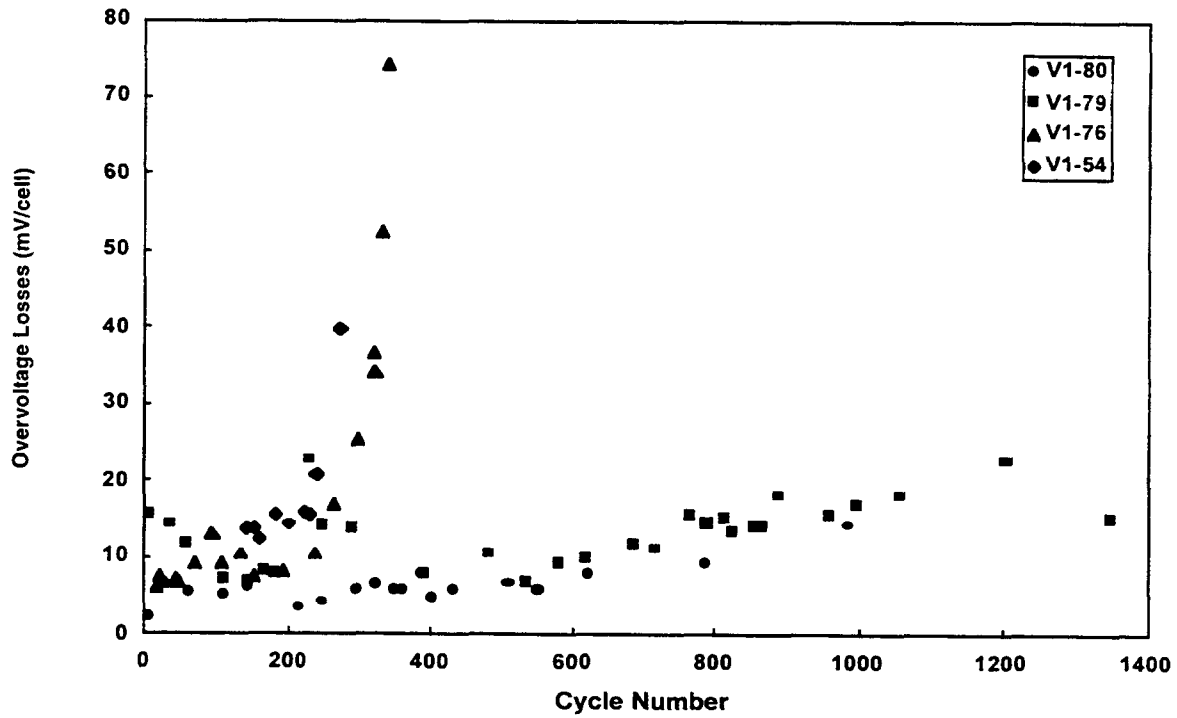


Figure 5-4. Battery Overvoltage Losses versus Cycle Life.

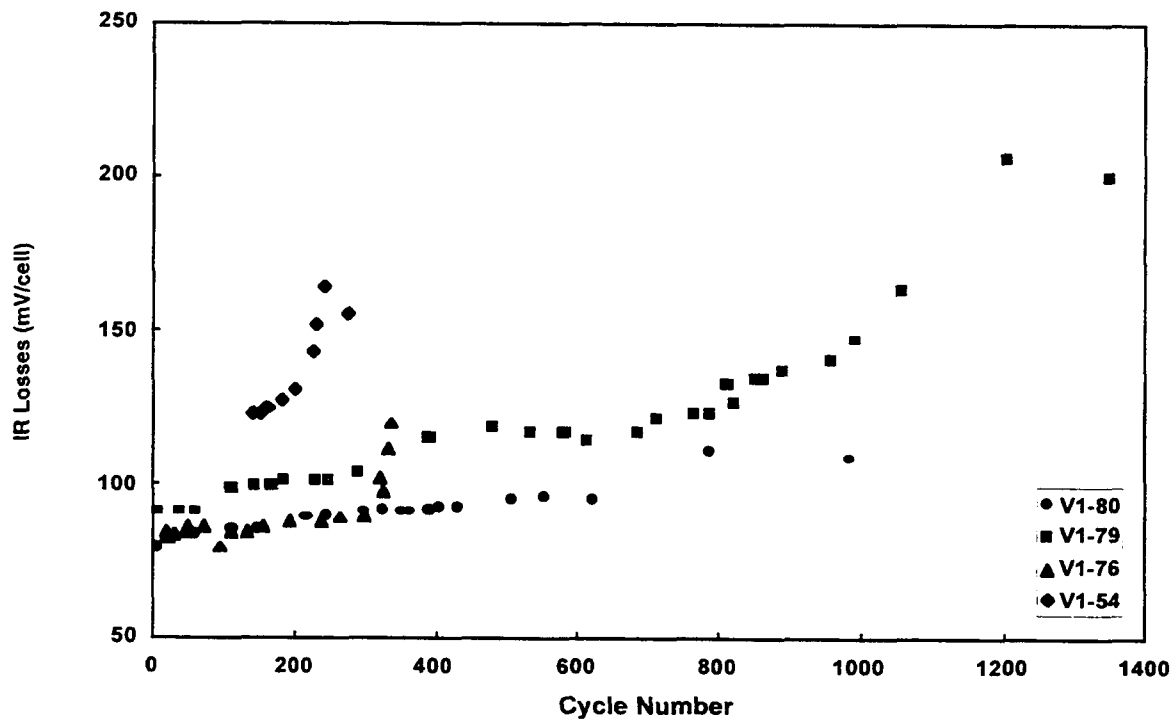


Figure 5-5. Battery IR Losses versus Cycle Life.

The overvoltage and IR losses of an 1170-cm² battery stack were also measured during a standard discharge cycle. The rapid decline in voltage near the end of discharge (the "knee" in the voltage profile) is associated with an increase in battery overvoltage (see Figure 5-6). The IR losses appear to increase nearly linearly during discharge, but the overvoltage increases more rapidly near the end of discharge. The increase in overvoltage was most probably caused by a reduction in the amount of bromine available for reaction and the nonuniform dissolution of zinc from the anode.

High-rate Discharge

The results of discharging a 60-cell, 2500-cm² battery stack at different rates are given in Table 5-4. Voltage profiles for the various discharge rates are shown in Figure 5-7. A standard charge cycle of 50 A for 4.5 hours was used for each test. This demonstrates that a battery stack is capable of producing 19 kWh of energy for discharges lasting three hours or more. For discharges of less than three hours, the energy output decreases significantly. The results at the higher-rate discharges are probably low because the amount of complexed second-phase delivered to the battery stack

during discharge was limited by the station design. Results might have been better if the amount of complexed bromine circulated during discharge could have been increased. Table 5-4 also shows that it was much more difficult to control the temperature while the battery was discharged at the higher rates. All cycles began charging at a temperature of about 25°C.

Electrode Reconditioning

In the past, failure of zinc/bromine batteries has usually been associated with a very rapid increase in overvoltage as the number of cycles increases, which causes efficiencies to drop very quickly near the end of cycle life. This trend can be seen in Figure 4-5 for battery V1-72. Tests have indicated that the high overvoltage of a poorly performing battery can be at least partially reversed. An electrode reconditioning technique was used to significantly lower overvoltage and to improve efficiencies of three 8-cell batteries, as seen in Table 5-5.

ZBB's electrode reconditioning process was patented in 1997 (U.S. Patent No. 5,650,239). The basic concept is that by lowering the pH of the electrolyte and

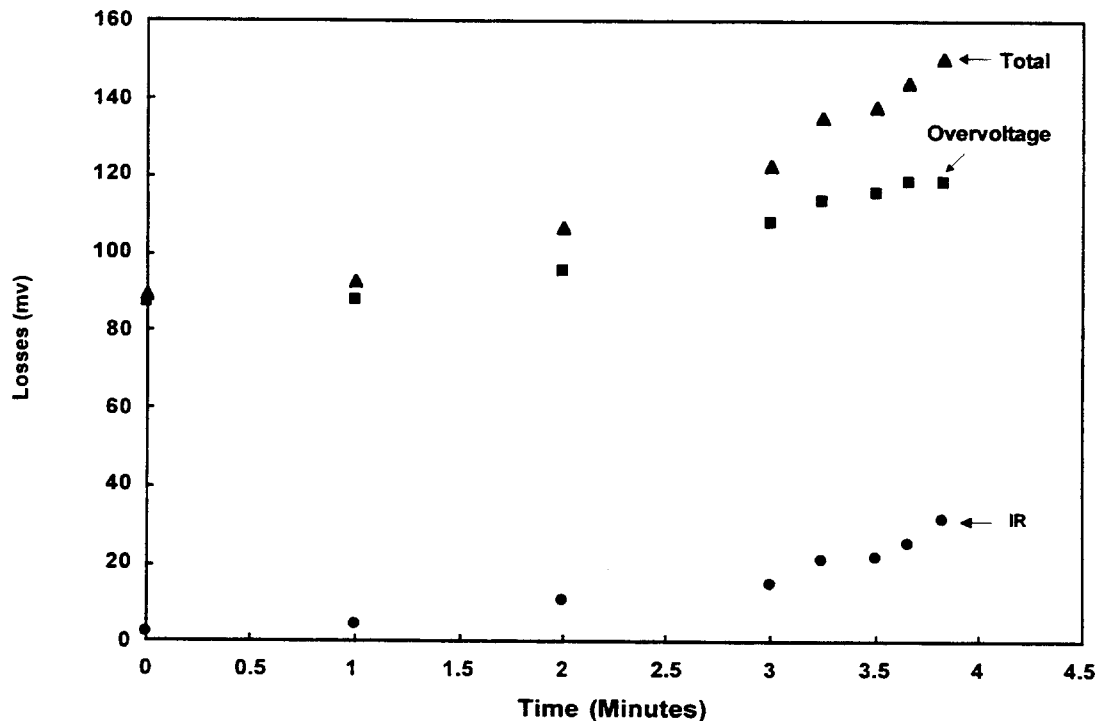


Figure 5-6. Overvoltage and IR Losses During Discharge Cycle (V1-80, 1-kWh).

**Table 5-4. Effect of Discharge Rate on Performance
for a 60-cell, 2500-cm² Battery Stack**

Discharge Current (A)	Discharge Time (Hours)	Maximum Temperature (°C)	Energy Output (kWh)
35.5	5.61	30.6	19.83
42.8	4.67	31.6	19.71
53.3	3.75	33.2	19.43
71.2	2.82	35.0	19.15
104.9	1.87	39.5	17.86
209.9	0.83	50.9	13.54

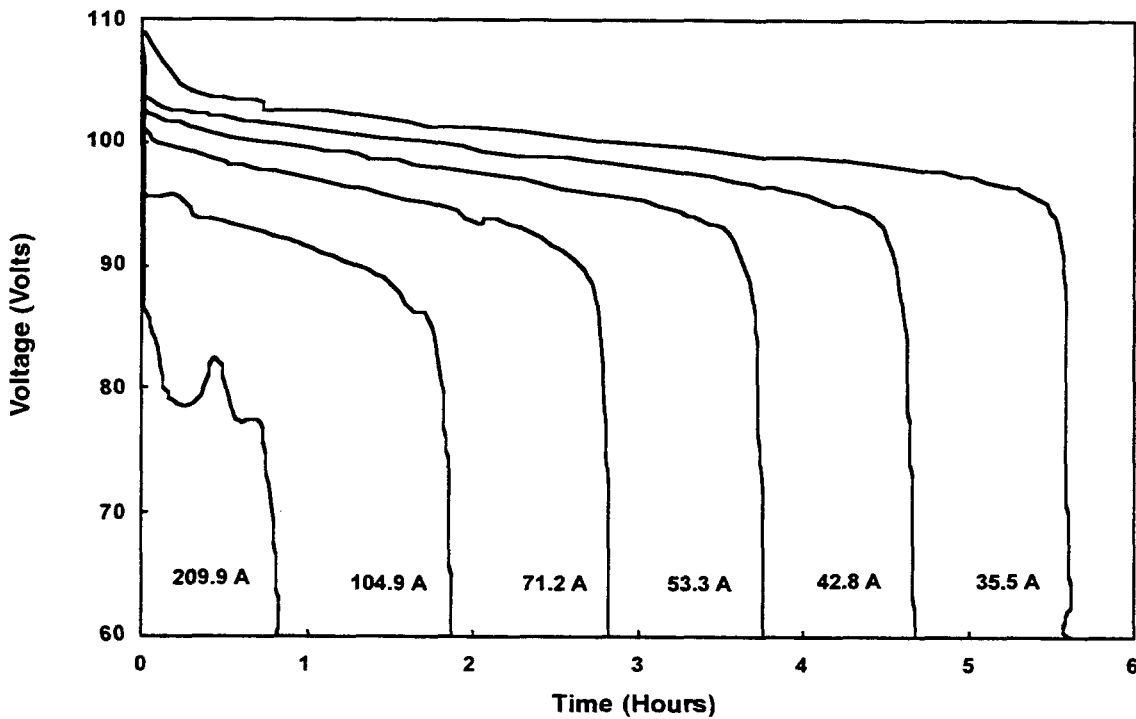


Figure 5-7. Discharge Voltage Profiles for a 60-Cell, 2500-cm² Battery Stack.

then reversing the direction of normal cycling current through the battery, the electrochemical activity of a poorly performing electrode can be significantly improved. The effects of the reconditioning can also be seen in the baseline cycle efficiency plots for Batteries V1-72, V1-76, and V1-77 given in Figures 4-5, 4-9, and 4-10, respectively.

This reconditioning procedure was also performed on Batteries V1-79 and V1-80 about every 50 cycles after the first 250 cycles. It was performed before the battery performance declined by 10% from the peak energy efficiency. Figures 4-12 and 4-13 show that performing this reconditioning procedure regularly increases battery life significantly. It may be important to use this type of procedure as a standard operating procedure for zinc/bromine batteries. More work will need to be done to optimize the reconditioning process.

Effect of Orientation on Battery Performance

The results of tests of vertical versus horizontal stack orientation using Battery VL-15 (50-cell, 1170-cm²) indicated no advantage for either orientation. No significant difference was observed for baseline cycles or for multiple cycles without stripping, as shown in Table 5-6. The flow was reversed periodically while the cell stack was in each orientation.

No stand tests were run on this battery, but later tests indicated that the stand loss was higher if the battery was in the horizontal orientation rather than in the vertical orientation.

Table 5-5. Baseline Cycle Efficiencies Before and After Electrode Reconditioning

Battery	Cycle	Coulombic Efficiency (%)	Voltaic Efficiency (%)	Energy Efficiency (%)
V1-72	Before	82.6%	78.1%	64.5%
V1-72	After	85.4%	80.4%	68.7%
V1-76	Before	79.3%	71.8%	57.0%
V1-76	After	84.9%	78.0%	66.2%

Table 5-6. Cycle Efficiencies for Vertical and Horizontal Orientation for Battery VL-15

Cycles	Orientation	Coulombic Efficiency (%)	Voltaic Efficiency (%)	Energy Efficiency (%)	Transport Inefficiency (%)	Residual Inefficiency (%)
Baseline	Vertical	86.2	84.1	72.5	6.4	7.4
Six No-strip	Vertical	90.6	84.9	77.0	7.4	2.0
Baseline	Horizontal	86.3	84.1	72.5	7.9	5.7
Six No-Strip	Horizontal	90.8	84.9	77.1	7.6	1.6
Six No-Strip	Horizontal	90.7	84.8	76.8	8.0	1.3

Simplified Frequency Regulation/ Spinning Reserve (SFRSR) Testing

In addition to standard load-leveling duty, an electric utility battery should also be able to fill other needs. The simplified frequency regulation/spinning reserve (SFRSR) discharge test is a simulation of a stationary energy storage application for an electric utility, modeled from the Puerto Rico Electric Power Authority battery energy storage system.¹ The frequency regulation part of the SFRSR test requires a series of constant-power discharge steps set at three different power levels. When the battery's state of charge falls to 76%, the discharge is stopped, the battery is given a full recharge, and then the discharge is started again. The basic test lasts for 160 minutes and is to be repeated 54 times or until 6.5 days have elapsed. A rapid spinning-reserve discharge is then performed.

A cycling unit from SNL was used for the testing. A Simplified Federal Urban Driving Schedule program was modified to apply frequency regulation steps in place of the existing steps. Each frequency regulation set contains a total of 32 five-minute steps. The frequency regulation test requires the three power levels listed in Table 5-7, which were calculated for an 8-cell zinc/bromine battery stack with load-leveling electrolyte. An example of an SFRSR voltage profile is shown in Figure 5-8.

The frequency regulation test was modified to include a periodic recharge as in the SFRSR. After estimating that the 76% state of charge would be reached after approximately three sets of steps, the controlling program was changed to add 20 Ah of constant-current charge at that point. The valve controlling the addition of complexed bromine was set to automatically open on discharge and to close on charge.

Several frequency regulation tests were attempted using Batteries V1-50 and V1-64. Initially, each charge was twice as long as it should have been, because of an error in the controlling program. This error caused Battery V1-64 to be significantly overcharged, which was indicated by an increase in voltage after each charge portion of the cycle.

Two tests were performed on a fully charged battery, Battery V1-64, until it was fully discharged. Each test lasted about 30 hours. The results, listed in Table 5-8, showed that the average efficiency was nearly the same as that in baseline constant current cycles run before and after the frequency regulation tests. The coulombic efficiency was slightly lower and the voltaic efficiency was higher than for the baseline cycles. Both of these effects were probably the result of a freshly deposited layer of bromine, generated during the previous step, on the bromine electrode surface as the battery was discharged.

Battery V1-50 was cycled several times using the frequency regulation steps, but each cycle terminated at about 45 to 50 hours (full test = 156 hours) because of a problem with the cycling unit. The efficiencies of two SFRSR cycles (see Table 5-9) are similar to the efficiencies of baseline cycles. Baseline Cycles 53 and 54 may be low in efficiency because the cycler had trouble maintaining a set current and had to be stopped and restarted several times.

These initial trials revealed a concern that required changes to the SFRSR test. The high-power recharge pulse of C/1.5 for five minutes was too high for the battery as it was configured. The battery voltage would often increase above 2.1 V/cell, causing the test to stop. The C/1.5 discharge step was not a problem for the battery. Therefore, in these tests, the recharge step was changed to C/2 for eight minutes to give the same number of amp-hours, but at a slightly lower voltage. Other strategies for lowering the voltage on charge could be investigated in the future. Such strategies include using

Table 5-7. Constant-power Discharge Tests

Rate	ZnBr ₂ Battery (W/kg)	8-cell Battery (W)
C/1.5	43	632.1
C/2.5	27	396.9
C/7.5	9	132.3

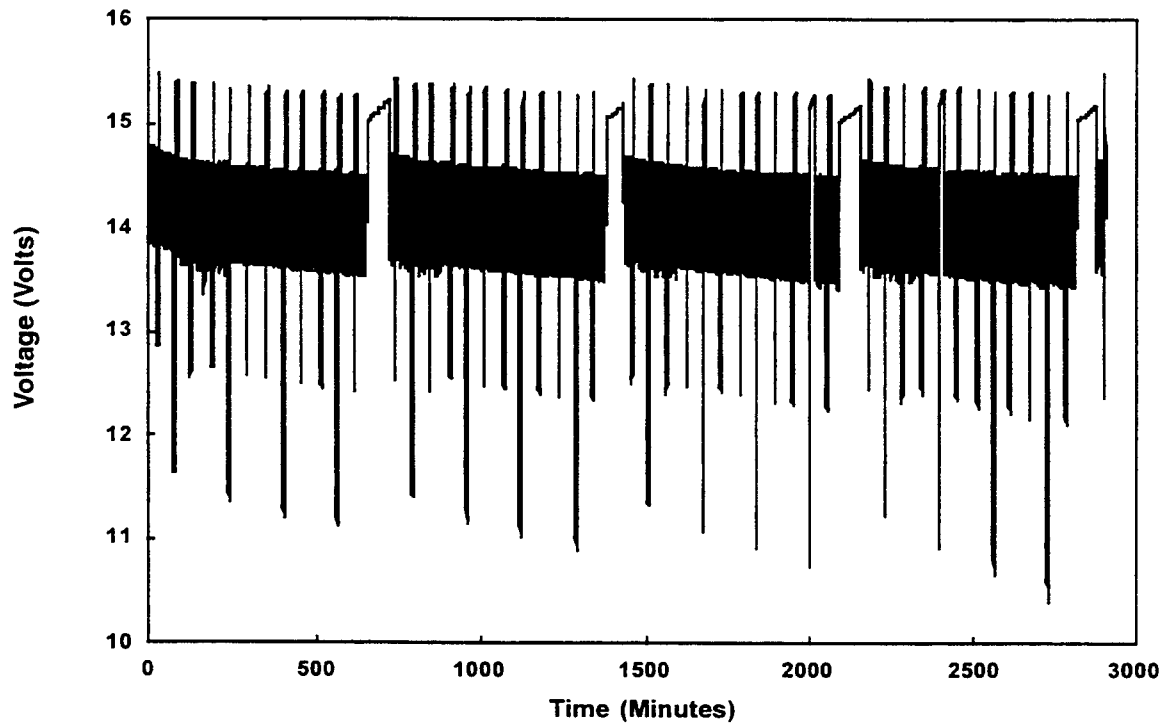


Figure 5-8. SFRSR Cycle for Zinc/Bromine Battery.

Table 5-8. Frequency Regulation Discharge for Battery V1-64

	Coulombic Efficiency (%)	Voltaic Efficiency (%)	Energy Efficiency (%)
FR-Cycle 47	82.2	84.9	69.7
FR-Cycle 49	79.2	84.0	67.9
Average Baseline*	84.0	82.4	69.2

* Average of four cycles

a conductivity additive in the electrolyte, momentarily increasing the circulation rate, or designing the battery for higher power by decreasing the internal resistance.

Low-temperature Study

In earlier studies, electrolytes based on 3.0 M ZnBr₂ and 0.5 M of a quaternary salt (either N-methyl, N-ethylpyrrolidinium bromide [MEP] or N-methyl,

N-ethylmorpholinium bromide [MEM]) were evaluated for low-temperature service. Adding 2 to 3 M calcium chloride (CaCl₂) extended the freezing point well below 0°C. Low-temperature studies during this contract were directed toward collecting information in two areas. First, it was important to determine how much the battery temperature could be reduced and still allow the battery to start a cycle. Once in action, a battery will generate enough heat to raise its own temperature significantly. Second, it was necessary to measure how low-temperature operation affects the battery performance.

Table 5-9. V1-50 Frequency Regulation Efficiencies

Cycle No.	Cycle Type	Coulombic Efficiency (%)	Voltaic Efficiency (%)	Energy Efficiency (%)	Transport Inefficiency (%)	Residual Inefficiency (%)
47	Baseline	87.1	80.8	70.4	8.9	6.1
51	SFRSR	77.0	84.2	64.8	17.9	5.1
52	SFRSR	78.6	83.6	65.7	14.8	6.6
53	Baseline	82.2	76.4	62.8	9.2	8.6
54	Baseline	76.0	79.3	60.3	16.1	7.9

Battery V1-50 was cycled in a cold chamber with load-leveling electrolyte containing 2.0 M CaCl₂. However, the AC pump motors supplied so much heat that the cold chamber was unable to cool the battery while it cycled. After allowing the battery to sit in the chamber overnight with the circulating pumps turned off, the battery temperature was reduced to -5°C. Some solids were seen in the electrolyte when the circulation was restarted. The temperature had risen to 10°C by the time the pumps were running smoothly enough to start the charge cycle. After an hour of charge, the voltage unexpectedly reached the high-voltage cutoff, and the cycle was terminated. Following this, no further work was done on low-temperature cycling.

Electrolyte Utilization Study

Battery V1-62 was used to study the effect of increased zinc utilization on efficiency. By increasing

the zinc utilization, the amount of electrolyte needed could be reduced and the battery weight lowered. The zinc utilization for a baseline cycle is 65.5%. The results in Table 5-10 indicate that there was only a slight decline in efficiency as the zinc utilization was increased. The effect of increased utilization on life expectancy of the battery was not investigated.

Stand Heating Study

When a charged zinc/bromine battery is allowed to stand, the bromine in the cell stack will slowly diffuse to the zinc electrode and chemically react with the electroplated zinc. The process has two effects. First, the battery is partially discharged, and second, the cell stack temperature increases from the chemical reaction and the lack of cooling. The electrolyte circulation is often turned off to limit the amount of bromine in the cell stack.

Table 5-10. Zinc Utilization Study for Battery V1-62

Zinc Utilization (%)	Coulombic Efficiency (%)	Voltaic Efficiency (%)	Energy Efficiency (%)	Transport Inefficiency (%)	Residual Inefficiency (%)
65.5	89.7	85.3	76.5	5.6	4.6
80.0	89.1	85.4	76.1	6.5	4.5
90.0	88.1	84.4	74.4	7.3	4.6

The effect of stand on capacity loss was measured previously by calculating the decrease in efficiencies for 8-cell stacks (see SAND99-1853). However, in cell stacks with only a few cells, the temperature increase will be less than in full-size stacks. Therefore, further tests were done with a 50-cell stack where the temperature increase caused by a stand could be measured.

A 50-cell stack was charged and put into stand several times. After each stand, the electrolyte leaving the battery stack increased for a short time when the pumps were restarted. Two tests showed temperature pulses of 9.5°C and 3.7°C, indicating that the stack was in fact warming during the stand period. The temperature of the electrolyte was probably somewhat less than the temperature of the interior of the battery. Also, the measurement was complicated by the presence of a gas bubble at the connections.

During the tests, the average transport loss was calculated in terms of a pseudo-current. The transport current during stand was about 0.05 A, while during a baseline cycle it was 0.084 A. This value was lower than during a normal baseline cycle because the quantity of bromine is slowly being depleted while the battery is standing.

Gas Generation at the Anode

Because hydrogen (H₂) gas accumulation has sometimes been observed in the sealed anolyte flow lines of test batteries, a beaker-scale test was performed to quantify the normal H₂ gassing rates on zinc electrodes. The beaker-scale tests were conducted using zinc/zinc metal electrode pairs in 0% state-of-charge (no Br₂) load-leveling electrolyte at pH 3.7. All gassing rate volumes were measured at atmospheric pressure.

The open-circuit H₂ gassing rate on fresh zinc metal electrodes was 3.2×10^{-3} ml/hr-cm². For a 50-cell battery stack with a 1175-cm² electrode area, this translates into a gassing rate of 189 ml/hr. A current density of 20 mA/cm² was imposed across a pair of zinc electrodes, resulting in a gassing rate of 5.5×10^{-2} ml/hr-cm². For a full-size, 50-cell battery stack, this rate would correspond to a fairly significant gas generation rate of 3200 ml/hr. The most likely source of this enhanced H₂ gassing is the slightly inefficient zinc electrodeposition current, which also caused a parasitic reduction reaction of water to hydrogen on the electrode. However, visual inspection seemed to indicate that some of the H₂ gassing was also occurring at

the discharging zinc electrode. This was perhaps a chemical reaction between freshly exposed high-surface-area zinc and water.

Factors that would be expected to increase gassing rates in batteries include areas of bare, exposed carbon plastic on zinc electrodes; electrolyte impurities; shunt-current-induced gassing; and increased temperatures (beaker-scale tests were conducted at room temperature). The gassing rates measured in the beaker-scale tests indicate that the zinc electrode is capable of producing a large amount of H₂ gas. This implies that water should have to be periodically added to the electrolyte. Each liter of hydrogen gas would require the electrochemical reduction of 1.6 ml of water. However, this was not usually required. Therefore, the unexpectedly high gassing rate results from beaker-scale testing will need to be examined using other tests.

Nonflow Zinc/Bromine Battery

A 16-run experiment designed to investigate the important parameters for nonflowing zinc/bromine batteries was completed. The factors studied included quaternary salt (quat) type, cathode layer thickness, charge rate, discharge rate, and zinc loading. Results indicated that none of the factors had a significant effect on the energy efficiency of the battery; however, some of these factors influenced hydrogen gas evolution. Using the factors that minimize hydrogen formation, the cell should perform at 80% energy efficiency and would be expected to give off 1.8 ml of hydrogen during a cycle.

The self-discharge of a single-cell, nonflow battery was examined by allowing a fully charged battery to stand for various lengths of time before discharging. A thermocouple was introduced into the anolyte gap to determine the amount of heat generated during stand. Results of the stand tests are given in Table 5-11. The battery temperature increased by less than 1°C during each of the stand loss tests.

Two other cell designs did not perform as well as the original. The first design, which incorporated an ion-exchange resin into the catholyte gap, gave about the same amount of transport as the original set of tests, but the residual losses were much higher (43.6%). An ion-exchange membrane used in place of the standard separator gave very high transport loss, 72.2% for the 24-hour stand. It is believed that the ion-exchange membrane was too thin to provide low self-discharge in a battery.

**Table 5-11. Energy Efficiencies for Single-cell
Nonflow Battery During Stand-Loss Cycling**

Stand Time (Hours)	Coulombic Efficiency (%)	Voltaic Efficiency (%)	Energy Efficiency (%)	Transport Inefficiency (%)	Residual Inefficiency (%)
0	88.0	90.0	79.2	10.3	1.7
24	56.4	84.1	47.4	38.5	5.1
61.3	21.6	78.4	16.9	70.7	7.8

Intentionally Left Blank

6. 2500-cm² Battery Design

Cell Stack Design

Using a computer-aided engineering design system, a new endblock for a 2500-cm² battery stack, to be made completely out of plastic, was designed. This design eliminates the need for aluminum inserts to maintain the dimensional stability of the battery stack. The goal was to minimize the thickness and weight of the parts while maintaining an acceptable level of stress and deflection under load. The drawings were changed to reflect the optimum design, and the injection molds were made.

Heating/Cooling Requirements

The cooling requirements of a zinc/bromine battery depend primarily on the efficiency of the battery in a particular application. This is because all of the heat generated in the battery comes directly from energy losses associated with running the battery. In this section, a background discussion of the thermodynamic efficiency will show that the practical limit of the battery's energy efficiency is about 82%. This will be followed by some observations of the cooling function of a large battery used in laboratory testing.

Thermodynamic Efficiency

Heat in the battery occurs through processes such as ohmic heating, electrode overvoltage, and Peltier heat. The first two effects are well known, while the third is much less familiar. Peltier heat is derived from the nature of the electrochemistry and can set a limit to the overall battery efficiency. The energy needed to drive (or given off by) a chemical reaction is the enthalpy (ΔH). Of this energy, only the free energy (ΔG) is available for electrochemical use. The remainder of the energy is tied to the entropy of the system (ΔS). In the following relationship, the enthalpy is related to free energy by the entropy.

$$\Delta H = \Delta G - T\Delta S$$

The term $T\Delta S$ is called "electrochemical Peltier heat." It is defined as the energy needed to maintain a constant temperature for an electrochemical reaction. The actual energy-loss mechanism results from a combination of solvation energies, electrolyte mixing, and

injection of electrons into the conduction bands of the electrode. The theoretical maximum energy efficiency is limited by the size of $T\Delta S$, and is determined by the ratio $\Delta G/\Delta H$. For zinc/bromine, the maximum energy efficiency is 91%.³

Independent measurement of the electrochemical Peltier heats for each electrode has been reported.⁴ In a further test, the efficiency of the electrode reactions under free discharge at steady state was measured. In this test, the electrodes were essentially shorted, except for the resistance of the ammeter in the connecting lead. The measured energy efficiency was 82%. This measurement included all three of the energy-loss terms mentioned previously, but did not include any losses caused by practical battery operation, such as shunt currents or separator resistance. Consequently, the 82% energy efficiency represents a reasonable ultimate goal to strive for in the laboratory.

It is well known that some batteries, such as the nickel/hydrogen battery, cool slightly when charging, and that the lead/acid battery does not get as hot as it could when discharging. These effects are the result of the electrochemical equivalent to heats of reaction (that is, when some salts are dissolved, the solution heats; and when other salts are used, the solution cools). The effect occurs for the zinc/bromine battery as well, and a first-order calculation of the heating and cooling has been done.

The electrochemical heat can be found by first looking at the thermoneutral potential,

$$E_t = -\Delta H/nF,$$

where n equals the moles of electrons and F is Faraday's constant. If the thermoneutral potential is below the reversible voltage, $E_r = -\Delta G/nF$, the battery will cool on discharge. If E_t is above the reversible voltage, the battery will cool on charge. The values of E_t and E_r for the zinc/bromine battery are 2.019 V and 1.818 V, respectively. The amount of heating or cooling is found by comparing the difference between the operating voltage and E_t . If they are equal at some point, there will be no electrochemical heating or cooling. Other factors are also important. The ohmic resistance, overvoltage losses, and self-discharge reaction always generate heat in the cell. The reaction of bromine with quaternary ions generates heat reversibly. When bromine is removed from the complex, the electrolyte is cooled.

A spreadsheet calculation shows that the heating and cooling processes offset each other to an extent, but more heating occurs on discharge than on charge. The electrochemical cooling process on charge is countered by the formation of the bromine complex. A reverse matching happens on discharge. The results of the spreadsheet calculations for a 25-A constant-current cycle are shown in Table 6-1, with the heat values given in watts (W). For comparison, the electrical power supplied to or received from the cell is also included.

The energy lost from the battery should be approximately equal to the heat generated. In a hypothetical 4-hour charge/3.5-hour discharge cycle, 100 Ah and 191.2 Wh will be put into each cell of the battery, and 87.5 Ah and 150.9 Wh will be taken out. These values are equivalent to 87.5% coulombic efficiency and 78.9% energy efficiency, which is a reasonable representation of actual laboratory data. The heat will be 18.64 Wh evolved during charge, and 30.63 Wh evolved during discharge. Finally, 40.31 Wh of electrical energy would be lost during the cycle, and 49.26 Wh of heat would be generated. Ideally, these two numbers should be equal, but considering all of the approximations made in this first order calculation, an 18% overestimation of the heat generated is quite reasonable.

The calculation shows that one-third of the total heat can be expected during charge, and two-thirds will come out during discharge. Therefore, the cooling system should be large enough to handle the higher rate of heating expected during discharge. The example above did not include heating from parasitic losses such as the pumps and shunt currents, which would need to be

included to calculate the total battery cooling requirement.

Practical Cooling Requirements

In a test using a 30-kWh V-design (1170-cm²) battery, a cooling ability of about 2 kW was sufficient to keep the temperature from rising during a baseline charge/discharge cycle. Data were taken from tests of a 200-cell battery made of four 50-cell stacks. All four cell stacks were connected to a single set of anolyte and catholyte reservoirs. The anolyte reservoir was cooled by water circulating through a plastic tubing heat exchanger. The cooling water was switched on whenever the anolyte temperature went above a preset temperature. In the three cycles tested, the temperature did not rise during the charge but did rise during two of the discharges.

The heat generated in the battery can be divided between the charge and discharge periods. It is estimated from previous calculations that about one-third of the heating occurs during charge. The heat capacity (C_p) of the battery is assumed to be about 0.9 Wh/kg°C (the C_p of water is 1.164 Wh/kg°C). The results listed in Table 6-2 show the calculation of the total heat during each cycle, how it was allocated to the charge and discharge portions of the cycle, and how some was taken up by the battery temperature increase. The final heating rates shown in Table 6-2 are also the effective rates of the water cooling system. No temperature increases were observed during charge. It is clear that up to a heating rate of 2.2 kW, the cooling system was adequate to hold the temperature constant. However, when the

Table 6-1. Calculated Heat* and Electrical Power in a Single Cell for a Constant-current Cycle at 25 A

	Charge @ -25 A	Discharge @ 25 A
Electrochemical, W	-2.69	7.37
Self-Discharge, W	2.02	2.02
Complex Formation, W	2.98	-2.98
Ohmic, W	2.34	2.34
Total Heat, W	4.66	8.75
Electric Power, W	47.79	43.10

* Negative sign indicates heat absorbed by the battery.

Table 6-2. Battery Cooling Requirements

	Cycle 3	Cycle 4	Cycle 5
Energy Charged, kWh	40.9	59.8	40.9
Efficiency, %	70.8	54.0	50.2
Temperature Increase During Discharge, °C	0	27.5	21.7
Total Heat Generated, kWh	12.0	27.5	20.4
Heat Removed in Charge, kWh	3.6	8.3	6.1
Heat Removed in Discharge, kWh	8.4	7.0	4.6
Heat for Battery Warming, kWh	0	12.2	9.7
Heating Rate in Charge, kW	0.8	1.3	1.4
Heating Rate in Discharge, kW	2.2	4.5	6.9

cooling demand was increased to 4.5 kW and higher, the battery temperature increased. Therefore, the cooling system as it was installed and operated had sufficient capacity to cool 2.2 kW but not 4.5 kW or higher discharges. The second two cycles were discharged at higher-than-baseline current, which explains the higher heating rates.

Environmental Impact

The literature was investigated to predict the environmental impact of zinc/bromine batteries. Some initial results are given here. The environmental effects could occur as the result of an accident while batteries or electrolyte were being transported or as the result of a serious mishap at an electric utility station. The immediate cause of an incident would be an uncontained spill of electrolyte. The electrolyte consists of an aqueous solution of zinc bromide, zinc chloride, bromine, and a quaternary ammonium ion compound, such as MEP or MEM.

Zinc Bromide and Zinc Chloride

Zinc bromide is a relatively benign salt with a relatively low toxicity. Zinc chloride is similar with respect to safety and environmental hazards. The U.S. Department of Transportation hazard notification level for zinc bromide spills is 1000 pounds.⁵ Once spilled, zinc bro-

mid remains highly soluble in water and will be readily diluted and rinsed away. Therefore, it would not be expected to remain at the spill site, but would be washed away with rainwater and normal hydrological conditions.

The biological effect of zinc bromide is primarily due to the zinc ions. At high levels, it is toxic to invertebrates and fish. The U.S. Environmental Protection Agency acute criteria (maximum) in soft water is 0.18 mg/l, and the chronic criteria (30-day average) is 0.047 mg/l. Typically, the toxic effects are decreased with increasing water hardness. In a test of the effect on furoid algae, a 50% reduction in growth rate was observed at zinc levels of 5 to 10 mg/l. Zinc is already present in the runoff water from many highways; levels of from 0.16 to 22 mg/l have been measured. Because it is rapidly diluted and carried away, it has not been a serious problem in the national watershed.⁶

Bromine

Bromine is a liquid at room temperature and pressure. It is widely used to sanitize swimming pools and spas. In the zinc/bromine battery, it is nearly completely in the form of a chemical complex formed with the quaternary amine complexing agents. The range of bromine dispersal is limited by the uptake of bromine. Even though the reactivity of the bromine is reduced by the complexing action, the bromine would be expected to oxidize most organic materials that it contacts. This

oxidation forms an innocuous bromide salt. Bromine also is readily absorbed into water, reacting to form soluble bromine as well as hypobromic acid and hydrobromic acid. Both are reactive, although less so than bromine.

Quaternary Ammonium Ion Salts

The environmental impact of the quaternary ammonium ion salts has not been directly determined. However, it is expected to be quite low. Similar compounds are used as sequestering agents in sewage treatment, and other derivatives are used in topically applied sunblocks.⁷

7. Battery System Design and Manufacture

Battery Stack Manufacturing

The 2500-cm² flow-frame injection mold die set was completed, and a number of flow frames, endblocks, and endblock covers were produced. Test stacks with six flow frames welded between two endblocks were manufactured from these parts. The weld integrity of the battery stacks was investigated by subjecting them to internal air pressure increasing at 1-psi increments each minute until the stack burst. The first two samples failed at 6 psi. In both cases, the center weld bead at the juncture between the first flow frame and the endblock was insufficiently welded.

Additional vents were then added to the injection mold die to allow the flow frame to be filled more evenly. A change in the gate arrangement was also made that was found to significantly reduce wrinkling at both ends of the center weld bead.

The next set of testing was done on two 8-cell, 2500-cm² battery stacks. One stack was prepared with the standard flow frames, while the other stack was manufactured using flow frames that were highly packed during the injection molding process. Each of these stacks burst at about 17 psi. The failure in each case was between the first flow frame and the endblock. It was believed that these failures were caused by a slight taper in the endblock.

The edges of the endblocks at the welded face are tapered, causing welding to occur only at the extreme outer edges before the remaining weld beads make contact. To compensate for this, the first flow frame welded to the endblock, and the final weld need to be welded down farther than normal. It is hoped that the taper associated with the endblocks can be minimized in the injection-molding process; however, it appears that vibration welding can still be accomplished with careful attention to the process.

Another set of burst tests was performed on stacks in which the first frames connected to the endblocks were overwelded. This was done to compensate for the endblock tapering. These stacks failed at about 20 to 22 psi, and the failures were along the side edge of the stack as opposed to the top. This burst pressure (20 to 22 psi) is what should be achieved if endblock parts without any taper can be produced.

Following initial burst testing of the battery stacks, the endblock mold was modified from a hot-manifold type to a three-plate mold. The purpose of this change was to eliminate the remaining variation in thickness at the edges of the part. Also, a new blowing agent was used in quantities of 0.25% to 0.75% to produce a finer pore structure. The next set of endblocks received from the vendor was markedly improved in appearance. The flared edges on the perimeter of the endblocks (both detailed and nondetailed endblocks) were reduced, but remained to a small extent.

The battery stacks built with the improved endblocks held up to 25 psi before bursting, and the failure was attributed to tooling misalignment in the center of the battery. Despite this misalignment, the burst pressure was within the range required for actual battery operation. These batteries burst at approximately the same pressure as the batteries made when the endblocks were welded very deeply. The fracture point was no longer at the weld between the endblocks and the first or last flow frame; it was between flow frames. The 25-psi burst pressure may be the limit for this type of battery stack. Under normal operating conditions, the battery stack observes a pressure of 7 to 8 psi, so a safety factor of about 3 is built into the battery stacks.

Several problems were discovered after the post-mortem analysis of the first 2500-series battery stacks. Additional seals needed to be added to the diverters and vanes, and the heights of existing seals were increased to improve the distribution of second-phase. The leakage problem was minimized by reducing sink marks during the injection molding process. Poor-quality welds in the area where weld beads cross a flow channel on the adjacent frame were improved by adding additional weld beads in this area.

Scaling up from 8-cell stacks to 60-cell stacks uncovered an additional problem with slippage of the endblock in the vibration-welding machine. The endblock tooling for the welder was modified to minimize the slippage during the manufacture of 60-cell stacks. Also, minor problems with the vibration welder surfaced during development, but modifications were made to eliminate the errors and to improve the consistency of the process.

2-kWh Control Station

A 2-kWh control station was designed as a prototype for controlling the 33-kWh modules to be used in the 100-kWh deliverable. The battery stack contained eight cells with an electrode area of 2500 cm². Directly coupled pumps/motors were tested, but displayed seal failure resulting in corrosion of the motor. Magnetically coupled pumps were installed to eliminate this failure. The 2-kWh station pumps and reservoirs were equipped with centrifugal pumps mounted vertically inside a recessed area in the cover of the electrolyte reservoirs. This was done to keep most of the plumbing inside of the reservoirs and to eliminate the need to prime the pumps.

The control station for the 8-cell, 2500-cm² battery was manufactured to demonstrate the viability of a fully automated battery system. Three pumps with AC motors were used for controlling the addition of second-phase and for circulating the aqueous catholyte and the anolyte. The second-phase was delivered to the intake of the aqueous catholyte pump during discharge and remained off during charge. Liquid levels were adjusted by modifying the speeds of the anolyte and catholyte motors. The second-phase motor was also controlled by the programmable logic controller (PLC). Most of the plumbing components were made of rigid Kynar™ and flexible Viton™. The reservoirs for the deliverable were constructed from rectangular polyethylene tanks.

A microprocessor controller was used to coordinate the operation and safety monitoring of the system. Voltage, current, liquid level, and leak data were converted to 24-V signals and sensed by the PLC. Temperature data were converted in a similar manner, but were monitored by a commercially available electronic package.

Charge and discharge currents were controlled by power metal-oxide semiconductor field-effect transistors (MOSFETs) that are switched either on or off by the PLC. They are also capable of controlling the direction of the current. Therefore, a fully charged battery does not need to be electrically isolated because the discharge circuit would be enabled, allowing only discharge to occur.

100-kWh Deliverable Battery Design

A chief design objective for the proposed 100-kWh battery station was that it operate independently of external controls. It would have to be a stand-alone system with internal controls and safeguards that would enable fail-safe cycling. The battery system would be

completely self-contained. The pump rates and electrolyte levels would be self-adjusting. Power for all of the parasitic systems such as cooling, controls, and electrolyte circulation would be taken from the battery system itself. If any electrolyte should leak, it would be contained within an outer shell and collect in a water-tight basin at the bottom.

The original 100-kWh deliverable battery proposal consisted of six battery stacks, two electrolyte reservoirs, and a support structure. The battery system was to be tested using a cycling unit at SNL. The statement of work for the contract was changed to call for delivery of a self-contained, stand-alone peak-shaving system to be connected to a utility grid. A three-module configuration, each module having individual reservoirs and circulation systems, was selected so that the battery modules could be electrically connected in both series and parallel arrangements. Details of the 100-kWh battery design and progress in the manufacture of the system are discussed below.

The demonstration unit consists of a 100-kWh stand-alone system housed in a portable chemical storage vault. It contains three battery modules, each rated at 33 kWh for a two-hour discharge. Each module consists of two 60-cell, 2500-cm² battery stacks connected in parallel, a pair of reservoirs, and an electrolyte circulation system as shown in Figure 7-1. A dry module weighs more than 700 pounds, and more than 1800 pounds when filled with electrolyte. Features allowing transport by forklift were incorporated into the modules. A finite-element analysis was run on the structure to ensure adequate strength, and the final design was reviewed by an outside consultant for verification.

The three modules are housed in a 9'1" × 8'6" × 8'3" HazMat building. The system is designed to sustain a 200-A discharge at an average of 250 V for two hours. Heat exchangers, a bromine scrubber, and electrical panels are located in an isolated quadrant in the building. The building contains a spill containment sump in addition to those for the individual modules. Additional safety devices in the building include bromine and hydrogen sensors, and an accelerometer for earthquake detection. The layout of the 100-kWh building, including battery modules and the isolated area for the heat exchanger and scrubber, is shown in Figure 7-2. A more detailed drawing of the battery module is provided in Figure 7-3.

The battery system is designed to comply with Zone 4 earthquake requirements, which are considered the most restrictive national guidelines. This is accomplished by using an epoxy-coated steel frame to support each module, with the reservoirs inserted into the structure of the frame and the two battery stacks located

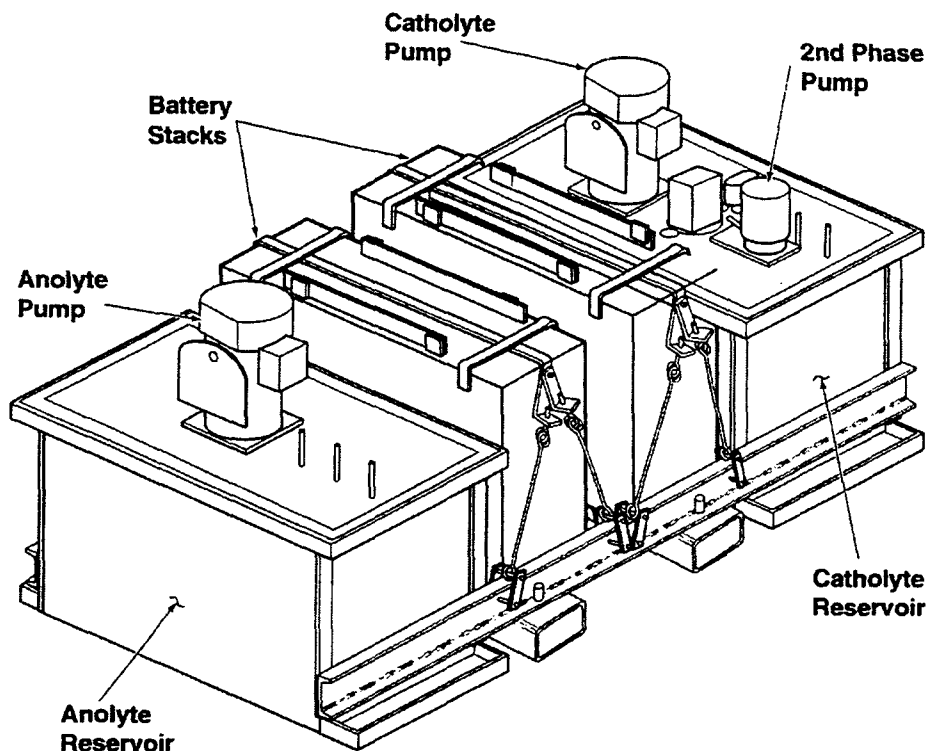


Figure 7-1. Depiction of a 33-kWh Battery Module.

between the reservoirs. The stacks are attached to the frame by plastic-coated steel cords that will restrain the stacks in the x, y, and z directions in case of an earthquake.

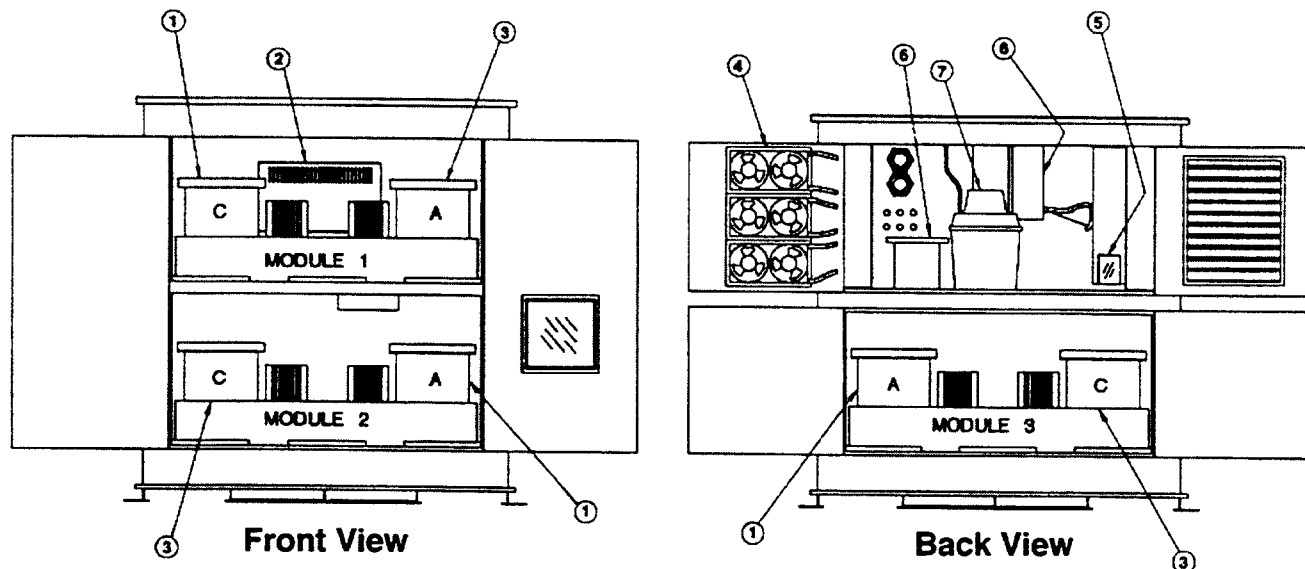
Each reservoir accommodates a recessed sump area in the cover where the pumps are located. The anolyte reservoir uses one pump, while two pumps are used to circulate both the catholyte-aqueous and complexed-bromine phases. Brushless DC motors run centrifugal pumps that are mounted vertically inside the recessed area in the reservoir covers. The inlets to the pumps are located below the liquid level in the reservoirs, which eliminates the need to prime the pumps. The majority of the plumbing is fused polyvinylidene fluoride, which is located inside the reservoir to minimize leakage from the system. Any minor leaks from this plumbing will be contained inside the reservoirs.

The plumbing from the reservoirs to the stacks is composed of reinforced Viton™, which was chosen because of its flexibility. The entire module is located inside of a larger spill tray, which can contain any minor leaks from the system.

Liquid-level sensors are located at the top of each reservoir. The analog sensors are accurate to 0.25 inches and supply data to the battery controller. The data are used to maintain constant electrolyte levels in each reservoir by adjusting pump motor speeds. Leak sensors are located in the module spill tray and in each reservoir sump area. They will indicate minor leaks of electrolyte into either location.

The 100-kWh system is designed so that batteries can be electrically connected in either parallel or series configurations. Each module has an open-circuit voltage of 109 V. The battery system specifications are given in Table 7-1.

An extensive data collection system was developed to verify the need for battery subsystems. Parasitic losses from the pumps, heat exchanger, and control systems can be quantified, and a paging system, which is automatically activated in the case of a potentially hazardous condition, were installed. An internal load-management system was integrated into the system by running all of the auxiliary equipment, such as the heater, scrubber, etc., off a 30-A circuit. For example, if the scrubber needs to be activated, the heater will automatically be disconnected from the circuit to maintain the 30-A load.



NO.	PART	REF. NO.
1	ANOLYTE RESERVOIR	10103
2	HEATER	10021
3	CATHOLYTE RESERVOIR	10103
4	HEAT EXCHANGER	10069
5	GAS ANALYZER	10127
6	FIRE SUPPRESSION	10021
7	SCRUBBER	ZBB
8	HEAT EXCHANGER RESERVOIR	10103

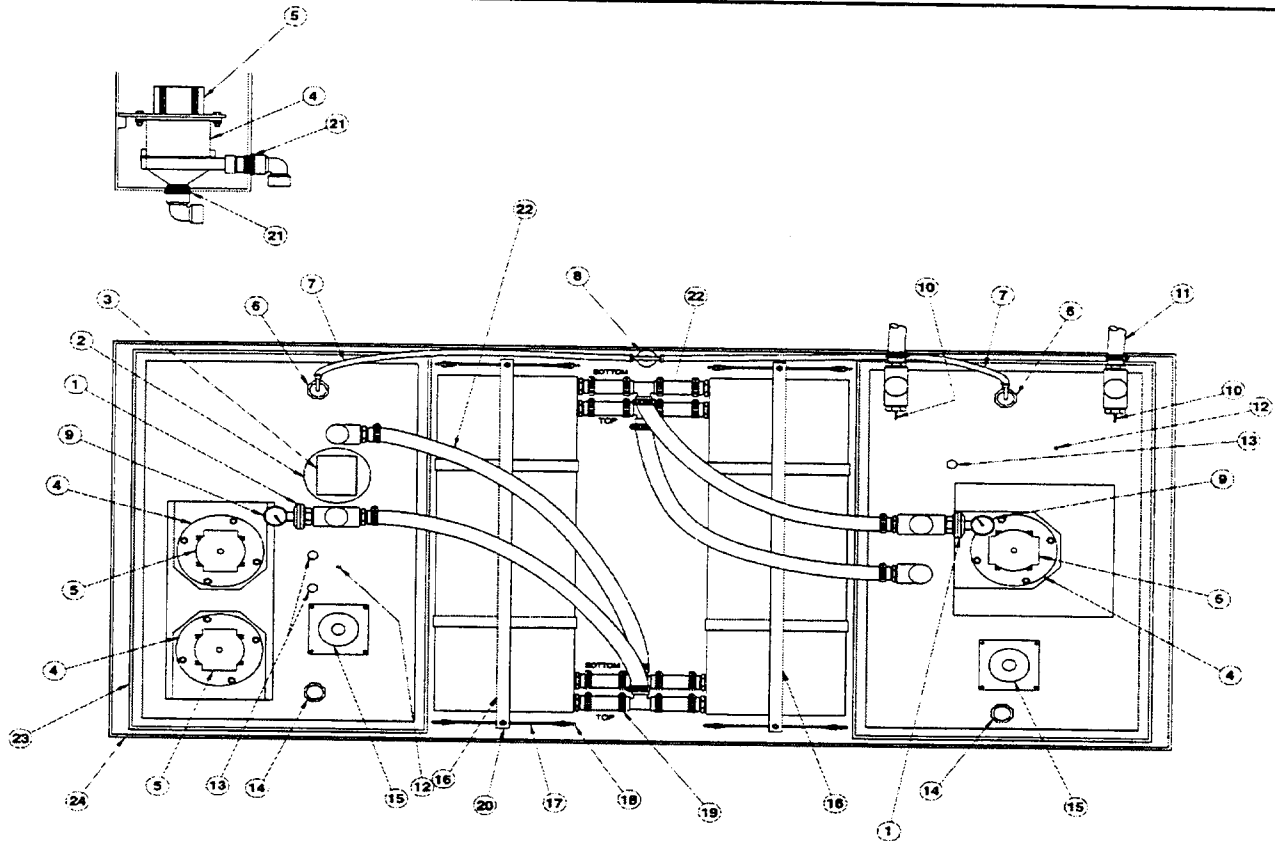
Figure 7-2. Front and Back Views of the 100-kWh HazMat Building.

Battery Controller and Software

A separate PLC monitors and controls each battery module. Each PLC has 2 KB of user memory and is capable of data acquisition through a full-duplex RS232C serial port. The PLCs monitor module voltage, stack current, pump motor currents, and electrolyte levels in the module reservoirs. The PLCs compare the measured parameters to preset limits to determine if the battery modules are performing properly. If the measured parameters fall outside the preset norms, the PLCs will adjust variables, such as pump speed, to compensate. If the measured parameters cannot be modified, the PLCs will generate either a "FAULT" or "SHUTDOWN" condition and proceed to turn off the system. A "FAULT" condition causes the battery to be discon-

nected from the power conversion system (PCS). A "SHUTDOWN" condition gives the same result as the "FAULT" condition, but the entire system, including pumps, shuts down.

An additional PLC (the system controller) coordinates the overall operation and safety of the system. This controller monitors system parameters such as electrolyte temperatures, bromine and hydrogen concentrations inside the building, building temperature, ambient temperature, peripheral current, and seismic activity. If a potentially hazardous condition (to the system and/or its surroundings) is sensed, the controller will completely shut down the system. Conditions that would result in a complete shutdown of the system include an electrolyte or coolant leak, an earthquake, or high levels of bromine.



NO.	PART	REF. NO.
1	GAUGE GUARD	10039
2	4-WAY VALVE	ZNBR 089
3	ACTUATOR	10039
4	PUMP	10001
5	MOTOR	10117
6	VENT CAP	10039
7	1/4" VENT TUBE	10071
8	BROMINE FILTER	10016
9	PRESSURE GAUGE	10039
10	WATER THERMISTOR	10087
11	COOLANT HOSE	10037
12	THERMISTOR	10087
13	BURP CAP	
14	FILL PORT	10039
15	FLOAT	10122
16	BATTERY HOLD DOWN (SEE DRAWING)	ZNBR 144
17	HOLD DOWN CABLE	10037
18	EYE BOLT	10037
19	HOSE CLAMP	10040
20	EYE BOLT	10037
21	VITON O-RING	10026
22	3/4" ID VITON HOSE	10025
23	RESERVOIR	10103
24	SPILL TRAY	

Figure 7-3. Detailed View of 33-kWh Battery Module.

Table 7-1. 100-kWh Battery Specifications

	Typical	(Maximum)
Charge Voltage	360 V	(378 V)
Charge Current	100 A	(150 A)
Open Circuit Voltage	328 V	
Discharge Current	100 A	(200 A)
Low Voltage Cutoff	180 V	
Strip Current Cutoff	0.5 A	

Microsoft Windows™-based software monitors the performance of the system. The PLCs monitoring the battery system send data over RS232C serial lines to a personal computer. Various screens generated by the software display the information collected by the monitoring PLCs. This information includes parameters such as module and system voltage and current, electrolyte pump speeds, temperatures, seismic activity, hydrogen and bromine gas concentrations, and parasitic load conditions. The information is saved on the personal computer's hard disk to be recalled at a later date. It can be presented in either a tabular or graphical format.

The software allows the operator to manually change the speed of the various pumps in the system and to manually shut down the system if necessary. If the system is shut down or halted either manually or by the PLCs controlling the system, the software, through a modem connected to the personal computer, will notify key personnel via personal pagers.

The software that controls the 100-kWh battery system is also Windows-based and is provided on a disk that can be used to install the software on any personal computer. The software gives the user the ability to monitor battery voltage, current, and state of charge.

100-kWh Battery System Manufacturing

Four 33-kWh battery modules, each consisting of two battery stacks, two reservoirs, and a circulation system, were manufactured. Three of the modules were used for the 100-kWh battery deliverable, and one additional module was used as a backup.

An Ansul-certified fire-suppressant system was installed in the 100-kWh building. The system consists of a dry chemical and a propellant that distributes the chemical to each of the four quadrants in the building. The system will be activated automatically by excessive heat in any of the quadrants, or it can be activated manually from outside the building. Also, a heater and heat exchanger were installed so that the battery system could be operated in cold or hot weather.

Three 33-kWh battery modules were installed in the 100-kWh building. Also, the other major components of the system (heat exchanger, scrubber, etc.) were installed and tested. Before initiating the battery test plan, a number of preliminary steps were taken. Communication between the personal computer and all four PLCs was established. The voltage and current sensors for the modules and the gas sensor monitor were calibrated. Finally, control of the batteries, pumps, scrubber, and heat exchanger was verified using the personal computer.

Short cycling of the modules through a cycling unit and later through the PCS was initiated for calibration purposes and to test fault conditions such as overcharge, overvoltage, and bromine detection. Noise in the system caused periodic system shutdowns, which resulted in initial delays in qualifying the battery system. Methods were developed to electrically isolate the battery; this electrical isolation allowed the PLCs to consistently read battery voltages without being affected by the noise from the PCS.

Once the noise problem was eliminated, all the safety protection features were entered into the system. The fault and shutdown conditions given in Table 7-2 were used to verify that the protection features of the zinc/bromine battery were functioning. Each event was

Table 7-2. Fault and Shutdown Conditions for 100-kWh Battery

Fault Condition	Shutdown Conditions
Overvoltage in Charge	Loss of 120 V, 30 A Supply
Overcurrent in Charge	Bromine Detection
Door Open	Accelerometer
Hydrogen Detection	Leak Detection
Above Maximum Temperature	Level Sensors Off
Below Minimum Temperature	Fire

documented by hard-copy printout as well as on the hard disk of the personal computer.

Originally, reaching the low-voltage cutoff was also considered a fault condition. However, instead of treating it as a fault condition, the response to a low-voltage cutoff was changed to open the DC contactor and connect the batteries to resistor banks so that the batteries could be stripped. However, before the batteries are put into strip, all battery modules must be within a specified voltage window.

The following is a list of the responses that occurred when a fault condition was observed:

1. Pump motors remain on.
2. DC contactor opens.
3. Alarm light turns on.
4. Test manager is paged.
5. Fault indicator to PCS opens.
6. Alarm screen appears on battery monitoring PC.
7. Alarm horn on battery-monitoring PC sounds.
8. Event is recorded to the PC hard disk.
9. Event is sent to the printer.
10. All subsequent operator actions are recorded to the PC hard disk.
11. All subsequent operator actions sent to the printer.

The following is a list of the responses that occurred when a shutdown condition was observed:

1. Pump motors are turned off.
2. Horn sounds.
3. Alarm light turns on.
4. Both louvers close.
5. Scrubber turns on.
6. Test manager is paged.
7. DC contactor opens.
8. Fault indicator to PCS opens.
9. Fault indicator to utility opens.
10. Alarm screen appears on the battery monitoring PC.
11. Alarm horn on battery monitoring PC sounds.
12. Event is recorded to the PC hard disk.
13. Event is sent to the printer.
14. All subsequent operator actions are recorded to the PC hard disk.
15. All subsequent operator actions sent to the printer.
16. The heat exchanger is turned off.

The shutdown conditions for a fire within the building were also modified. In the event of a fire, all power is removed from the system and a warning bell is activated.

Once testing of the batteries was initiated, some problems were encountered that resulted from erratic currents through individual battery stacks. The cause of these problems appeared to be the inability to strip the batteries following discharge. Because of this, the batteries were not all at the same state of charge at the beginning of each cycle. Individual stack currents became more inconsistent on each subsequent cycle. Strip resistors for each of the three battery modules and

electrical contactors that switch from the PCS to the resistor banks, were installed inside the 100-kWh building. The ability to strip the batteries improved the performance of the system. Once the system was running properly, all the battery stacks were replaced with new stacks to complete the battery test plan. The complete test plan, including a description of the acceptance testing procedures, and the results of the testing are described in a subsequent report.

8. Summary and Conclusions

In Phase 2 of the contract, zinc/bromine battery technology was greatly improved in both safety and performance. The unique, sealed cell stack has been shown to be leak-free when properly designed and manufactured. Improved properties of the base components of the battery (electrode substrate, terminal electrode, cathode layer, and separator) have increased the efficiencies of 8-cell battery stacks to greater than 80% energy efficiency on baseline cycling. Life expectancies have also been dramatically increased. A number of batteries have achieved greater than 500 baseline cycles with less than 10% degradation in performance. One battery stack cycled more than 1000 times.

The size of the battery stack was increased from 1170 cm² to 2500 cm² for utility applications. Some problems were encountered with several of the first larger-sized battery stacks, but the majority of these problems were overcome by redesigning the injection molds and improving welding techniques. Battery stacks, both 8-cell and 60-cell, have achieved over 77% energy efficiency on baseline cycling.

Additional testing was performed during the course of the contract. No-strip cycling demonstrated increased energy efficiency compared to baseline cycles.

Overvoltage and IR testing showed that recent batteries are lower in resistance and that the cathode layer has been improved. Batteries have been discharged over three-to-six-hour rates with very little variation in performance. Finally, a process that appears to recondition battery electrodes has been identified. This process has decreased electrode overvoltage and extended the life expectancy of the battery.

Alternative bromine complexing agents were examined, and one was found to give slightly better performance than the standard material. Some quaternary amines, which form very strong complexes with bromine, were found to perform poorly in zinc/bromine batteries.

A 100-kWh stand-alone zinc/bromine battery system was manufactured, and testing of the system was initiated. The system contains three separate modules, each consisting of two battery stacks, two reservoirs, and an electrolyte circulation system. Many changes were made from the original design to obtain a system (battery and PCS) that needs minimal operator involvement.

Testing of the 100-kWh battery and PCS are documented in a subsequent report.

8. SUMMARY AND CONCLUSIONS

Intentionally Left Blank

9. References

1. J. W. Braithwaite, J. M. Freese, and A. A. Akhil, "Draft Standard SES-Battery Test Procedure," Sandia National Laboratories memorandum, May 28, 1991.
2. R. J. Bellows and P. G. Grimes, "Zinc/Halogen," in *Power Sources for Electric Vehicles*, p. 621, B. D. McNicol and D. A. J. Rand, eds., Elsevier Science Publishing Co., 1984.
3. H. F. Gibbard, "Thermal Properties of Battery Systems," in *J. Electrochem. Soc.*, Vol. 125, p. 353, 1978.
4. V. S. Donepudi and B. E. Conway, "Electrochemical Calorimetry of the Zinc and Bromine Electrodes in Zinc-Bromine and Zinc-Air Batteries," in *J. Electrochem. Soc.*, Vol. 131, p. 1477, 1984.
5. 40 CFR 302, EPA Designated Reportable Quantities, May 13, 1991.
6. T. V. Dupuis, et al., *Effects of Highway Runoff on Receiving Waters, Vol III: Resource Document for Environmental Assessments*, Federal Highway Administration Report No. FHWA/RD-84/064, Rexnord, Inc., 1985.
7. C. Anselmi, "Staying on the Surface," in *Chemtech*, p. 99, February 1992.
8. P. C. Butler, Eidler, P.A., Grimes, P.G., Klassen, S.E., and Miles, R.C., "Zinc/Bromine Batteries," Chapter 37 of *Handbook of Batteries*, ed. D. Linden, McGraw-Hill, Inc., New York, 1995.

9. REFERENCES

Intentionally Left Blank

10. Publications

P. J. Lex and P. A. Eidler. "Demonstration of a 100 kWh Peak Shaving Zinc/Bromine Utility Battery," *Proceedings of the 5th International Conference, Batteries for Utility Energy Storage*, San Juan, Puerto Rico, July 1995.

P. Eidler, P. Lex, J. Bolstad, and R Miles. "The Zinc/Bromine Battery For Utility Storage Applications," *Proceedings of the 4th International Conference, Batteries for Energy Storage*, Berlin, Germany, September 1993.

P. J. Lex and J. F. Mathews. "Recent Developments in Zinc/Bromine Technology at Johnson Controls." presented at the 35th International Power Sources Symposium, Cherry Hill, NJ, June 22-25, 1992.

10. PUBLICATIONS

Intentionally Left Blank

Distribution

Bob Weaver
777 Wildwood Lane
Palo Alto, CA 94303

Eric Rudd
35 Harmon Ave
Painesville, OH 44077

Robert W. Fenn
6335 Coleridge Road
Painesville, OH 44077

Per Danfors
ABB Power T&D Co., Inc.
16250 West Glendale Drive
New Berlin, WI 53151

Hans Weinerich
ABB Power T&D Co., Inc.
1460 Livingston Ave.
P.O. Box 6005
North Brunswick, NJ 08902-6005

Jim Balthazar
Active Power
11525 Stonehollow Dr.
Suite 255
Austin, TX 78758

Robert Wills
Advanced Energy Systems
Riverview Mill
P.O. Box 262
Wilton, NH 03086

B. Tiedeman
Alaska State Div. of Energy
333 West Fourth Ave.
Suite 220
Anchorage, AK 99501-2341

Percy Frisbey
Alaska State Div. of Energy
333 West Fourth Ave.
Suite 220
Anchorage, AK 99501-2341

P. Crump
Alaska State Div. of Energy
333 West Fourth Ave.
Suite 220
Anchorage, AK 99501-2341

Michael L. Gravely
American Superconductor Corp.
8371 Bunchberry Court
Citrus Heights, CA 95610

C. Shih
American Elec. Pwr. Serv. Corp.
1 Riverside Plaza
Columbus, OH 43215

Christopher G. Strug
American Superconductor Corp.
Two Technology Drive
Westborough, MA 01581

Meera Kohler
Anchorage Municipal Light & Pwr
1200 East 1st Avenue
Anchorage, AK 99501

Tim Ball
Applied Power Corporation
Solar Engineering
1210 Homann Drive SE
Lacey, WA 98503

Ralph M. Nigro
Applied Energy Group, Inc.
46 Winding Hill Drive
Hockessin, DE 19707

Christian St-Pierre
ARGO-TECH Productions, Inc.
Subsidiary of Hydro-Quebec
1580 de Coulomb
Boucherville, QC J4B 7Z7
CANADA

Gary Henriksen
Argonne National Laboratories
9700 South Cass Avenue
CTD, Bldg. 205
Argonne, IL 60439

Ira Bloom
Argonne National Laboratories
9700 South Cass Avenue
CTD, Bldg. 205
Argonne, IL 60439-4837

Herb Hayden
Arizona Public Service
400 North Fifth Street
P.O. Box 53999, MS8931
Phoenix, AZ 85072-3999

Ray Hobbs
Arizona Public Service
400 North Fifth Street
P.O. Box 5399, MS8931
Phoenix, AZ 85072-3999

Robert Hammond
Arizona State University East
6001 S. Power Rd.
Bldg. 539
Mesa, AZ 85206

Edward C. Kern
Ascension Technology, Inc.
P.O. Box 6314
Lincoln, MA 01773-6314

Greg Kern
Ascension Technology, Inc.
4700 Sterling Drive
Unit #
Boulder, CO 80301

Rick Lawrence
AVO International
P.O. Box 9007
Valley Forge, PA 19485-1007

Glenn Campbell
Babcock & Wilcox
P.O. Box 785
Lynchburg, VA 24505

Richard L. Hockney
Beacon Power Corp.
6 Gill St.
Woburn Industrial Park
Woburn, MA 01801-1721

Michael L. Bergey
Bergey Windpower
2001 Priestley Avenue
Norman, OK 73069

Klaus Kramer
Berliner Kraft und Licht (BEWAG)
Stauffenbergstrasse 26
1000 Berlin 30
GERMANY

Massoud Assefpour
BHP Research & Tech Dev.
600 Bourke Street
Melbourne Victoria, 3000
AUSTRALIA

Samuel B. Wright
Boeing
Inform., Space & Defense Sys.
P.O. Box 3999 MS 82-97
Seattle, WA 98124-2499

Gerald W. Braun
BP Solarex
630 Solarex Court
Frederick, MD 21703

Salim Jabbour
Business Management Consulting
24704 Voorhees Drive
Los Altos Hills, CA 94022

Dr. Les Holden
C&D Charter Pwr. Systems, Inc.
Washington & Cherry Sts.
Conshohocken, PA 19428

Larry S. Meisner
C&D Powercom
1400 Union Meeting Road
P.O. Box 3053
Blue Bell, PA 19422-0858

Dr. Sudhan S. Misra
C&D Technologies
Washington & Cherry Streets
Conshohocken, PA 19428

Jon Edwards
California Energy Commission
1516 Ninth Street, MS-46
Sacramento, CA 95814

J. Holmes
California State Air Resc. Board
Research Division
P.O. Box 2815
Sacramento, CA 95812

Pramod P. Kulkarni
California Energy Commission
Research & Dev. Office
1516 9th Street, MS43
Sacramento, CA 95814-5512

Rod Boucher
Calpine Corporation
50 W. San Fernando
Suite 550
San Jose, CA 95113

Tom Lovas
Chugach Elec. Association, Inc.
5601 Minnesota Dr.
P.O. Box 196300
Anchorage, AK 99519-6300

John Cooley
Chugach Elec. Association, Inc.
P.O. Box 196300
Anchorage, AK 99519-6300

M. Lebow
Consolidated Edison
4 Irving Place
New York, NY 10003

N. Tai
Consolidated Edison
4 Irving Place
New York, NY 10003

R. Stack
Corn Belt Electric Cooperative
P.O. Box 816
Bloomington, IL 61702

R. B. Sloan
Crescent EMC
P.O. Box 1831
Statesville, NC 28687

J. Michael Hinga
Delphi Energy & Engine
Management Systems
P.O. Box 502650
Indianapolis, IN 46250

Bob Galyen
Delphi Energy. & Engine
Management Systems
P.O. Box 502650
Indianapolis, IN 46250

Bob Rider
Delphi Energy & Engine
Management Systems
P.O. Box 502650
Indianapolis, IN 46250

Joseph J. Iannucci
Distributed Utility Associates
1062 Concannon Blvd.
Livermore, CA 94550

Alan Collinson
EA Technology Limited
Chester CH1 6ES
Capenhurst, England
UNITED KINGDOM

Jim DeGruson
Eagle-Picher Industries, Inc.
C & Porter Street
Joplin, MO 64802

M. Stanton
East Penn Manufact. Co., Inc.
Deka Road
Lyon Station, PA 19536

Daniel R. Bruck
ECG Consulting Group, Inc.
55-6 Woodlake Road
Albany, NY 12203

Steve Eckroad
Elec. Pwr. Research Institute
P.O. Box 10412
Palo Alto, CA 94303-0813

Robert Schainker
Elec. Pwr. Research Institute
P.O. Box 10412
Palo Alto, CA 94303-0813

Steve Chapel
Elec. Pwr. Research Institute
P.O. Box 10412
Palo Alto, CA 94303-0813

Phillip C. Symons
Electrochemical Engineering
Consultants, Inc.
1295 Kelly Park Circle
Morgan Hill, CA 95037

Dave Feder
Electrochemical Energy
Storage Systems, Inc.
35 Ridgedale Avenue
Madison, NJ 07940

Michael Dodge
Electrosource
P.O. Box 7115
Loveland, CO 80537

Harald Haegermark
Elforsk-Swedish Elec Utilities R&D Co
Elforsk AB
Stockholm, S-101 53
SWEDEN

Chuck Whitaker
Endecon Engineering
2500 Old Crow Canyon Road
Suite 220
San Ramon, CA 94583

Jennifer Schilling
Energetics, Inc.
501 School Street SW
Suite 500
Washington, DC 20024

Phil DiPietro
Energetics, Inc.
501 School Street SW
Suite 500
Washington, DC 20024

Paula A. Taylor
Energetics, Inc.
7164 Gateway Drive
Columbia, MD 21046

Mindi J. Farber De Anda
Energetics, Inc.
501 School Street SW
Suite 500
Washington, DC 20024

Howard Lowitt
Energetics, Inc.
7164 Gateway Drive
Columbia, MD 21046

Rich Scheer
Energetics, Inc.
501 School Street SW
Suite 500
Washington, DC 20024

Laura J. Johnson
Energetics, Inc.
7164 Gateway Drive
Columbia, MD 21046

Greg J. Ball
Energy & Env. Economics, Inc.
353 Sacramento Street
Suite 1540
San Francisco, CA 94111

Amber Gray-Fenner
Energy Communications Consulting
7204 Marigot Rd. NW
Albuquerque, NM 87120

Dale Butler
EnerTec Pty. Ltd.
349 Coronation Drive
PO Box 1139, Milton BC Old 4044
Auchenflower, Queensland, 4066
AUSTRALIA

Robert Duval
EnerVision
P.O. Box 450789
Atlanta, GA 31145-0789

David H. DaCosta
Ergenics, Inc.
247 Margaret King Avenue
Ringwood, NJ 07456

Erik Hennig
EUS GmbH
MunscheidstraBe 14
Gelsenkirchen, 45886
GERMANY

John Breckenridge
Exide Electronics
8609 Six Forks Road
Raleigh, NC 27615

J. Mills
Firing Circuits, Inc.
P.O. Box 2007
Norwalk, CT 06852-2007

James P. Dunlop
Florida Solar Energy Center
1679 Clearlake Road
Cocoa, FL 32922-5703

Steven J. Durand
Florida Solar Energy Center
1679 Clearlake Road
Cocoa, FL 32922-5703

Steven Kraft
Frost & Sullivan
2525 Charleston Road
Mountain View, CA 94043

Dave Coleman
Frost & Sullivan
2525 Charleston Road
Mountain View, CA 94043

Bob Zrebiec
GE Industrial & Pwr. Services
640 Freedom Business Center
King of Prussia, PA 19046

Nick Miller
General Electric Company
1 River Road
Building 2, Room 605
Schenectady, NY 12345

Declan Daly
General Electric Drive Systems
1501 Roanoke Blvd.
Salem, VA 24153

Gerry Woolf
Gerry Woolf Associates
17 Westmeston Avenue
Rottingdean, East Sussex, BN2 8AL
UNITED KINGDOM

Anthony B. LaConti
Giner, Inc.
14 Spring Street
Waltham, MA 02451-4497

George Hunt
GNB Tech. Ind. Battery Co.
Woodlake Corporate Park
829 Parkview Blvd.
Lombard, IL 60148-3249

Joe Szymborski
GNB Tech. Ind. Battery Co.
Woodlake Corporate Park
829 Parkview Blvd.
Lombard, IL 60148-3249

Sanjay Deshpande'
GNB Technologies
Woodlake Corporate Park
829 Parkview Blvd.
Lombard, IL 60148-3249

John Boehm
GNB Tech. Ind. Battery Co.
Woodlake Corporate Park
829 Parkview Blvd.
Lombard, IL 60148-3249

Steven Haagensen
Golden Valley Elec. Assoc., Inc.
758 Illinois Street
P.O. Box 71249
Fairbanks, AK 99701

Ben Norris
Gridwise Engineering Company
121 Starlight Place
Danville, CA 94526

Clyde Nagata
Hawaii Electric Light Co.
P.O. Box 1027
Hilo, HI 96720

George H. Nolin
HL&P Energy Services
P.O. Box 4300
Houston, TX 77210-4300

Carl D. Parker
ILZRO
2525 Meridian Parkway
P.O. Box 12036
Research Triangle Park, NC 27709

Patrick Moseley
ILZRO
2525 Meridian Parkway
P.O. Box 12036
Research Triangle Park, NC 27709

Jerome F. Cole
ILZRO
2525 Meridian Parkway
PO Box 12036
Research Triangle Park, NC 27709

Ron Myers
Imperial Oil Research Centre
3535 Research Road NW
Room 2E-123
Calgary, Alberta, T2L 2K8
CANADA

Ken Belfer
Innovative Power Sources
1419 Via Jon Jose Road
Alamo, CA 94507

Albert R. Landgrebe
Int'l Electrochemical Sys & Technology
B14 Sussex Lane
Long Neck, DE 19966

David Warar
Intercon Limited
6865 Lincoln Avenue
Lincolnwood, IL 60646

A. Kamal Kalafala
Intermagnetics General Corp.
450 Old Niskayuna Road
P.O. Box 461
Latham, NY 12110-0461

John Neal
International Business & Tech.
Services, Inc.
9220 Tayloes Neck Road
Nanjemoy, MD 20662

Gerard H. C. M. Thijssen
KEMA T&D Power
Utrechtseweg 310
P.O. Box 9035
ET, Ernhem, 6800
THE NETHERLANDS

Elton Cairns
Lawrence Berkeley Nat'l Lab
University of California
One Cyclotron Road
Berkeley, CA 94720

Frank McLarnon
Lawrence Berkeley National Lab
University of California
One Cyclotron Road
Berkeley, CA 94720

Kim Kinoshita
Lawrence Berkeley Nat'l Lab
University of California
One Cyclotron Road
Berkeley, CA 94720

J. Ray Smith
Lawrence Livermore Nat'l Lab
University of California
P.O. Box 808, L-641
Livermore, CA 94551

Susan M. Schoenung
Longitude 122 West, Inc.
1010 Doyle Street
Suite 10
Menlo Park, CA 94025

Joseph Morabito
Lucent Technologies, Inc.
600 Mountain View Ave.
P.O. Box 636
Murray Hill, NJ 07974-0636

Cecilia Y. Mak
Lucent Technologies
3000 Skyline Drive
Room 855
Mesquite, TX 75149-1802

Stephen R. Connors
Massachusetts Inst of Tech
The Energy Laboratory
Rm E40-465
Cambridge, MA 02139-4307

Dutch Achenbach
Metlakatla Power & Light
P.O. Box 359
3.5 Mile Airport Road
Metlakatla, AK 99926

D. Nowack
Micron Corporation
158 Orchard Lane
Winchester, TN 37398

Dr. Christine E. Platt
Nat'l Institute of Standards & Tech.
Room A225 Administration Bldg.
Gaithersburg, MD 20899

Byron Stafford
Nat'l Renewable Energy Lab
1617 Cole Boulevard
Golden, CO 80401-3393

Holly Thomas
Nat'l Renewable Energy Lab
1617 Cole Boulevard
Golden, CO 80401-3393

Richard DeBlasio
Nat'l Renewable Energy Lab
1617 Cole Boulevard
Golden, CO 80401-3393

Jim Green
Nat'l Renewable Energy Lab
1617 Cole Boulevard
Golden, CO 80401-3393

Larry Flowers
Nat'l Renewable Energy Lab
1617 Cole Boulevard
Golden, CO 80401-3393

Susan Hock
Nat'l Renewable Energy Lab
1617 Cole Boulevard
Golden, CO 80401-3393

Anthony Price
National Power PLC
Harwell Int'l Business Ctr.
Harwell, Didcot, OX11 0QA
UNITED KINGDOM

Steven P. Lindenberg
National Rural Elec Cooperative Assoc.
4301 Wilson Blvd.
SSER9-207
Arlington, VA 22203-1860

Bill Brooks
NC Solar Center
Corner of Gorman & Western
Box 7401 NCSU
Raleigh, NC 27695-740

Andrew L. Rosenthal
New Mexico State University
Southwest Tech. Dev. Institute
Box 30001/Dept. 3SOL
Las Cruces, NM 88003-8001

Bart Chezar
New York Power Authority
1633 Broadway
New York, NY 10019

Gary G. Karn
Northern States Power Co.
1518 Chestnut Avenue North
Minneapolis, MN 55403

Denise Zurn
Northern States Power Co.
414 Nicollet Mall
Minneapolis, MN 55401

Jack Brown
NPA Technology
Two University Place
Suite 700
Durham, NC 27707

John Stoval
Oak Ridge National Laboratory
P.O. Box 2008
Bldg. 3147, MS-6070
Oak Ridge, TN 37831-6070

Robert Hawsey
Oak Ridge National Laboratory
P.O. Box 2008
Bldg. 3025, MS-6040
Oak Ridge, TN 37831-6040

James VanCoevering
Oak Ridge National Laboratory
P.O. Box 2008
Bldg. 3147, MS-6070
Oak Ridge, TN 37831-6070

Brendan Kirby
Oak Ridge National Laboratory
P.O. Box 2008
Bldg. 3147, MS-6070
Oak Ridge, TN 37831-6070

Hans Meyer
Omnion Pwr. Engineering Corp.
2010 Energy Drive
P.O. Box 879
East Troy, WI 53120

Douglas R. Danley
Orion Energy Corporation
10087 Tyler Place #5
Ijamsville, MD 21754

John DeStreese
Pacific Northwest Nat'l Lab
Battelle Blvd.
P.O. Box 999, K5-02
Richland, WA 99352

Daryl Brown
Pacific Northwest Nat'l Lab
Battelle Blvd. MS K8-07
P.O. Box 999
Richland, WA 99352

Thomas H. Schucan
Paul Scherrer Institut
CH - 5232 Villigen PSI
SWITZERLAND

Brad Johnson
PEPCO
1900 Pennsylvania NW
Washington, DC 20068

Stan Sostrom
POWER Engineers, Inc.
P.O. Box 777
3870 US Hwy 16
Newcastle, WY 82701

P. Prabhakara
Power Technologies, Inc.
1482 Erie Blvd.
P.O. Box 1058
Schenectady, NY 12301

Rick Winter
Powercell Corporation
6724 Preston Avenue
Suite C
Livermore, CA 94550

Reznor I. Orr
PowerCell Corporation
99 South Bedford Street
Suite 2
Burlington, MA 01803

Jerry Neal
Public Service Co. of New Mexico
Alvarado Square MS-BA52
Albuquerque, NM 87158

Roger Flynn
Public Service Co. of New Mexico
Alvarado Square MS-2838
Albuquerque, NM 87158

Wenceslao Torres
Puerto Rico Elec. Pwr. Authority
P.O. Box 364267
San Juan, PR 00936-4267

Norman Lindsay
Queensland Department of
Mines and Energy
G.P.O. Box 194
Brisbane, 4001
QLD. AUSTRALIA

J. Thompson
R&D Associates
2100 Washington Blvd.
Arlington, VA 22204-5706

Al Randall
Raytheon Eng. & Constructors
700 South Ash Street
P.O. Box 5888
Denver, CO 80217

K. Ferris
RMS Company
135 Post Office Rd.
South Salem, NY 10590-1106

George V. Fantozzi
S&C Electric Company
6601 North Ridge Blvd.
Chicago, IL 60626-3997

Jim McDowall
SAFT America, Inc.
3 Powdered Metal Drive
North Haven, CT 06473

Guy Chagnon
SAFT Research & Dev. Ctr.
107 Beaver Court
Cockeysville, MD 21030

Michael C. Saft
SAFT Research & Dev. Ctr.
107 Beaver Court
Cockeysville, MD 21030

G. E. "Ernie" Palomino
Salt River Project
P.O. Box 52025
MS PAB 357
Phoenix, AZ 85072-2025

Dr. Charles Feinstein
Santa Clara University
Dept. of Dec. & Info. Sciences
Leavey School of Bus. & Admin.
Santa Clara, CA 95053

Robert Reeves
Sentech, Inc.
9 Eaton Road
Troy, NY 12180

Kurt W. Klunder
Sentech, Inc.
4733 Bethesda Avenue
Suite 608
Bethesda, MD 20814

Rajat K. Sen
Sentech, Inc.
4733 Bethesda Avenue
Suite 608
Bethesda, MD 20814

Nicole Miller
Sentech, Inc.
4733 Bethesda Avenue
Suite 608
Bethesda, MD 20814

Clay Aldrich
Siemens Solar
4650 Adohr Lane
P.O. Box 6032
Camarillo, CA 93011

Deepak Divan
Soft Switching Technologies
2224 Evergreen Road
Suite 6
Middleton, WI 53562

Scott Sklar
Solar Energy Ind. Assoc. (SEIA)
1111 North 19th St
Suite 2604th Floor
Arlington, VA 22209

Naum Pinsky
Southern California Edison
2244 Walnut Grove Ave.
P.O. Box 800, Room 418
Rosemead, CA 91770

Bruce R. Rauhe, Jr.
Southern Company Services, Inc.
600 North 18th Street
P.O. Box 2625
Birmingham, AL 35202-2625

K. Vakhshoorzadeh
Southern Company Services, Inc.
600 North 18th Street
P.O. Box 2625
Birmingham, AL 35202-2625

Richard N. Schweinberg
Southern California Edison
6070 N. Irwindale Avenue
Suite I
Irwindale, CA 91702

C. Seitz
SRI International
333 Ravenswood Avenue
Menlo Park, CA 94025

George Zink
Stored Energy Engineering
7601 E. 88th Place
Indianapolis, IN 46256

Bob Bish
Stored Energy Engineering
7601 E. 88th Place
Indianapolis, IN 46256

Jon Hurwitch
Switch Technologies
4733 Bethesda Avenue
Suite 608
Bethesda, MD 20814

Terri Hensley
Tampa Electric Company
P.O. Box 111
Tampa, FL 33601-0111

Harold Gotschall
Technology Insights
6540 Lusk Blvd.
Suite C-102
San Diego, CA 92121

Thomas J. Jenkin
The Brattle Group
44 Brattle Street
Cambridge, MA 02138-3736

Haukur Asgeirsson
The Detroit Edison Company
2000 2nd Ave.
435 SB
Detroit, MI 48226-1279

Charles E. Bakis
The Pennsylvania State University
227 Hammond Building
University Park, PA 16802

Michael Orians
The Solar Connection
P.O. Box 1138
Morro Bay, CA 93443

Tom Anyos
The Technology Group, Inc.
63 Linden Avenue
Atherton, CA 94027-2161

Bill Roppenecker
Trace Engineering Division
5916 195th Northeast
Arlington, WA 98223

Bill Erdman
Trace Technologies
161G South Vasco Road
P.O. Box 5049
Livermore, CA 94550

Michael Behnke
Trace Technologies
161G South Vasco Road
P.O. Box 5049
Livermore, CA 94550

Donald A. Bender
Trinity Flywheel Power
6724D Preston Avenue
Livermore, CA 94550

Jim Drizos
Trojan Battery Company
12380 Clark Street
Santa Fe Springs, CA 90670

James Fanguie
TU Electric
R&D Programs
P.O. Box 970
Fort Worth, TX 76101

Paul C. Klimas
U.S. Agency for Intn'l Development
Center for Environment
Washington, DC 20523-3800

Jim Daley
U.S. Department of Energy
1000 Independence Ave. SW
EE-12 FORSTL
Washington, DC 20585

Dan T. Ton
U.S. Department of Energy
1000 Independence Ave. SW
EE-11 FORSTL
Washington, DC 20585

James E. Rannels
U.S. Department of Energy
1000 Independence Ave. SW
EE-11 FORSTL
Washington, DC 20585-0121

Gary A. Buckingham
U.S. Department of Energy
Albuquerque Operations Office
P.O. Box 5400
Albuquerque, NM 87185

Mark B. Ginsberg
U.S. Department of Energy
1000 Independence Ave. SW
EE-90 FORSTL 5E-052
Washington, DC 20585

Alex O. Bulawka
U.S. Department of Energy
1000 Independence Ave. SW
EE-11 FORSTL
Washington, DC 20585

Tien Q. Duong
U.S. Department of Energy
1000 Independence Ave. SW
EE-32 FORSTL, Rm. 5G-030
Washington, DC 20585

J. A. Mazer
U.S. Department of Energy
1000 Independence Ave. SW
EE-11 FORSTL
Washington, DC 20585

J. P. Archibald
U.S. Department of Energy
1000 Independence Ave. SW
EE-90 FORSTL
Washington, DC 20585

Richard J. King
U.S. Department of Energy
1000 Independence Ave. SW
EE-11 FORSTL, 5H-095
Washington, DC 20585

Russ Eaton
U.S. Department of Energy
Golden Field Office
1617 Cole Blvd., Bldg. 17
Golden, CO 80401

Kenneth L. Heitner
U.S. Department of Energy
1000 Independence Ave. SW
EE-32 FORSTL, Rm. 5G-030
Washington, DC 20585

Bob Brewer
U.S. Department of Energy
1000 Independence Ave. SW
EE-10 FORSTL
Washington, DC 20585

Neal Rossmeissl
U.S. Department of Energy
1000 Independence Ave. SW
EE-13 FORSTL
Washington, DC 20585

Allan Jelacic
U.S. Department of Energy
1000 Independence Ave. SW
EE-12 FORSTL
Washington, DC 20585

R. Eynon
U.S. Department of Energy
1000 Independence Ave. SW
EI-821 FORSTL
Washington, DC 20585

Alex G. Crawley
U.S. Department of Energy
1000 Independence Ave. SW
EE-90 FORSTL
Washington, DC 20585

Philip N. Overholt
U.S. Department of Energy
1000 Independence Ave. SW
EE-11 FORSTL
Washington, DC 20585-0121

W. Butler
U.S. Department of Energy
1000 Independence Ave. SW
PA-3 FORSTL
Washington, DC 20585

Pandit G. Patil
U.S. Department of Energy
1000 Independence Ave. SW
EE-32 FORSTL
Washington, DC 20585

Allan Hoffman
U.S. Department of Energy
1000 Independence Ave. SW
EE-10 FORSTL
Washington, DC 20585

Jack Cadogan
U.S. Department of Energy
1000 Independence Ave. SW
EE-11 FORSTL
Washington, DC 20585

Joe Galdo
U.S. Department of Energy
1000 Independence Ave. SW
EE-10 FORSTL
Washington, DC 20585

Paul Maupin
U.S. Department of Energy
19901 Germantown Rd
ER-14 E-422
Germantown, MD 20874-1290

Dr. Gerald P. Ceasar
U.S. Department of Commerce
NIST/ATP
Bldg 101, Room 623
Gaithersburg, MD 20899

Dr. Imre Gyuk
U.S. Department of Energy
1000 Independence Ave. SW
EE-14 FORSTL
Washington, DC 20585

Steve Bitterly
U.S. Flywheel Systems
1125-A Business Center Circle
Newbury Park, CA 91320

Wayne Taylor
U.S. Navy
Code 83B000D, NAWS
China Lake, CA 93555

Edward Beardsworth
UFTO
951 Lincoln Avenue
Palo Alto, CA 94301-3041

John Herbst
University of Texas at Austin
J.J. Pickel Research Campus
Mail Code R7000
Austin, TX 78712

Max Anderson
University of Missouri - Rolla
112 Electrical Eng. Bldg.
Rolla, MO 65401-0249

Mariesa L. Crow
University of Missouri-Rolla
233 EECH
Rolla, MO 65409-0040

G. Alan Palin
Urenco (Capenhurst) Ltd.
Capenhurst, Chester, CH1 6ER
UNITED KINGDOM

Steve Hester
Utility Photo Voltaic Group
1800 M Street NW
Washington, DC 20036-5802

Mike Stern
Utility Power Group
21250 Califa Street
Suite 111
Woodland Hills, CA 91367-5029

Rick Ubaldi
VEDCO Energy
12 Agatha Lane
Wayne, NJ 07470

Gary Verno
Virginia Power
Innsbrook Technical Center
5000 Dominion Blvd.
Glen Ellen, VA 23233

Alex Q. Huang
Virginia Polytechnic Instit. & State Uni
Virginia Power Electronics Center
672 Whittemore Hall
Blacksburg, VA 24061

Randy Bevin
Walt Disney World
Design and Eng'g
P.O. Box 10,000
Lake Buena Vista, FL 32830-1000

Gerald J. Keane
Westinghouse Elec. Corp.
Energy Management Division
4400 Alafaya Trail
Orlando, FL 32826-2399

Howard Saunders
Westinghouse STC
1310 Beulah Road
Pittsburgh, PA 15235

Frank Tarantino
Yuasa, Inc.
2366 Bernville Road
P.O. Box 14145
Reading, PA 19612-4145

Nicholas J. Magnani
Yuasa, Inc.
2366 Bernville Road
P.O. Box 14145
Reading, PA 19612-4145

Gene Cook
Yuasa-Exide, Inc.
262 Valley Road
Warrington, PA 18976

R. Kristiansen
Yuasa-Exide, Inc.
35 Loch Lomond Lane
Middleton, NY 10941-1421

Henry W. Zaininger
Zaininger Engineering Co., Inc.
9959 Granite Crest Court
Granite Bay, CA 95746

Robert J. Parry
ZBB Technologies
11607 West Dearbourn Ave.
Wauwatosa, WI 53226-3961

Phillip A. Eidler
ZBB Technologies, Inc.
11607 West Dearbourn Ave.
Wauwatosa, WI 53226-3961

MS-0340/01832	Jeff W. Braithwaite
MS-0457/02000	Gary N. Beeler
MS-0537/02314	Stanley Atcitty
MS-0953/02500	William E. Alzheimer
MS-0953/02501	J. Thomas Cutchen
MS-0613/02521	Daniel H. Doughty
MS-0613/02521	Terry M. Unkelhaeuser
MS-0613/02521	Rudolph G. Jungst
MS-0614/02522	Paul C. Butler
MS-0614/02523	Robert W. Bickes, Jr.
MS-0613/02525	Garth P. Corey
MS-0613/02525	Gustavo P. Rodriguez
MS-0613/02525	James T. Crow
MS-0613/02525	Nancy H. Clark
MS-0613/02525	John D. Boyes (10)
MS-0612/04912	Review & Approval For DOE/OSTI (1)
MS-0899/04916	Technical Library (2)
MS-0741/06200	Samuel G. Varnado
MS-0704/06201	Abbas A. Akhil
MS-0455/06201	Marjorie L. Tatro
MS-0708/06214	Henry M. Dodd
MS-0753/06218	Christopher P. Cameron
MS-0753/06218	Russell H. Bonn
MS-0753/06218	Thomas D. Hund
MS-0753/06218	John W. Stevens
MS-0753/06218	Ward I. Bower
MS-9403/08723	James C. F. Wang
MS-9018/08940-2	Central Technical Files
MS-1193/09531	Dean C. Rovang
MS-0212/10251	Julie A. McBride